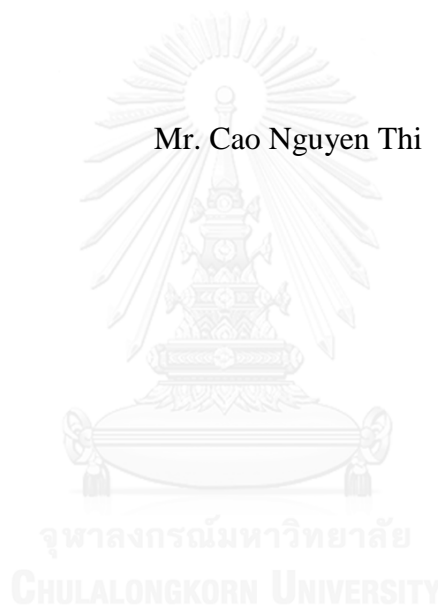FLEXURAL BEHAVIOR OF FIRE-
DAMAGED REINFORCED CONCRETE SLABS REPAIRED WITH NEAR-
SURFACE MOUNTED (NSM) CARBON FIBER REINFORCED POLYMER (CFRP)
RODS

Mr. Cao Nguyen Thi

A Dissertation Submitted in Partial Fulfillment of the Requirements
for the Degree of Doctor of Philosophy Program in Civil Engineering
Department of Civil Engineering
Faculty of Engineering
Chulalongkorn University
Academic Year 2015
Copyright of Chulalongkorn University

พฤติกรรมการดัดของแผ่นพื้นคอนกรีตเสริมเหล็กที่เสียหายจากเพลิงไหม้ซ่อมแซมด้วยแท่งพอลิเม
อร์เสริมเส้นใยคาร์บอนติดตั้งแบบใกล้ผิว

นายกาว เหงวียน ถิ

Thesis Title	FLEXURAL BEHAVIOR OF FIRE-DAMAGED REINFORCED CONCRETE SLABS REPAIRED WITH NEAR-SURFACE MOUNTED (NSM) CARBON FIBER REINFORCED POLYMER (CFRP) RODS
By	Mr. Cao Nguyen Thi
Field of Study	Civil Engineering
Thesis Advisor	Associate Professor Withit Pansuk, Ph.D.
Thesis Co-Advisor	Professor Lluis Torres, Ph.D.

Accepted by the Faculty of Engineering, Chulalongkorn University in Partial Fulfillment of the Requirements for the Doctoral Degree

.... Dean of the Faculty of Engineering
(Associate Professor Supot Teachavorasinskun, Ph.D.)

THESIS COMMITTEE

.... Chairman
(Associate Professor Thanyawat Pothisiri, Ph.D.)
.... Thesis Advisor
(Associate Professor Withit Pansuk, Ph.D.)
.... Thesis Co-Advisor
(Professor Lluis Torres, Ph.D.)
.... Examiner
(Associate Professor Akhrawat Lenwari, Ph.D.)
.... Examiner
(Associate Professor Jaroon Rungamornrat, Ph.D.)
.... External Examiner
(Hwa Kian Chai, Ph.D.)

กาว เหงวียน ถิ : พฤติกรรมการดัดของแผ่นพื้นคอนกรีตเสริมเหล็กที่เสียหายจากเพลิงไหม้ซ่อมแซมด้วยแท่ง พอลิเมอร์เสริมเส้นใยคาร์บอนติดตั้งแบบใกล้ผิว (FLEXURAL BEHAVIOR OF FIRE-DAMAGED REINFORCED CONCRETE SLABS REPAIRED WITH NEAR-SURFACE MOUNTED (NSM) CARBON FIBER REINFORCED POLYMER (CFRP) RODS) อ.ที่ปรึกษาวิทยานิพนธ์หลัก: ผศ. ดร. วิทิต ปานสุข, อ.ที่ปรึกษาวิทยานิพนธ์ร่วม: หลุยส์ ตอร์เรส, 94 หน้า.

หลังจากคอนกรีตเสริมเหล็กถูกเพลิงไหม้ ความสามารถในการรับแรงจะลดลงและส่งผลให้เกิดความเสียหาย ถึงอย่างไรก็ตามองค์อาคารคอนกรีตที่เสียหายจากเพลิงไหม้ยังสามารถนำมาใช้ใหม่ได้หากได้รับการฟื้นฟูสภาพที่มี ประสิทธิภาพ งานวิจัยมากมายได้เสนอวิธีต่างๆในการซ่อมแซมความเสียหายของโครงสร้างที่เสื่อมสภาพจากเพลิงไหม้ โดยการศึกษาทดสอบด้วยการใช้พอลิเมอร์เสริมเส้นใยได้รับความนิยมในช่วงปัจจุบันเนื่องจากมีประโยชน์ในหลายด้าน จุดสำคัญของการศึกษาด้านนี้คือข้อกำหนดต่างๆของระบบพอลิเมอร์เสริมเส้นใยที่สามารถคืนสภาพและปรับปรุงสภาวะ ใช้งานของโครงสร้างที่อ่อนแอโดยมีการเปลี่ยนแปลงขนาดโครงสร้างเพียงเล็กน้อยเมื่อเปรียบเทียบกับขนาดเดิม และมี ความจำเป็นที่จะต้องคำนึงถึงการออกแบบวิธีการซ่อมแซมเพื่อป้องกันระบบพอลิเมอร์เสริมเส้นใยจากปัจจัยภายนอก ระหว่างการใช้งานภายหลังจากการฟื้นฟูสภาพ

งานวิจัยนี้มีเป้าหมายเพื่อหาวิธีการซ่อมแซมองค์อาคารคอนกรีตเสริมเหล็กรับแรงดัดหลังจากถูกเพลิงไหม้ ด้วยวิธีการติดตั้งแบบใกล้ผิวด้วยแท่งพอลิเมอร์เสริมเส้นใยคาร์บอนและวัสดุซ่อมแซม จุดประสงค์ของงานวิจัยนี้คือการ นำเสนอการออกแบบซ่อมแซมซึ่งมีความเป็นไปได้ที่จะฟื้นฟูสภาพองค์อาคารคอนกรีตรับแรงดัดที่เสียหายจากเพลิงไหม้ ด้วยวัสดุพอลิเมอร์เสริมเส้นใยโดยไม่มีการเปลี่ยนแปลงขนาดเดิมของโครงสร้าง ในการศึกษานี้แผ่นทดสอบจำนวนหนึ่ง ได้รับการประเมินพฤติกรรมรับแรงดัดหลังจากถูกเพลิงไหม้ และทำการทดสอบเช่นเดียวกันกับแผ่นทดสอบที่ได้รับการ เสริมกำลัง การจัดวางหรือตำแหน่งของแท่งพอลิเมอร์เสริมเส้นใยคาร์บอนเป็นตัวแปรหลักที่ได้รับการศึกษาเพื่อการ ประเมินประสิทธิภาพของวิธีนี้ ในขณะเดียวกัน ได้ทำการทดสอบพันธะยึดเหนี่ยวโดยตรงด้วยตัวอย่างทดสอบคอนกรีต รูปตัวซี เพื่อตรวจสอบพฤติกรรมของพันธะยึดเหนี่ยวระหว่างแท่งพอลิเมอร์เสริมเส้นใยคาร์บอน คอนกรีต และวัสดุ ซ่อมแซม โดยมีการเปลี่ยนแปลงตำแหน่งฝังแท่งพอลิเมอร์เสริมเส้นใยคาร์บอนทั้งสิ้นสามตำแหน่ง จากผลการทดลอง สามารถสรุปได้ชัดเจนว่าแผ่นทดสอบที่ได้เสริมกำลัง ไม่เพียงแค่ได้เพิ่มขีดความคงทน แต่ยังเพิ่มความสามารถในการรับ น้ำหนักบรรทุกและค่าสติฟเนส เมื่อเปรียบเทียบกับตัวอย่างทดสอบควบคุมและแผ่นทดสอบที่เสียหายจากเพลิงไหม้ โดยเฉพาะอย่างยิ่งจากผลการทดสอบของแผ่นทดสอบเสริมกำลังด้วยแท่งพอลิเมอร์เสริมเส้นใยคาร์บอนที่ฝังอยู่ในชั้นของ วัสดุซ่อมแซม พบว่าเป็นวิธีการซ่อมแซมที่มีประสิทธิภาพที่สุดในการศึกษานี้ จากนั้นทำการจำลองเชิงตัวเลขโดยใช้ ระเบียบวิธีไฟไนต์เอลิเมนต์สามมิติแบบไม่เชิงเส้น ABAQUS เพื่อพัฒนาแบบจำลองพฤติกรรมรับแรงดัดของแผ่น ทดสอบที่เสียหายจากเพลิงไหม้และเสริมกำลังด้วยวิธีที่นำเสนอ จากการเปรียบเทียบกับผลการทดสอบพบว่าแบบจำลอง สามารถทำนายความสัมพันธ์ระหว่างน้ำหนักบรรทุกและการเสียรูปของแผ่นคอนกรีตเสริมเหล็กทั้งก่อนและหลังความ เสียหายจากเพลิงไหม้ และแบบจำลองเชิงตัวเลขยังสามารถทำนายพฤติกรรมของแผ่นทดสอบที่ได้เสริมกำลังด้วยวิธี ดังกล่าวอีกด้วย นอกจากนั้นได้ทำการศึกษาตัวแปรเพื่อหาอิทธิพลจากการเปลี่ยนความยาวของแท่งพอลิเมอร์เสริมเส้นใย คาร์บอน และประเมินผลกระทบของระบบพันธะยึดเหนี่ยวแบบบางส่วน

ภาควิชา	วิศวกรรมโยธา	ลายมือชื่อนิสิต	_____
สาขาวิชา	วิศวกรรมโยธา	ลายมือชื่อ อ.ที่ปรึกษาหลัก	_____
ปีการศึกษา	2558	ลายมือชื่อ อ.ที่ปรึกษาร่วม	_____

CAO NGUYEN THI: FLEXURAL BEHAVIOR OF FIRE-DAMAGED REINFORCED CONCRETE SLABS REPAIRED WITH NEAR-SURFACE MOUNTED (NSM) CARBON FIBER REINFORCED POLYMER (CFRP) RODS. ADVISOR: ASSOC. PROF. WITHIT PANSUK, Ph.D., CO-ADVISOR: PROF. LLUIS TORRES, Ph.D., 94 pp.

After exposure to fire, the decrease in load capacity of reinforced concrete (RC) structure will take place and may lead to a damage. However, the fire-damaged concrete member still can be reused if an effective rehabilitation method is applied. Many researches have proposed a lot of techniques on repairing fire-deteriorated structures. Among them, the experimental studies using Fiber Reinforced Polymer (FRP) materials have become popular in recent years due to its high advantage. An important point in this field is the requirement for a FRP system that could restore and enhance the serviceability of weakened structure with only a small change in comparison with its initial size. Moreover, it is also necessary to consider a repairing design in order to protect the FRP system from external agents during service process after the rehabilitation.

This research aims to carry out a method to repair flexural reinforced concrete members after exposure to fire based on near-surface mounted (NSM) technique with the application of carbon fiber reinforced polymer (CFRP) rods and repairing material. The purpose is in order to propose a repairing design that could be possible to rehabilitate fire-damaged flexural concrete members by using FRP materials without changing original size of structure. In this study, a series of slabs were conducted to evaluate the flexural behavior of structures after exposure to fire as well as strengthened specimens. The arrangement or the location of CFRP bars was the main factor that had been considered to evaluate the effectiveness of this method. Besides, the direct bond test on C-shaped concrete block specimens was carried out to investigate the bond behavior between CFRP rods and concrete-repairing material substrate in three different embedding positions of FRP bars. Based on the experimental data, it is clear to conclude that the strengthened slabs not only improved endurance limits but also improved load-carrying capacities and stiffness values as compared to control specimen and fire-damaged slab. Especially, based on the results from slab strengthened with CFRP rods embedded in repairing material overlay, it could be considered that this is the most effective method among the proposed techniques in this study. In addition, a numerical simulation was conducted by using 3D nonlinear finite element software ABAQUS in order to develop a model for simulating the flexural behavior of fire-deteriorated slabs strengthening with the proposed method. Based on the comparison with experimental results, the model is possible to predict the load-deflection relation of RC slabs before and after exposure to fire. This numerical simulation is also capable to predict the behavior of strengthened slabs mentioned in experiment. Furthermore, a parametric study was carried out to determine the influence of changing the length of CFRP bars and evaluate the effect as a partially-bonded system could be applied.

Department: Civil Engineering   Student's Signature ....

Field of Study: Civil Engineering   Advisor's Signature ....

Academic Year: 2015   Co-Advisor's Signature ....

ACKNOWLEDGEMENTS

CONTENTS

LIST OF FIGURES

LIST OF TABLES

Chapter 1

INTRODUCTION

1.1 Background

In recent years, design and repair of fire-damaged concrete structure have emerged as a subject of remarkable interest to both specialist and public. When concrete structures are exposed to high temperatures, mechanical losses of its properties take place [1]. This may result in cracking and loss in the bearing capacity of components [2]. After fire, concrete suffers a reduction of its strength as well as its damage that can be observed at the surface. Furthermore, another main problem is the reduction of bond strength between concrete and steel reinforcement, which cause reduction in the structural load carrying capacity. Consequently, after exposure to fire, reinforced concrete (RC) structures cannot be used as effectively and safely. Nowadays, a lot of different techniques may be used for repairing and retrofitting of fire-damaged RC structures. Among these techniques, the use of fiber reinforced polymer (FRP) composites has become increasingly popular due to their unique properties, including a high strength-to-weight ratio, ease of installation, excellent corrosion resistance and long fatigue life. For flexural strengthening, this technique can be employed by using different kinds of FRP products as for example sheets, strips or rods to the tension side of the member in order to take advantage of their high strength in tension. Two popular strengthening methods are distinguished by the different ways in which FRP materials are applied, namely Externally Bonded (EB) Reinforcement and Near Surface Mounted (NSM) reinforcement.

Most of researches on strengthening or repairing flexural fire-damaged structures focused on using EB FRP systems. Haddad, Al-Mekhlafy [2] used carbon FRP (CFRP) and glass FRP (GFRP) sheets to repair heat damaged slabs (heated at 600°C for 2h). Based on the results, the authors concluded that CFRP and GFRP strengthened elements regained up to 158 and 125% of the control slab's ultimate load capacity with a substantial increase in stiffness, first cracking load, with a corresponding decrease in mid-span deflections at ultimate load. Kai, Guohui [3] carried out a series of tests with T-beams (5400x200x200 mm and flange 900x80 mm) exposed to fire at 1000°C. After fire exposure, the fire damaged beams were strengthened with CFRP sheets following three steps: 1) serious fire damaged concrete was removed before strengthening; 2) epoxy bonding adhesive was used to retrofit the damaged surface of the T-beams; and 3) CFRP sheets were used to strengthen the beams. External strengthening with CFRP sheets was found to increase the yield and ultimate loads of the fire-damaged T-beams.

The second strengthening method indicated above, NSM reinforcement, has become an emerging retrofitting technique for RC members and masonry which has attracted an increasing interest of research as well as practical applications [4, 5]. In the NSM FRP technique, grooves are first cut into the concrete cover of a RC member and the FRP reinforcement is bonded therein with groove filler. This technique offers various advantages over the EB FRP method such as: it is less prone to debonding from the

concrete surface, provides greater protection from external damage, can be more easily pre-stressed and the aesthetic of the strengthened structure is virtually unchanged [6, 7]. Based on those benefits, the NSM technique could be an effectively choice for strengthening or repairing fire-damaged RC structures.

However, after fire attack, it could be observed that the concrete cover is the most deteriorated part in RC member. Therefore NSM FRP reinforcements cannot be applied in usual way that has been conducted in prior works. FRP reinforcement should not be installed in the weakened layer; this layer must be replaced by repairing material.

According to the previous considerations, a study on the repairing of fire-damaged flexural RC elements using the NSM FRP technique and repairing material was carried out. This work aims to propose a repairing technique without changing the original size of member and can protect FRP bars from the external agents.

Due to the lack of research works on the utilization of NSM FRP bars in RC slab after fire damage, an experimental program which focus on repairing and strengthening fire-damaged one way slab by NSM method has been carried out. The specimens in this experimental campaign were prepared based on the following main steps: a) the RC slabs were exposed to fire; b) after exposure to fire, the damaged concrete layer was removed; c) the NSM CFRP reinforcements were applied on the tension side of the remaining part of slab; and d) the removed layer was replaced by repairing material and it was required to restore the full size of the slab.

Three different positions of the installed CFRP rods have been studied in this work: inside the original concrete part; between the concrete and repairing material parts; inside the repairing material layer. Besides, pull-out tests on C-shaped concrete blocks were carried out to study the bond behavior between FRP bars and surrounding substrate corresponding to the three different locations of FRP reinforcement as mentioned above. Subsequently, the slabs were tested under bending to obtain the load-deflection response. The results are presented and discussed to evaluate the effectiveness of the proposed methods.

Furthermore, a numerical analysis using finite element code ABAQUS to simulate the flexural behavior of RC slabs has also been carried out. The numerical results have been compared with the experimental data. The developed models could be used to predict the flexural behavior of RC slab after exposure to fire as well as fire-damaged RC slab repairing by CFRP rods.

1.2 Research objectives

The main objective of this research is to study and examine a method for repairing and flexural strengthening fire-damaged RC slabs based on the concept of NSM FRP technique combined with using repairing material. Beside the experimental work, a numerical simulation study which employed finite element code ABAQUS was conducted to simulate the specimens and compare the results with testing data. The experiment and numerical simulation aimed to propose models which could be applicable to predict the flexural behavior of RC structures before and after fire damage, as well as the behavior of repaired members by NSM FRP system. The specific objectives of this study could be summarized as follows:

- To evaluate the behavior of RC slabs after exposed to fire.

- To study the flexural behavior of fire-damaged RC slabs repaired by using CFRP bars installed with the NSM FRP methodology in combination with repairing material through of different designs in order to propose an effective method for rehabilitating structures after fire damage. The evaluated parameters in the experimental campaign were the location of CFRP bars and the strength of concrete.

- To study the bond stress-slip behavior between CFRP rods with surrounding concrete – repairing material substrate through pull out test of C-shaped specimens.

- To simulate the behavior of the specimens tested under bending in the experiment by using the simulation software ABAQUS. The developed models could be used to predict the load-deflection relation of RC slabs after exposure to fire, as well as the slab strengthening by system FRP bar - repairing material.

- A parametric study was conducted based on the developed model to determine the effect of changing the length of NSM FRP reinforcement. Different lengths of CFRP bars were analyzed. Moreover, the application of partially-bonded CFRP bars instead of fully-bonded systems was also analyzed.

1.3 Research project

To achieve the above objectives, the program was divided into two main parts. One included the experimental work, while the second included the analytical work as shown in **Fig. 1.1**.
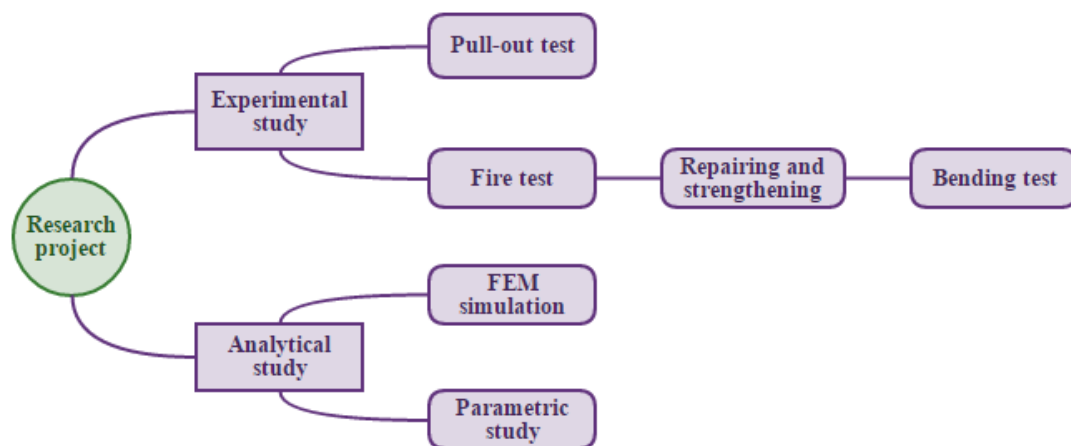
Figure 1.1 Research program.

The experimental work consisted of two phases. The first phase includes the pull-out tests of 6 specimens of CFRP rods embedded in a C-shaped concrete block composed of 2 parts: concrete and repairing material. The main parameter in the test was the

position of the CFRP rod with 3 cases considered: inside the concrete; between the concrete and the repairing material; inside the repairing material.

The second phase includes a process of fire test, repairing process and bending test of 8 RC slabs. The different strengthening designs, different location of CFRP bars, was the main parameter need to be evaluated based on the comparison on load-deflection relation of all slabs.

The numerical work includes conducting an analytical model to be used in a commercially available non-linear finite element program ABAQUS. This work aimed to analyze and predict the flexural behavior of RC slabs before and after exposure to fire, as well as the behavior of specimens strengthened in flexure using the NSM FRP bars. The efficiency and accuracy of the model were compared against the experimental results. The developed model was also used for studying the influence when changing CFRP bars length and the application of partially-bonded systems.

1.4 Outline of the thesis

This thesis is divided into six chapters as shown in **Fig. 1.2**.
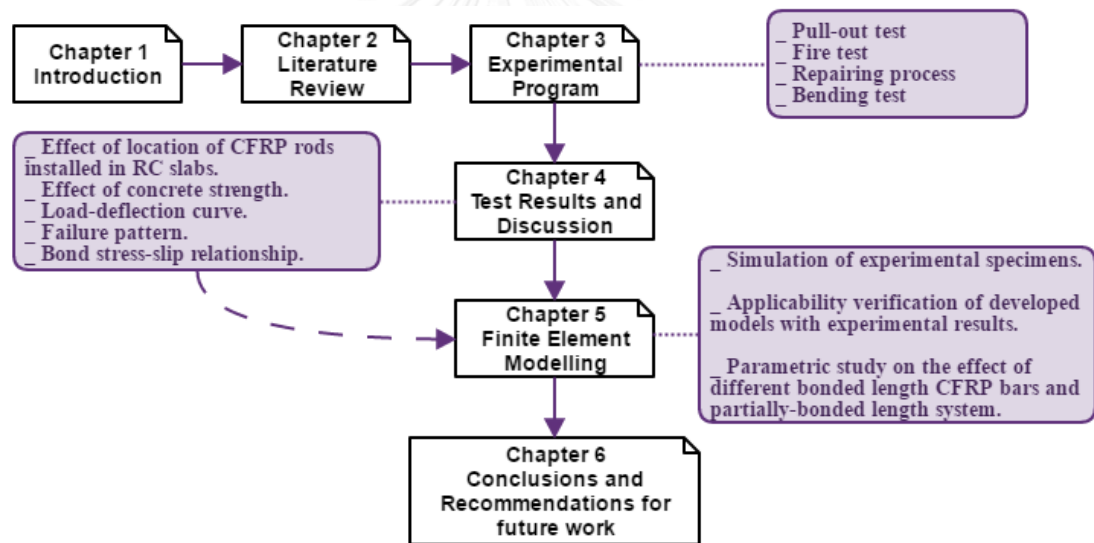
Figure 1.2 The structure of dissertation.

Chapter 1 provides the introduction to flexural strengthening techniques using FRP material and mentions to a method on repairing fire-damaged RC slabs base on NSM FRP technique combines with repairing material. The methodology to achieve these research objectives and the outline of the thesis are written in this part.

Chapter 2 presents a literature review includes a background in FRP material, overview on behavior of reinforced concrete structure after exposure to fire and the general of flexural strengthening techniques using FRP materials consists of EBR and NSM techniques. This chapter also reviewed the bonding behavior between concrete and NSM FRP rod through of failure modes, local bond strength, local bond-slip behavior and development length. A series of previous researches on repairing and flexural strengthening RC structures by NSM techniques are referred. In addition,

another FRP strengthening technique using partially-bonded system are introduced according to the prior studies.

Chapter 3 describes the experimental program consists of pull-out test on C-shaped specimens, process of repairing fire-damaged RC slabs and bending test on these specimens.

Chapter 4 reports the test results and discussions for pull-out test and bending test. The effect of position of CFRP bars installed in slabs were considered as the main parameter to propose an effective strengthening method. The effectiveness of technique is evaluated based on the data such as failure patterns, loading capacity and load-deflection relationship obtained from bending test. Besides, the influence of concrete strength are considered also.

Chapter 5 discusses the numerical simulation that was carried out using the finite element software ABAQUS. The numerical models were compared with experimental results. Besides, a parametric study was conducted based on the developed model to predict the effect of CFRP bars length. Furthermore, the flexural response of slabs in case of using NSM FRP bars with partially-bonded system was evaluated using numerical simulation.

Chapter 6 presents the conclusions and recommendations for future work.

Chapter 2

LITERATURE REVIEW

2.1 Reinforced concrete exposed to fire

Fire causes heat to flow into the concrete structure. The temperature in the concrete mass will rise, causing thermal expansion of the constituents, evaporation of moisture, buildup of pore pressures and degradation of the mechanical properties [8]. Most of the damage in the concrete exposed to high temperature comes from the mostly irreversible processes occurring in the heating phase and during the rest period at high temperature. The chemical composition and physical structure of the concrete change considerably by the following factors: loss of evaporable water in the cement paste (40-105°C) and in the aggregates (beyond 200°C), reduction of chemically-combined water in the hydration products (105-850°C), crystalline transformation of siliceous aggregates, dissociation of calcium hydroxide (350-500°C) and decarbonation of calcareous aggregates (600-900°C). These factors, together with the different thermal expansion of the hardened cement paste and of the aggregates, cause micro-strains and micro-cracking, to the detriment of the integrity of concrete microstructure [9]. Moreover, the fire is generally extinguished by water and CaO turns into [Ca(OH)$_2$] causing cracking and crumbling of concrete [10]. When a RC structure is exposed to fire, steel rebar loses a significant part of its elastic modulus and yield strength during thermal loading but recovers almost all of them when it cools down to the ambient temperature [11]. On the contrary, concrete is not able to recover its original characteristics during the cooling process. With regard to horizontal members such as beams and one-way slabs exposed to fire, the bending failure can be the most common type of failure. Given the fact that only fire exposure of the bottom side is considered, failure can occur by either rupture of the reinforcement, which is common for sagging bending moments, or crushing of the concrete in the compression zone, which is more likely for hogging bending moments near the supports [8].

To repair a fire-damaged concrete structure, it is necessary to have a post-fire investigation before repairing. The main objective of repairing a fire-damaged concrete structure is to bring back the structure to its original state and destination, through the following steps [9]: the reinforced should be refurbished and protected, and the concrete sections should be brought back to their original size; the repaired structure should have the same residual life, same load-bearing capacity, fire-safety requirements as before the fire. Some methods are carried out to determine the depth of the thermal deterioration that need to be removed and replace. The external layers that have been subjected to temperatures in excess of 300°C should be removed according to the following, well-proved techniques [9]: chiseling and sand blasting, cleaning with high-pressure water jets. Drill small cores can be used as a useful method to evaluate the depth of the deterioration as well as strength and modulus of elasticity. Cores are also useful for giving incidental information about cracking in the

interior of a member, the bond to reinforcing steel, and interior temperatures as revealed by color changes. Some of the information that can be obtained is shown in the schematic drawing of **Fig. 2.1**.

After the depth of the deterioration concrete layer is defined and removed, the tensile strength of the new concrete layer should be assessed by means of pull-off test. The correlation between the pull-off load and concrete tensile strength makes it possible to have sufficient information on concrete strength for the application of protective coatings.
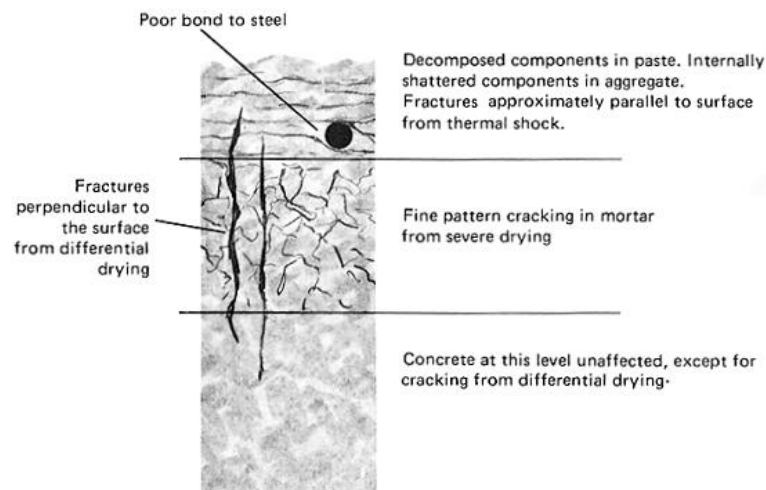
Figure 2.1 A core of fire-damaged concrete taken at appropriate intervals [12].

2.2 Fiber Reinforced Polymer

Fiber reinforced polymer (FRP) is a name to determine the composite material that made of a polymer matrix reinforced with fibers. Composite materials are man-made or natural materials that consist of at least two different constituent materials, the resulting composite material being different from the constituent materials [13]. Normally, FRPs consist of two main components: (a) the reinforcing or fiber phase provides strength and stiffness to the composite and generally carry most of the applied load [14]; (b) the matrix phase, in which the fibers are embedded. The functions of the matrix phase are to bind fibers to fabricate structural shapes, protect them from environmental degradation, to provide for transfer of forces between the individual fibers through shear stresses. Generally, matrix materials can be grouped into two classifications: thermoplastic and thermosetting resins. Thermoplastics involve such polymer compounds as polyethylene, nylon, and polyamides, while thermosetting materials include epoxies and vinyl esters. Meanwhile, the fibers provide the strength and stiffness of an FRP. Because the fibers use in most structural FRP applications are continuous and are oriented in specified directions, FRPs are orthotropic, and they are much stronger and stiffer in the fiber direction(s). Fibers are generally selected to have: high stiffness, high ultimate strength, low variation of strength between individual fibers, stability during handling and uniform diameter [15]. Many kinds of fibers are available to produce FRP such as glass fibers, carbon fibers, aramid fibers and basalt fibers. They are chosen for the use depending on their respective advantages and each individual case.

Figure 2.2 Assorted FRP products used for civil engineering structures [15].

FRP were originally developed for aircraft and have been used for civil engineering structures since the 1980s. A large number of projects have been carried out to demonstrate the use of this composite in the rehabilitation of reinforced and pre-stressed concrete structures [16]. FRPs have significant advantages over classical structural materials such as steel, including high strength-to-weight ratios, corrosion resistance, ease of application and outstanding fatigue characteristics (carbon FRP). The samples of FRP products used for civil engineering are shown in **Fig. 2.2**. They can be successfully used for the rehabilitation of all structural elements such as beams, columns, slabs, walls, tanks and chimneys. FRPs have been applied to the existing structures to increase properties including axial, flexural, or shear load capacities, ductility for improved seismic performance, improved durability against adverse environmental effects, increased fatigue life; stiffness for reduced deflections under service and design loads [16].

The application of any material strongly depends on the mechanical properties including the stress-strain response, creep, fatigue, fracture, and bond behavior. Many previous researches and standard test methods have been carried out to determine the mechanical properties of FRPs for the use in civil engineering structures. In general the mechanical properties of an FRP depend on several factors: the relative proportions of fiber and matrix, the mechanical properties of the constituent materials (fiber, matrix, and any additives), the orientation of the fibers within the matrix and the method of manufacture [15]. The typical stress-strain curves for several FRP materials are shown in **Fig. 2.3** for a comparison of each other and also includes stress-strain curves for reinforcing and prestressing steel. It is clear that the modulus of glass and aramid FRPs is significantly lower than that of steel in the pre-yield zone, while the modulus of CFRPs is higher than steel. It is also evident to observe the ultimate strengths of FRPs can be many times greater than steel and they specially have no yielding. **Table 2.1** also provides a comparison between various types of FRPs.

Table 2.1 Comparison of typical approximate properties for reinforcing materials for Concrete [15].

Property	Steel Rebar	Steel Tendon	GFRP Rebar	CFRP Tendon	AFRP Tendon
Tensile Strength (MPa)	483-690	1379-1862	517-1207	1200-2410	1200-2068
Yield Strength (MPa)	276-414	1034-1396	N/A	N/A	N/A
Tensile Elastic Modulus (GPa)	200	186-200	30-55	147-165	50-74
Ultimate Elongation (%)	>10	>4	2-4.5	1-1.5	2-2.6
Compressive Strength (MPa)	276-414	N/A	310-482	N/A	N/A
CTE (10-6/˚C)*	11.7	11.7	9.9	0	-1--0.5
Specific Gravity	7.9	7.9	1.5-2.0	1.5-1.6	1.25

* Coefficient of thermal expansion (CTE)
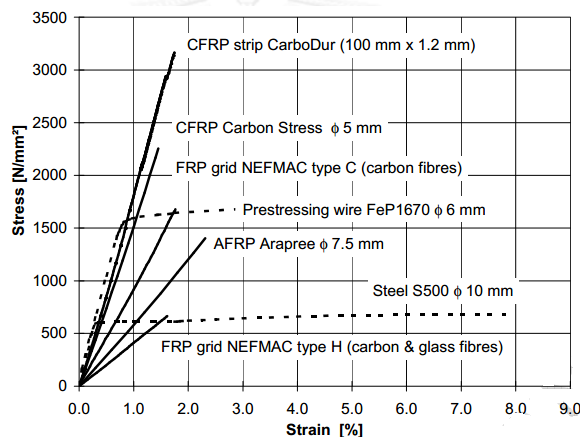
Figure 2.3 Stress-strain behavior of some FRP elements compared to steel [17].

2.3 Overview of FRP strengthening techniques in flexural structures

2.3.1 Externally bonded reinforcement (EBR) method

Over the past decades, since FRP material started to be applied in civil engineering, a widespread technique has been using for strengthening reinforced concrete structures namely externally bonded reinforcement (EBR). This technique has not only been investigated in many laboratories but also implemented in a large number of practical projects. In this method, FRP plates or sheets are bonded to the exterior of RC elements on the tension face using the wet lay-up procedure with an epoxy resin. By this way, the flexural strength can increase up to 160%, ductility and serviceability constraints limit the percentage increase to about 40% that have been reported in the literature [16]. Moreover, FRPs also increase the shear capacity of RC members by bonding to their side faces. Typical applications are shown in **Fig. 2.4**.
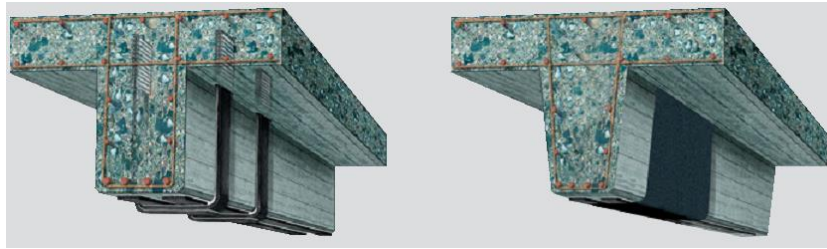
Figure 2.4 Flexural and shear strengthening of reinforced concrete beams [18].
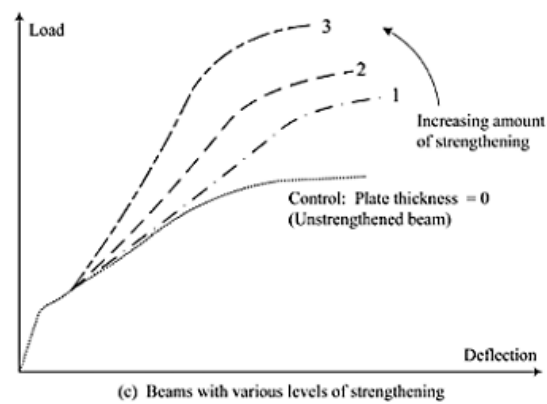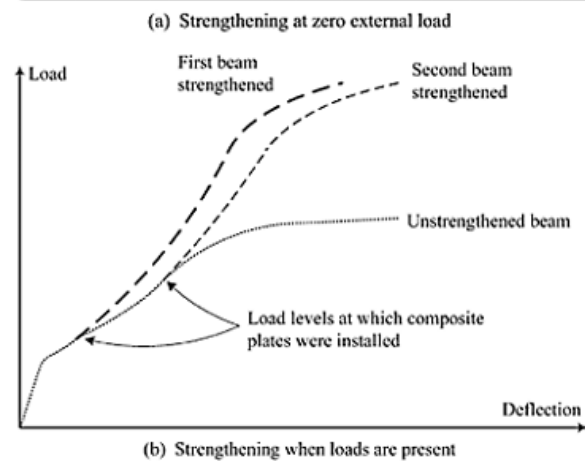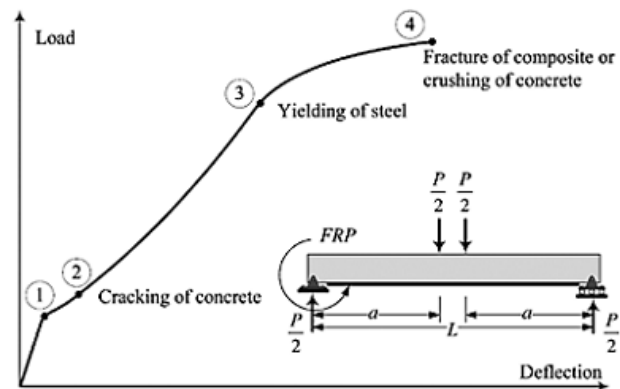
Figure 2.5 Typical load–deflection curves of strengthened reinforced concrete beams [16].

The load–deflection response of a simply supported beam strengthened with FRP (with no previous external loads) is shown in **Fig. 2.5a**. The beam strengthened at zero load essentially behaves like the reinforced concrete beam with extra reinforcement with the following notable differences [16]:

- The cracking load (moment) is slightly larger due to the extra force provided by the composite.

- In the post-crack, preyielding region, between points 2 and 3 in **Fig. 2.5a**, the slope will be higher. The higher stiffness is a function of FRP plate cross-sectional area and modulus of elasticity of the fiber. For example, carbon plates will provide a larger increase than glass plates. However, in the normal strengthening range (strength increase less than 50%) the stiffness increase in not significant.

- The load (moment) at which yielding of steel occurs will also increase. The increase is again function of composite thickness and its modulus of elasticity (composite stiffness).

- The contribution of composite becomes very significant in the post yielding stage, between points 3 and 4 of **Fig. 2.5a**. Since additional contribution of steel is zero in the yield plateau, post-yield part of the curve is flat for a reinforced concrete beam. The composite strengthened beam continues to provide strength increase because the composite force contribution continues at the same level.

Fig. 2.5b shows the curves in case of the FRP is installed when certain external loads are present. In most cases, the beam will be in the post-crack, preyielding stage. Even if some of the loads such as live loads are removed, the beams are still in cracked condition. The behavior is similar to the previous case, except that the composite has more strain capacity and, hence, can achieve larger deflections. Since composites can generate large strains compared to yield strain of steel, the loads should be reduced as much as possible during the installation.

The influence of composite thickness is shown in **Fig. 2.5c**. Larger plate thicknesses provide larger stiffness increase, higher load at steel yielding, higher load post-yield increase, and higher failure loads. However, as the thickness increases, failure by delamination of the plate could become a possibility.

2.3.2 Near surface mounted (NSM) method

The EBR FRP method is currently the most commonly used technique for flexural and shear strengthening of RC beams and slabs. However, EBR FRP may be highly susceptible to damage from collision, fire and temperature, ultraviolet rays, and moisture absorption. In some situations, it cannot reach a high effectiveness and may narrow the service life of the structure. To minimize these problems and to develop an application of the FRP materials. The NSM method was recently introduced as an attractive and promising technique for strengthening masonry and reinforced concrete members. In comparison with EBR, the NSM system has a number of advantages: (1) Due to the concrete cover, NSM reinforcement is less prone to debonding from the substrate and less exposed to accidental impact, mechanical damage; (2) the amount of site installation work may be reduced, as surface preparation other than grooving is no longer required; (3) NSM reinforcement can be more easily anchored into adjacent

members to prevent debonding failures; (4) NSM reinforcement can be more easily pre-stressed; (5) The aesthetic of the strengthened structure is virtually unchanged. (6) The technique could also provide better resistance in the event of a fire; therefore, it could reduce the cost of fire protection measures [7].

Even though the use of NSM FRP reinforcement for strengthening is relatively recent, NSM steel bars were used in Europe for the strengthening of RC structures [19]. In 1949, Asplund carried out tests on concrete beams strengthened with NSM steel bars grouted into diamond-sawed grooves filled with cement mortar and compared their behavior with that of conventional concrete beams reinforced with steel bars [20]. Due to many advantages of FRP materials, FRP rods or strips have been applied for this application instead of using steel bars. They bring out high tensile strength with the lightweight properties. Therefore, rods with smaller diameters can be used for a given required tensile force whereby groove size needed for embedment can reduce in comparison with using steel bars.

Types of NSM FRP reinforcement strongly affect the behavior and effectiveness of the strengthening method. Carbon FRP (CFRP) and glass FRP (GFRP) have been employed commonly in many cases to strengthen RC members. Typical products of this type of reinforcements are presented in **Fig. 2.6**. However, the tensile strength and elastic modulus of CFRP are much greater than those of GFRP. Therefore, at the same tensile capacity, a CFRP rod needs a smaller cross-sectional area and a smaller groove than a GFRP rod. This in turn leads to save groove-filling material, less risks of interfering with the internal steel reinforcement. The shape of NSM FRP reinforcement can be round, square, rectangular or oval bars, as well as strips. Different cross-sectional shapes bring out distinctive advantages and different choices for practical applications. FRP bars are manufactured with a variety of surface textures, which strongly affect their bond behavior as NSM reinforcement [7]. Their surface can be smooth, sand-blasted, sand-coated, roughened and spirally wound with a fiber tow.
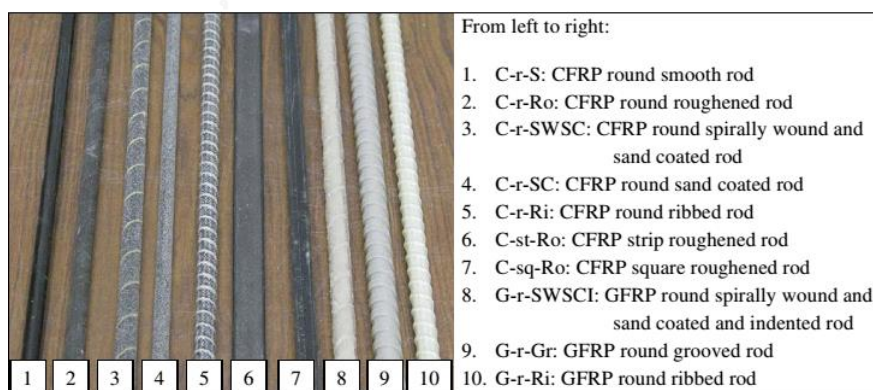
Figure 2.6 Types of NSM FRP reinforcements [21].

When using the NSM FRP procedure, the groove is first saw-cut onto the surface of the concrete substrate of a RC member. Then, the filling material, such as epoxy or cement paste, is filled half-way in the groove and the FRP bar will be put into the groove and lightly pressed. Finally, more filling material is applied to fill the groove and the surface is leveled. Details of NSM FRP reinforcements that are applied in concrete substrate are shown in **Fig. 2.7** and **Fig. 2.8**.
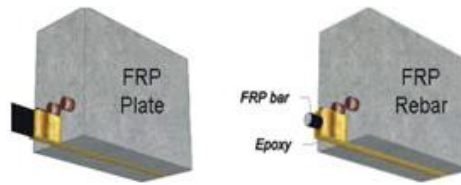
Figure 2.7 The representation of NSM FRP reinforcement in application [22].
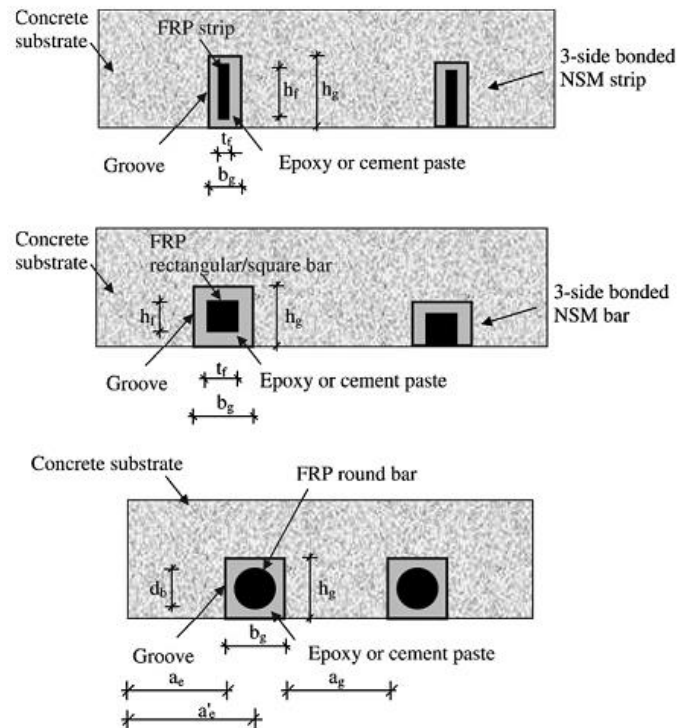
Figure 2.8 Different NSM systems [7].

The effect of type of FRP reinforcement, groove filler, groove dimensions and groove position are also factors that affect the behavior of NSM FRP system. In terms of structural behavior, tensile and shear strength of groove filler are the most significant mechanical properties. The tensile strength is especially important when the embedded bars have a deformed surface, which produces high circumferential tensile stresses in the cover formed by the groove filler as a result of the bond action. In addition, the shear strength is important when the bond capacity of the NSM reinforcement is controlled by cohesive shear failure of the groove filler [7].Two-component epoxy is the most common material used as a groove filler due to its high tensile and shear strength. For round bars, De Lorenzis [23], based on results of bond tests with square grooves ($b_g=h_g$) and defining $k=b_g/d_b$, proposed a minimum value of 1.5 for k for smooth or lightly sand-blasted bars and a minimum value of 2.0 for k for deformed bars. Parretti and Nanni [24] suggested that both b_g and h_g should be not less than $1.5d_b$. For NSM strips, Blaschko [25] proposed that the depth and width of the cut groove should be about 3 mm larger than the height and thickness of the corresponding FRP strip respectively, so to obtain an adhesive layer thickness of about 1–2 mm. Also for NSM strips, Parretti and Nanni [24] recommended that the

minimum width of a groove be no less than $3t_f$ and the minimum depth is not less than $1.5h_f$. In order to position of FRP bar, if a single bar is applied to the tension side of the RC member, it should be located in the central over the beam width. The distance between the edge of the member and the adjacent bar are also important parameters need to be evaluated.

2.4 Researches of the bond behavior between concrete and NSM CFRP bars

2.4.1 Failure modes

In general, previous researchers summarized three main bond failure modes of NSM FRP systems including: (1) bond failure at the bar-epoxy interface; (2) bond failure at the epoxy-concrete interface; (3) splitting of the epoxy cover.

The first failure mode can be pure interfacial failure (BE-I) or cohesive shear failure in the groove filler (BE-C) [7]. The BE-I failure mode is critical for bars when their degree of surface deformation is insufficient to provide mechanical interlocking between bar and groove filler. In case of round bars, this mode is also critical as the groove size is sufficiently large to avoid splitting failure of the groove filler. The BE-C failure mode can occur when the shear strength of the epoxy is exceeded with respect to the NSM strips.

In case of the second failure mode, pure interfacial (EC-I) and shear failure in the concrete (EC-C) can be observed [7].The EC-I failure mode was observed with respect to pre-cast grooves. The EC-C failure mode has never been observed in bond tests, but it has been observed in bending tests on beams within the strengthened region [26].

Splitting of the epoxy cover may occur as longitudinal cracking of the groove filler or fracture of the surrounding concrete along inclined planes and was observed to be the critical failure mode in case of deformed round bars. The mechanic of this failure mode is similar to splitting bond failure of steel deformed bars in concrete. For an NSM FRP bar, the radial component of the bond stresses is balanced by circumferential tensile stresses in the epoxy cover which may lead to the formation of longitudinal splitting cracks of the cover. The concrete surrounding the groove is also subjected to tensile stresses and may eventually fail when its tensile strength is reached, causing fracture along inclined planes [7].

2.4.2 Local bond strength

Bond behavior of the NSM FRP round deformed bars is controlled by splitting tensile stresses in the epoxy cover and the surrounding concrete. In the proposed approach of Hassan and Rizkalla [27], transfer of stresses from a deformed NSM FRP rod to the concrete is assumed to be mainly through the mechanical interlocking of the lugs to the surrounding adhesive or epoxy as presented in **Fig. 2.9**. Herein, a typical stress distribution around a NSM FRP bar is proposed by the authors with a stress discontinuous at the concrete-epoxy interface as shown in **Fig. 2.10**. Two different types of debonding failures can occur for NSM FRP bars [27]. The first mode of failure is due to splitting of the epoxy cover as a result of high tensile stresses at the FRP-epoxy interface, and is termed "epoxy split failure". Increasing the thickness of

the epoxy cover reduces the induced tensile stresses significantly. Furthermore, using adhesives of high tensile strength delays epoxy split failure. The second mode of failure is due to cracking of the concrete surrounding the epoxy adhesive and is termed "concrete splitting failure". This mode of failure takes place when the tensile stresses at the concrete-epoxy interface reach the tensile strength of the concrete. Widening the groove minimizes the induced tensile stresses at the concrete-epoxy interface and increases the debonding loads of NSM bars. Base on the test results, Hassan and Rizkalla [27] proposed two formulae to predict the local bond strengths for the bar–epoxy and the epoxy–concrete interfaces respectively. The two formulae are:

$$\tau_{\max\,bar-epoxy} = \frac{f_{at}\mu}{G_2} \tag{2-1}$$

$$\tau_{\max\,epoxy-concrete} = \frac{f_{ct}\mu}{G_1} \tag{2-2}$$

where f_{at} is the tensile strength of epoxy, f_{ct} is the tensile strength of concrete, μ is the coefficient of friction, G_1 and G_2 are coefficients which were evaluated by finite element analysis and are dependent on the groove depth-to-bar diameter and the groove width-to-bar diameter ratios. G_1 and G_2 range between 0.58 and 1.3 and between 0.5 and 0.72, respectively.
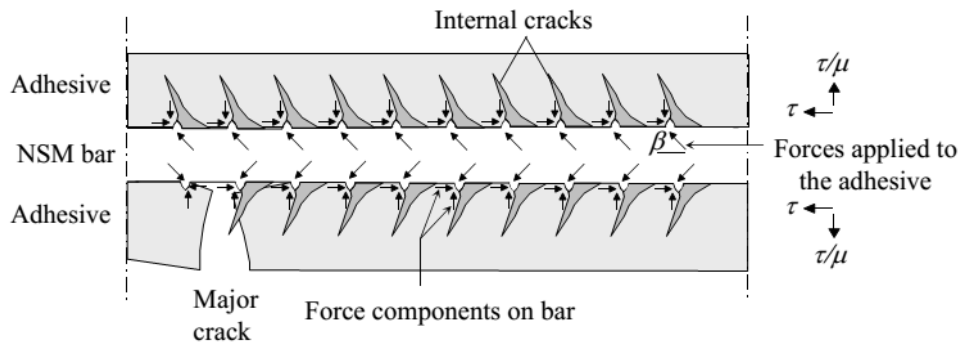
Figure 2.9 Forces between a NSM FRP bar and adhesive [27].
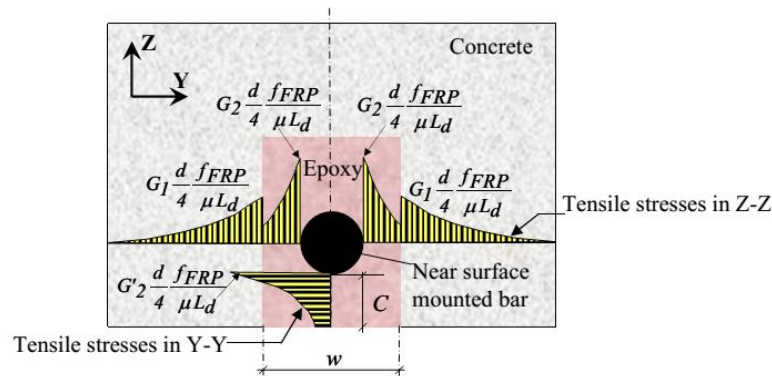
Figure 2.10 Typical stress distribution around a NSM bar [27].

2.4.3 Local bond-slip behavior

Three different types of local bond–slip behavior (types I–III), of which the first two are shown in **Fig. 2.11** and the third type (for sand-blasted round bars) differs from the second in that the abrupt decay from the maximum bond stress to the frictional bond stress level is replaced by a linearly decreasing branch [7].
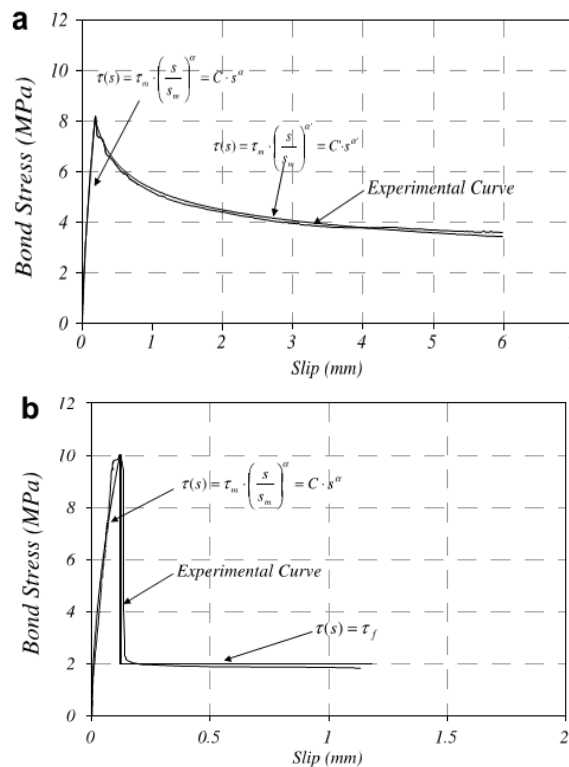
Figure 2.11 Typical bond-slip curves of NSM FRP reinforcement: (a) Type I curve; (b) Type II curve [7].

Type I curve show cases such as bond failure of the epoxy-concrete interface of round bars, splitting of the epoxy cover of CFRP ribbed round bars and bond failure of the bar-epoxy interface of strips. In type I curve, the bond-slip behavior has an initial ascending branch and followed by a rather smooth softening branch after the peak point. In the ascending branch, the bond stress increases rapidly until it reaches a maximum value and follow an equation:

$$\tau(s)=\tau_m \left(\frac{s}{s_m}\right)^{\alpha}, \; 0 \leq s \leq s_m \tag{2-3}$$

where τ is the local bond stress, s is the local slip, τ_m and s_m are bond stress and slip at the peak point, and α is a parameter that varies between 0 and 1. After peak point, the bond stress decreases abruptly to a value that remains approximately constant or decreases afterwards, follow an equation:

$$\tau(s)=\tau_m \left(\frac{s}{s_m}\right)^{\alpha'}, \; s \geq s_m \tag{2-4}$$

where α' varies between -1 and 0. In the descending brand, the stress value decreases with the bond stress approaching zero for infinite values of slip. If α' is smaller than -1, this area becomes finite, and the joint may be predicted to be unable to develop the full tensile capacity of the bar [7]. In this case, a significant amount of post-peak friction develops because of the interfacial friction and the aggregate interlocking of the cracked concrete. Meanwhile, type II curve shows an abrupt decrease in bond stress upon the attainment of the peak value with respect to the cover splitting failure of ribbed and spirally wound bar [7]. However, after the complete loss of the cover, a low value of residual friction is maintained because half of the perimeter of the bar is still in contact with the epoxy.

2.4.4 Development length

The maximum stress that can be resisted by a bonded joint between an NSM bar and the concrete substrate with a sufficiently long bond length is given by [7]:

$$\sigma_{max} = \sqrt{2E\frac{\Sigma}{A}G_f} \tag{2-5}$$

with

$$G_f = \int_0^\infty \tau(s)d_s \tag{2-6}$$

where G_f, being the area underneath the bond–slip curve, is the fracture energy of the bonded joint, Σ is the perimeter over which the bond stress acts, A is the cross-sectional area over which the tensile stress acts, and E is the elastic modulus of the material on which the tensile stress is applied. In case of round bars bonded to epoxy, σ_{max} can be changed to:

$$\sigma_{max} = \sqrt{8\frac{E_b}{d_b}G_f} \tag{2-7}$$

where E_b is the elastic modulus of the bar. If σ_{max} computed by Eq. (2-5) is below the tensile strength of the reinforcement, its full capacity cannot be developed no matter how long the bond length is. In this case, a value of bond length exists and can be called "the effective bond length" that has been well established for externally bonded FRP laminates. However, in particular for bond–slip curves with infinite values of G_f, the full capacity of the reinforcement can be developed, and the corresponding value of bond length is usually termed "the development length" [7].
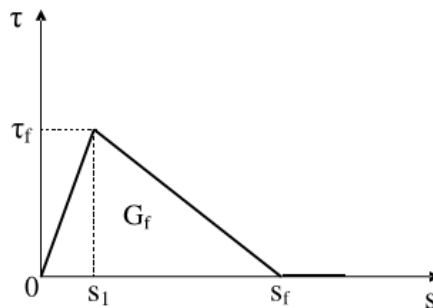
Figure 2.12 Idealized bilinear local bond–slip model of FRP laminates externally bonded to concrete [7].

Regarding to EBR method such as externally bonded laminates, a simplified local bond-slip model is shown in **Fig. 2.12**. The G_f value in this case is finite, and its value is usually insufficient for the reinforcement to develop its full tensile strength; hence no development length but an effective bond length can be computed. But in the case of NSM FRP reinforcement, the value of G_f is usually infinite, hence a development length generally exists. Besides, the shortest bond length required for an FRP bar to resist a given load is herein termed the anchorage length for that load. It depends on the load level and the anchorage length corresponding to the FRP bars rupture failure load is equal to the development length [7].

2.5 Previous researches on repairing and strengthening flexural RC structures based on the NSM FRP technique

The early researches using the NSM FRP system for strengthening flexural RC structures have been reported since more than two decades. Based on the results of in-place tests on RC bridge decks strengthened with NSM sandblasted CFRP rods, Alkhrdaji et al. [28] showed an increase in the moment capacity of 27% compared with the unstrengthen deck. Blaschko and Zilch [25] indicated that the bond characteristics of NSM CFRP strips are superior to externally bonded CFRP strips. On the other hand, based on experimental results, El-Hacha [19] observed that using NSM FRP reinforcements did not contribute to increasing the stiffness and strength in the elastic range of strengthened beams. In this research, beam strengthened with NSM CFRP bars showed a smaller increase in strength in comparison with the NSM CFRP strips (69% and 99% were measured in comparison with the control beam). The reason was due to early debonding of the CFRP reinforcing bars at failure and the smaller bonding surface of the NSM CFRP bars compared with NSM CFRP strips [19]. The author also concluded that the beam strengthened by NSM FRP system achieved higher ultimate load than beams strengthened by EB FRP reinforcement. In addition, an experiment was carried out by F. Ceroni [29] to compare the effectiveness between using the two techniques EBR CFRP laminate and NSM CFRP reinforcement. The results obtained from four-point test on beams showed a high load increase (46-72%) for the NSM system, greater than the beams strengthened with EBR CFRP laminates.

The global behavior of RC beams (300x150x280cm) strengthened by NSM technique was investigated to study the effects of concrete strength (30 and 60 MPa) and strengthening length (210 and 270 cm) in Firas Al-mahmoud et. al [30]. Some main aspects were pointed out from this research: if the CFRP rod is longer than the cracked span length of the beam at the ultimate stage, the failure is due to the pull-out of the rods including almost simultaneous splitting of the cracked concrete surrounding the groove; if the load causes some cracks which reach the end of the CFRP rod, the failure is due to the peeling-off of the concrete covering the groove from the end of the rod; the concrete strength does not influence the load-carrying capacity of the strengthened beam when the failure occurs by NSM system failure [30]. When the RC beam had a reinforcement ratio in the range of ρ_{min} to 0.4 ρ_{bal}, the NSM-FRP system was more efficient based on the experimental results of Shehab et al [31]. This study showed that the bonded length increased the ultimate carrying capacity up to a certain limit (in the range of 48 times the bar diameter of FRP bar).

As the bonded length increased beyond this limit, it would not result in any increase in the capacity.

The flexural response of RC beams strengthened by NSM FRP reinforcement of a limited bond length was carried out in an experimental research of I.A. Sharaky et al. [32]. Two types of FRP bars, carbon and glass, were used and the limited bond length of NSM FRP bars was 2.0 m. The beams had a rectangular cross section of 160x280 mm and 2.6 m total length. The number of NSM bars was also a variable to be evaluated in this study (**Fig. 2.13**). The results showed that increasing the number of NSM CFRP bars from one to two increased the yielding and the maximum loads by 25.6% and 7.5% respectively. Increasing the number of NSM GFRP bars increased the yielding and maximum loads by 11.7% and 13% respectively. The value of end slips for the beams strengthened with two NSM bars were slightly higher than those of the beam with one NSM bar, due to a lower confinement in the case of two NSM bars [32].
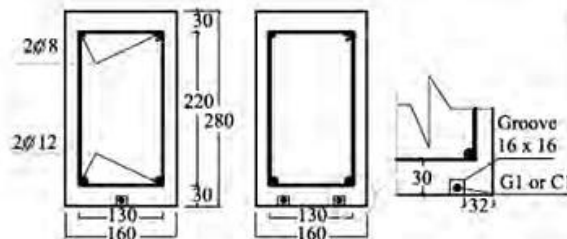
Figure 2.13 Detail of strengthened beams [32].

Most researches on NSM technique have focused on the strengthening of RC beams, while significantly less investigations have been performed on RC slabs. An experimental investigation on RC two-way slabs strengthened with NSM CFRP (**Fig. 2.14**) was conducted by Gilles Foret et al [33]. The RC slab with dimension of 7 cm x 115 cm x 165 cm was tested under static load and strengthened with 5 NSM CFRP rods per linear meter in both directions. The strengthened slab presented a more ductile behavior and its flexural strength was increased about 67% in comparison with the control RC slab.

Figure 2.14 NSM rods strengthening in research of Gilles Foret et al [33].

A common point among studies is that the specimens did not simulate exactly the real behavior of RC structures in actual environmental conditions, such as the structures exposed to corrosive environment or fire. In that case, the original members had been deteriorated by external impacts before the repairing method was applied. Therefore, laboratorial specimens should be prepared under a possible condition similar to that in practice. In regard to this purpose, an study was carried out to repair a corroded RC

beam with NSM CFRP rods by Amjad Kreit et al [34]. This experimental program included RC beams which were stored in a chloride environment during 23 years under service loading before testing. After exposure to chloride environment, the corrosion damage was observed with the completely splitting at each corner of the cross sectional areas. The concrete located far from the reinforcing bars was not significantly affected by the corrosion of the steel bars [34]. The authors assumed that the concrete was still of good quality and applied NSM CFRP rod in the middle of the cross-section in the tension area of the beams (**Fig. 2.15**). The groove was cut into the concrete cover in the longitudinal direction at the tension side of the beam. Then, it was half filled and the CFRP rod was then placed inside and lightly pressed. More filling material was applied to completely fill the groove and the surface was leveled. The beam was tested after one week to ensure the filling material strength.
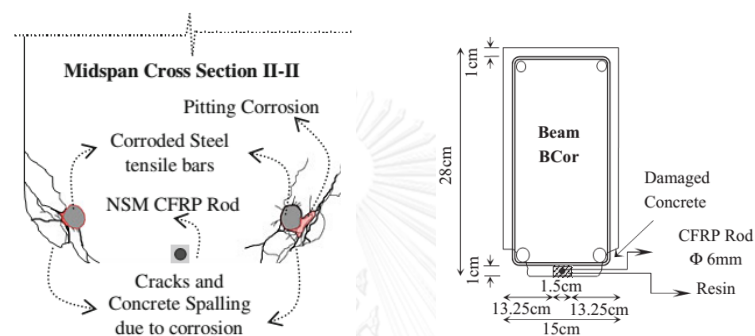
Figure 2.15 Location of NSM CFRP rod in the tension side of repaired corroded beam [34].

The experimental results showed that the ultimate moment of the strengthened beam was about 30% higher than the corroded beam. Despite the concrete in the corroded zone was damaged by corrosion, the NSM FRP repairing technique was efficient. However, the tension stiffness effect of the strengthened beam achieved a small increase (<10%), which was not the expectation of the authors. This was attributed to the small cross-section area of the CFRP rod (6 mm diameter) and the weak modulus of elasticity of the filling material.

Besides the strengthening for corroded structures, it is a challenge for engineers to rehabilitate or repair the RC structures after exposed to fire for a long period of time. A series of 16 under-reinforced high strength concrete one-way slabs were cast and heated at 600°C for 2h in a research of R.H. Haddad [2]. These heat damaged slabs were tested under four-point loading to investigate the coupling effect of water recurring and repairing with advance composite materials on increasing the flexural capacity. Carbon and glass FRP sheets were used to repair the heat damaged slabs after being recurred in water saturated burlap for 28 days. EBR method was chosen in this study. One layer of CFRP and GFRP sheets were applied at the tension side of heat damaged slabs, bonded to existing concrete along the entire span using a special epoxy. The stiffness of heat-damaged slabs after recurring was increased by 56% due to the significant regain in the modulus of elasticity [2]. Based on the results, the authors concluded that CFRP and GFRP regained up to 158 and 125% of the control slab's ultimate load capacity with a substantial increase in stiffness, first cracking loads, and a corresponding decrease in mid-span deflections at ultimate load.

For strengthening of fire damaged beams, Xiang Kai et al. [3] carried out an experiment with T-beams (5400x200x200 mm and flange 900x80 mm) that were exposed to fire at 1000°C. The specimens were separated into 2 groups, which were fired for 60 and 75 minutes respectively. After fire exposure, the fire damaged RC T-beams were strengthened with CFRP sheets following three steps [3]: firstly, serious fire damaged concrete should be removed before strengthening; secondly, epoxy bonding adhesive was used to retrofitting the strengthened surface of T-beams; thirdly, CFRP sheets were used to strengthening the fire-damaged T-beams. External strengthening with CFRP sheets was found to increase the yield and ultimate loads of fire-damaged T-beams. This technique also increased the stiffness of the fire-damaged specimens.

In case of EBR technique, the adhesive used to bond FRP and concrete substrate can be weakened by fire or aggressive chemical environments, thus affecting the quality of the repaired structure in long-term use. This can result in the debonding of FRP materials. In order to solve this problem, Do-Young Moon et al. proposed a strengthening technique for RC beams by using CFRP rods embedded in a mortar overlay whereby additional strengthening benefits are expected, such as crack-bridging effects; chemical and fire resistance [35]. To avoid the separation from the concrete substrate after flexural cracking, anchor bolts were used to confine the mortar to concrete and to transfer the tensile stress in the CFRP. The mortar overlay was applied with the thickness of 2.5 cm. Detail of this technique is shown in **Fig. 2.16**.
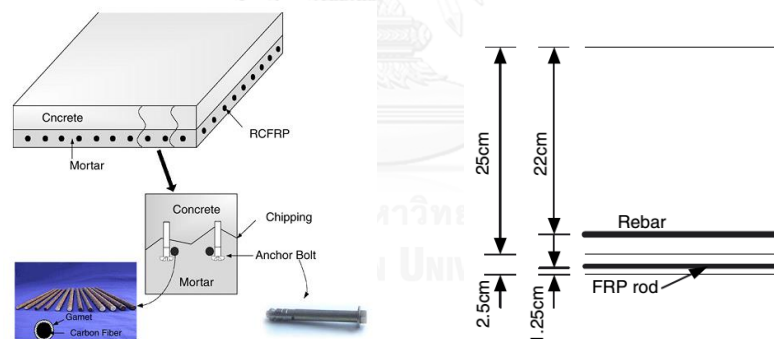
Figure 2.16 Strengthening detail of FRP rod in the research of Do-Young Moon et al [35].

The results in this paper indicated that the failure mode of the strengthened beams depended on the anchoring scheme. The separation of the mortar overlay was achieved only at the mid-point of the beam with respect to the beams which were anchored only in the end block. When the beams were anchored along the entire beam length, the mortar overlay did not fully separate from the bottom of the beam. The ultimate strength of the strengthened beams increased 40-50% under static load.

The NSM technique seems less influenced by external impact in comparison with the EBR technique because the FRP bar was installed inside concrete cover. However it always exists the possibility that the structure might be exposed to new destructive agents after repairing. In this case, the NSM system still can get debonding problem because of the concrete cover, even the new layer after repairing is deteriorated. In order to overcome this weak point, Aniello et al [36] applied a fire protection system

for RC beams strengthened with the NSM FRP system. The detail of the fire insulation system is shown in **Fig. 2.17**.
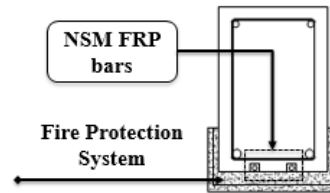
Figure 2.17 The fire protection system proposed by Aniello [36].

The fire protection systems investigated in that work were a calcium silicate protection board, and one insulation system composed by two ceramic based coatings. Tests results indicated that insulated NSM FRP strengthened beams could achieve a satisfactory fire endurance of one hour. Furthermore, the authors suggested that if insulation system is able to maintain the adhesive temperature at relatively low temperature, the FRP concrete bond degradation under fire is limited and the FRP strengthened beam is still able to retain part of the original strength [36]. However, it can be observed that using a fire protection system will change the aesthetic of building and it may take high cost if applies for big members.

Based on prior studies, it is clear to say that the NSM FRP method brings out a good effect to apply on flexural RC members. In order to supply more data and develop this technique in repairing fire-damaged RC structures, the present study aims to study a method based on the NSM FRP technique for retrofitting fire-damaged concrete slabs along with a combination with repairing material. The proposed method is expected to enhance the flexural capacity of heated slabs without changing the original size of the members and it might have the ability to protect the FRP system against the destructive agents that may act in long-term use.

2.6 Strengthening technique with partially bonded (PB) system

2.6.1 Background

FRP flexural strengthening methods include EBR and NSM systems have shown many advantages and become popular in studies as well as in practical application for the rehabilitation of RC structures. In both systems, the FRP is bonded to concrete using epoxy and a full bonded FRP strengthening has been carried out as conducted in many researches. This usage is to make sure the load capacity and stiffness improve and to avoid sudden premature failure due to debonding. As a result, the ultimate load carrying capacity of the strengthened structure is increased compared to the unstrengthened member. However, it can be observed that the ductility of strengthened structure dramatically decreased in comparison with unstrengthened situation. This lower ductility may lead to sudden failure without enough warning for strengthened members. Therefore, a balanced improvement between load carrying capacity and ductility should be assured in FRP strengthened flexural structures [37]. Nevertheless, although most of the studies have evaluated the influence of many different parameters but they still have focused on the increase of load carrying capacity alone.

In order to overcome this drawback for FRP strengthened members, some researchers developed a concept called partially bonded (PB) system and conducted experiments on RC beams. A partially-bonded FRP strengthening system is similar to the fully bonded system except that a portion of the FRP length is intentionally unbonded [38]. In this case the FRP is unbonded in the middle portion of the beam while the end portion still is bonded. This concept is described in **Fig. 2.18** for a sample of FRP partially bonded strengthened beam using EBR method. The test results on strengthened beams with partially bonded indicated improvement in ductility and reached load capacity with a slight decrease in comparison with fully bonded system [39-41].
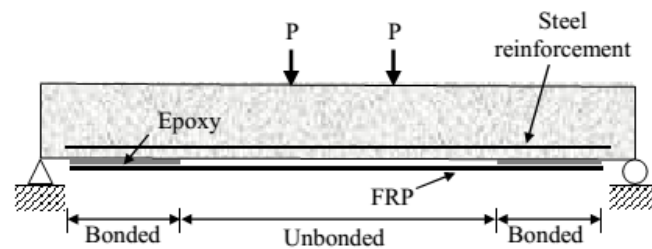
Figure 2.18 Partially bonded system [38].

2.6.2 Ductility and Deformability

For a safety design of concrete structures, a sufficient warning before failure should be considered in order to prevent sudden collapse and to provide enough time for evacuation. This problem could be achieved if an adequate deformation capacity of structure is provided. With regard to RC structures ductility is defined as the ability of the structural members to sustain large plastic deformation, and thus dissipate energy before failure [38]. For the flexural behavior of steel RC structure, a typical load – deflection diagram of RC beam is carried out in **Fig. 2.19a**. Based on this curve, the total energy (E_{tot}) including dissipated plastic energy and elastic energy (E_{el}) could be specified. When the beam fails the accumulated elastic energy in the system is dissipated. Before failure the RC beam has a large energy dissipation capacity because of large plastic deformation. Meanwhile, FRP reinforced beams shows lower energy dissipation prior to failure and a large elastic energy could be dissipated at failure (**Fig. 2.19b**). This may cause a sudden failure.

a) Steel reinforced beam   b) FRP reinforced beam
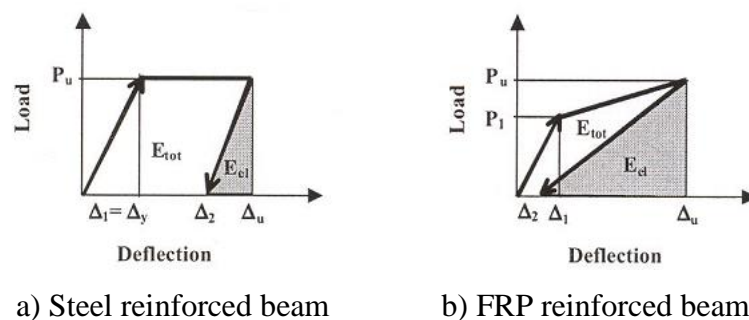
Figure 2.19 Typical load – deflection diagram for steel and FRP reinforced beam [38].

The value of ductility can be defined in a simple way by the equation:

$$\mu_{\Delta 1} = \frac{\Delta_u}{\Delta_y} \tag{2-8}$$

where Δ_u and Δ_y are the deflection at the ultimate load and the yielding point respectively.

On the other hand, plastic behavior is limited in FRP reinforced structures and FRP strengthened members because the FRP material does not yield. Therefore the term ductility is not really applicable in these cases, so a new term related to deformability has been developed to quantify deformation capacity [38]. This term was first used by Mufti et al. [42] and defined as the factor of the deflection at ultimate state to the deflection at serviceability limit state. In addition, deformability can be defined as the amount of deformation that occurs prior to failure, and so no plastic work is necessary [38]. Hence the basic equation to measure the deformability is shown by equation:

$$\mu_{\Delta 2} = \frac{\Delta_u}{\Delta_s} \tag{2-9}$$

where Δ_u and Δ_s are the deflection at the ultimate load and the service load respectively. For FRP strenghthened beams, a service load is defined as 67% of the ultimate load [43].

2.6.3 Flexural behavior of beam strengthened by partially bonded system

According to the analytical model proposed in [38], the flexural response of a RC structure strengthened with a partially bonded system could be interpreted through the strain profile at mid-span and the tensile stress distribution in FRP reinforcement for a simply supported beam subjected to mid-span loading (**Fig. 2.20**).
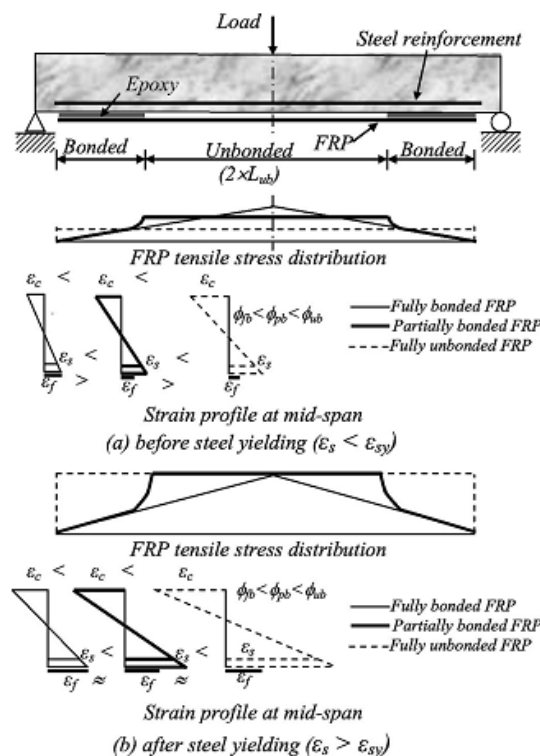
Figure 2.20 Flexural behavior of partially bonded beam [37].

Before the steel yielding, the maximum tensile stress in FRP reinforcement in case of a fully bonded system is higher than that of partially bonded system due to the unbonded part at mid-span. This also means that the stress in steel reinforcement and concrete with respect to the partially bonded case are higher than for the fully bonded situation. Nevertheless, at the post-yielding stage the stress in steel reinforcement does not increase, so the stress in the FRP will increase. As a result, the tensile stress in the FRP for the case of partially bonded system increases and it is almost equal to that of the fully bonded system. At this stage, the stress in FRP is uniform within the unbonded part and the curvature of beam increases significantly to satisfy the strain compatibility at the mid-span. This leads to the increase of rotation capacity and deflection of the beam.

2.6.4 Previous experimental study

There are not many studies aimed to evaluate the increase of deformability for flexural RC structures using partially bonded FRP system. Lees and Burgoyne [39]carried out a research to investigate the behavior of partially bonded prestressed AFRP concrete beams. The results from this study indicated an increase of deformability when a partially bonded system is applied. Another study of Chahrour and Soudki [44] used a partially bonded CFRP plate with mechanical anchors to strengthen RC beams. Based on the experimental results, it could be observed that the proposed system with end-anchored partially bonded CFRP showed an enhancement in load carrying capacity and deformability compared to the no end-anchor fully bonded system. Choi et al. [40] conducted an experiment to strengthen concrete T-beams using NSM CFRP bars. In this study, both of fully bonded and partially bonded systems were applied for a comparison in flexural behavior of the beams. Four strengthened beams with different unbonded lengths were tested in order to study the effect of partially bonded system. To create the unbonded region, these authors installed a thin plastic-tube at the mid-span of the beam as shown in **Fig. 2.21**.
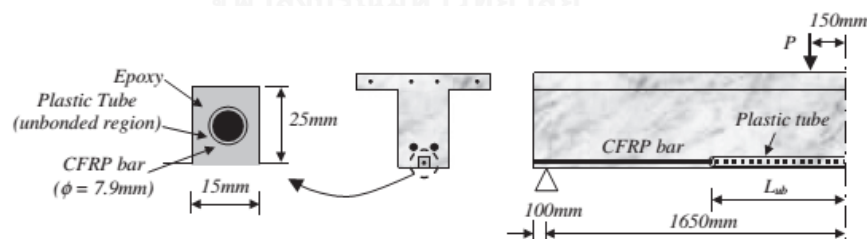
Figure 2.21 Details of partially unbonded system in the research of Choi [40].

According to this study, the stiffness of the partially bonded strengthened beams decreased as the unbonded length increased at the post-yielding stage. Therefore, the deformability of the specimens was increased at any applied load after the yielding point. In comparison with the fully bonded beam, the ultimate deflection in partially bonded systems was slightly increased, while the ultimate load carrying capacity slightly decreased. I.A. Sharaky et al. [41] showed out the results of the series of RC beams under four points bending test in order to investigate the flexural response of partially bonded system. The data from these specimens were compared to the fully bonded beam and both of systems were applied based on NSM method. However, the strengthening detail for partially bonded system was different from the technique of

Choi for creating the unbonded length of FRP bars. In this experiment, the beams strengthened with partially bonded FRP reinforcements had no bond in the constant moment region and the bond started from the point beneath the load into each shear span [41]. The details of this design are shown in **Fig. 2.22**.
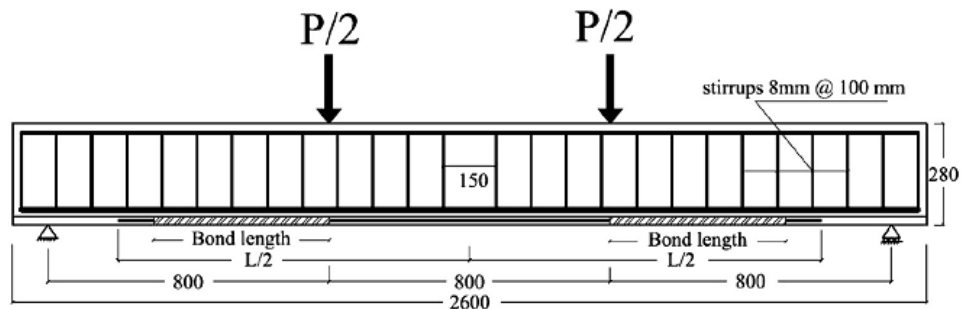
Figure 2.22 The detail of partially bonded system in the test of Sharaky et al. [41].

Two different partially bonded lengths (384mm and 480mm) were examined and compared with the fully bonded length. According to the results, fully bonded beams showed higher stiffness and bearing capacity than the partially bonded beams. However, a slight effect of bond length on deflection was observed in the partially bonded specimens. There was no increase in the yield load between specimens with two different bonded lengths. But a significant increase was measured when the bonded length increased from 480mm to 1000mm (fully bonded length). In addition, the stiffness of partially bonded beams with no bonding in the constant moment region was the same.

The prior studies have shown the possibility of partially-bonded FRP bars system in order to enhance the deformability for concrete structures. In this study, this technique was applied to evaluate the enhancement of deformability for strengthened slabs through of numerical simulation on developing models.

Chapter 3

EXPERIMENTAL PROGRAM

3.1 Bond test

To investigate the bond behavior between NSM CFRP rods and surrounding substrate with different rod locations, a bond test of C-shaped concrete block with a square groove in the middle for embedment of NSM rod was carried out. The dimensions of tests were designed based on some previous researches [4, 5, 7, 45] as shown in **Fig. 3.1**. Three different positions of NSM CFRP rods are shown in **Fig. 3.2** and summarized in **Table 3.1**: Group A – inside concrete; Group B – between concrete and repairing material overlay; Group C – inside repairing material overlay.
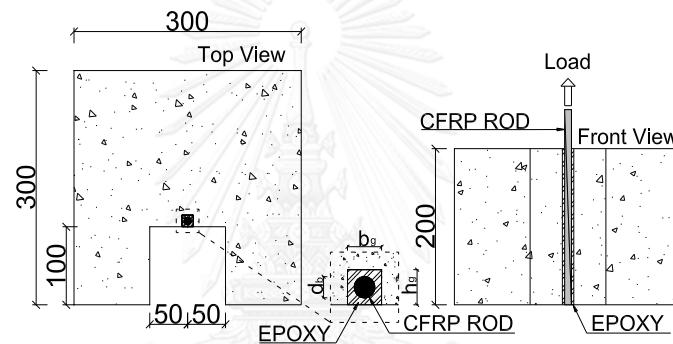
Note: d_b-diameter of FRP bar (9 mm); b_g-groove width; h_g-groove high.

Figure 3.1 Dimensions of C-shaped Specimens.
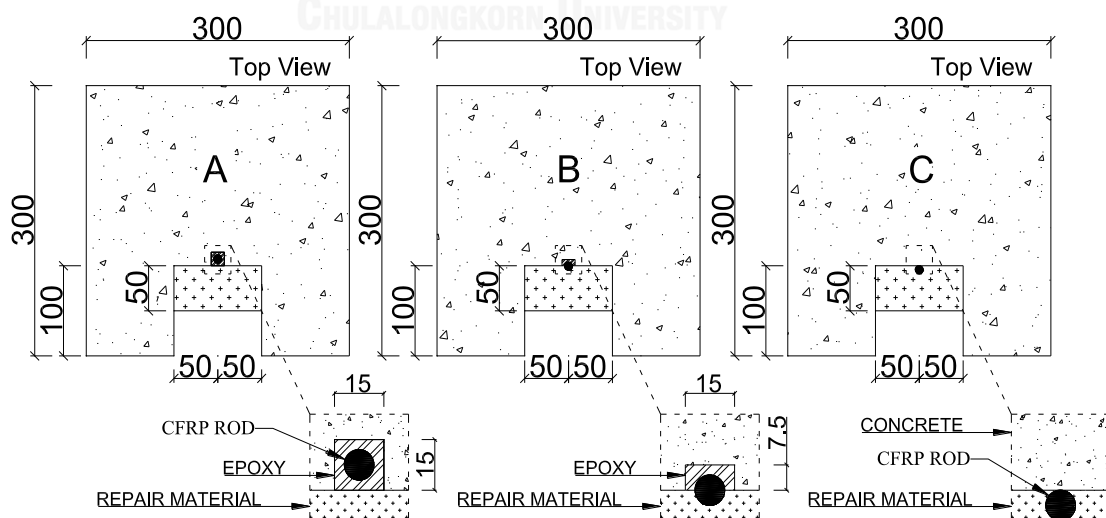
Figure 3.2 Different locations of CFRP rods in C-shaped specimens.

The concrete blocks were cast using ready mixed concrete with concrete grade of 35 MPa and the specimens were not fired. After 28 days of curing, the groove was first cut into the concrete block and NSM CFRP rods were applied therein. Epoxy paste SIKADUR®-30 was used as a groove-filling material. The dimension of grooves was 15x15 mm in case of specimens A and 15x7.5 mm for specimens B. On the contrary, grooves and epoxy were not used in case of specimens C. After the FRP rod had been placed in the groove with the surrounding epoxy for bonding to surrounding concrete, a thin layer of resin SIKADUR®-32TH was brushed on the concrete surface where the repairing material would be applied. This resin was used for improving the bond between concrete and repairing material. Then a layer of repairing material SIKA®MONOTOP®-614T was covered above with 5 cm depth. This was also the depth of fire-damaged concrete layer that had been observed in slabs after fire. The details of the six specimens with three different NSM FRP rod positions and variable groove sizes are indicated in **Table 3.1**.

Table 3.1 Bond tests program.

Group	Specimen Code	Rod Type	d_b (mm)	Groove filling material	b_g (mm)	h_g (mm)	Concrete grade (MPa)
A	C-1	CFRP	9	Epoxy	15	15	35
	C-2	CFRP	9	Epoxy	15	15	35
B	C-3	CFRP	9	Epoxy	15	7.5	35
	C-4	CFRP	9	Epoxy	15	7.5	35
C	C-5	CFRP	9	-	-	-	35
	C-6	CFRP	9	-	-	-	35

Besides, four strain gauges were glued onto the surface of every CFRP rod (**Fig. 3.3** and **Fig. 3.4**) to measure the axial strains. All of the specimens had been cured at temperature room before they were tested. The load was applied to the loaded end of the CFRP rod by a testing machine with a capacity of 500 kN, under displacement control at a rate of 1 mm/min. One LVDT was used to measure the free end slip. The applied tensile load and load end slip were measured from the test machine.
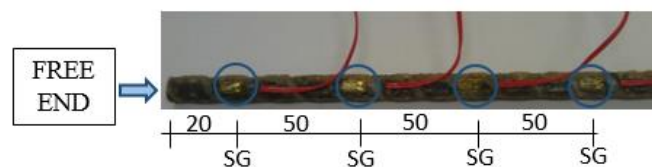
Figure 3.3 Position of strain gauges (SG) on the CFRP rod.

Figure 3.4 CFRP rod and epoxy applied in the groove.

3.2 Flexural test

This test was performed to investigate the bending behavior of fire-damaged RC slabs repaired and strengthened with repairing material and NSM CFRP rods. The experimental process is represented in **Fig. 3.5** through six main steps.
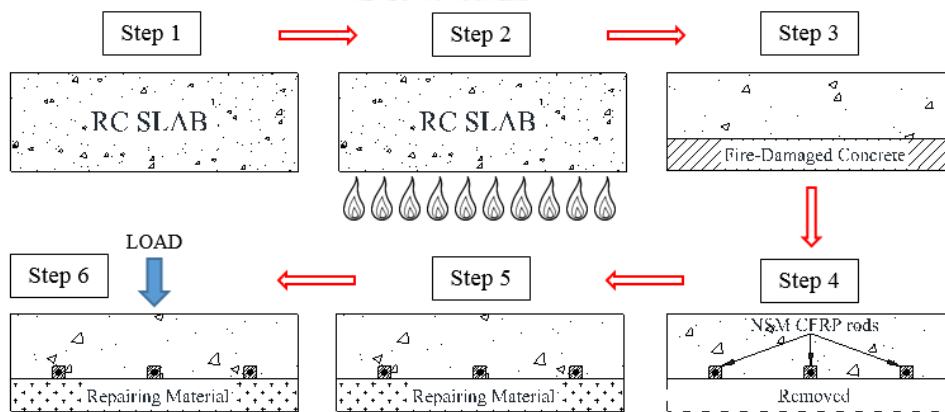
Figure 3.5 The process of flexural test.

3.2.1 Step 1: casting of RC slabs

Eight RC slabs were designed under standard ACI 318-08 [46] and cast in the laboratory. Every slab had the same design as described in **Fig. 3.6**. The slabs had the dimension of 1000x900x150 mm and were reinforced longitudinally in flexure with 10 mm diameter steel bars. The concrete cover had a depth of 20 mm. The slabs were divided into two series with concrete strength of 24 and 35 MPa. They were cured for 28 days before conducting the fire test. Two slabs (SC1 and SC2) were used as control specimens without firing or strengthening. The other six slabs (SF1-SF6) were subjected to fire.

Steel bar - 4 ϕ10mm @ 180mm

150

Steel bar - 3 ϕ10mm @ 270mm

A-A

1000

110

20   20

B-B

B

230

1000

230

1000

230

1000

A   A

230

B

900
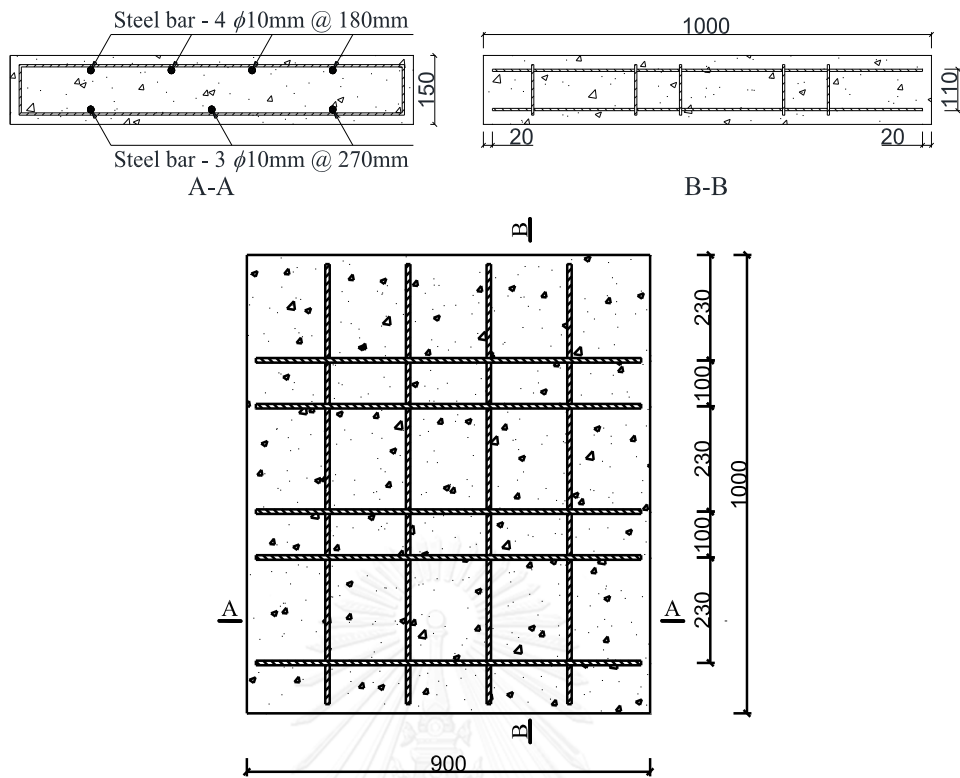
Figure 3.6 Design of the RC slabs.

3.2.2 Step 2: fire test

The installation and testing of fire exposure were operated under ASTM E119 standard [47]. The slabs were fired for 1 hour and 30 minutes to reach the peak point of temperature curve about 1000°C. The specimens were exposed to fire on one side reinforced longitudinally by three steel bars. The fire test was carried out by using a furnace as shown in **Fig. 3.7**.

SLAB   SLAB   SLAB

FURNACE
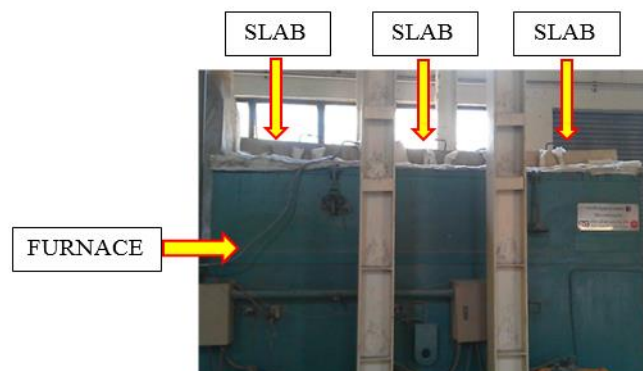
Figure 3.7 Fire test.

3.2.3 Step 3: removing the fire-damaged concrete layer

After fire, a fire-damaged concrete layer in every slab was observed on the side directly exposed to fire (**Fig. 3.8**). The depth of the weakened concrete layer was defined based on the results from a previous research carried out by Daungwilailuk [48]. The conditions and installation of the fire test in that research were similar to the test in this study. A semi-destructive test or core test was carried out by drilling the fire-damaged slabs to collect the cores having a diameter of 50 mm. The depth of the weakened concrete layer was assessed by color change as well as pull-off tests on different depths. Based on it, a degraded concrete layer of 50 mm was removed on the fire-damaged slabs in this experimental study, to arrive at the sound material.

Figure 3.8 The slab after exposure to fire.

A hammer machine was used to remove this weakened layer. To make the work easier, a concrete saw was used to cut lines on the slab surface and then the degraded concrete could be chiseled out by a hammer machine (**Fig. 3.9**). In this study, a pull-off test was also carried out to determine the tensile strength of concrete on the surface that was exposed to fire based on standard ASTM C1583-04 [49] (**Fig. 3.10**). This test can be used as an indicator of the adequacy of the surface preparation before applying a repairing material. The correlation between the pull-off load and concrete tensile strength makes it possible to have sufficient information on concrete strength for the application of mortar and protective coating [9]. The values of pull-off test are shown in **Table 3.2**. These values were collected at the depth of 0 mm and 50 mm from the surface.

a) Cutting lines on surface of slab   b) The surface after removing weakened layer
Figure 3.9 Removing damaged concrete layer.

Figure 3.10 The pull-off test.

Table 3.2 Values from pull-off tests.

Slab	Control slab		Fire-damaged slab					
	SC1	SC2	SF1	SF2	SF3	SF4	SF5	SF6
Concrete grade (MPa)	24	35	24	24	24	35	35	35
Depth (mm)	0		50					
Load (kN) – First Time	4.35	7.10	0.70	4.50	2.10	1.00	1.60	3.50
Load (kN) – Second Time	5.80	7.30	-	0.25	1.80	1.90	1.60	2.70
Load (kN) – Third Time	4.90	6.50	0.75	0.50	1.50	0.90	1.00	1.65
Average Load (kN)	5.02	6.97	0.73	1.75	1.80	1.27	1.40	2.62
Average Stress (MPa)	2.55	3.55	0.37	0.88	0.90	0.62	0.70	1.35

3.2.4 Step 4: installing the NSM CFRP rods

After the fire test, except for the slab SF1, which was not repaired, the remaining specimens (SF2-SF6) were strengthened by NSM CFRP rods and repairing material. After the weakened layer had been removed, a concrete saw was used to cut the grooves in the new surface along the slab (**Fig. 3.11**). The concrete surface was smoothed by a grinder machine and cleaned by a blower machine. Subsequently, epoxy was installed into the grooves for bonding the rods to the surrounding concrete by using a small trowel (**Fig. 3.12a**). Then the CFRP rod was installed into the groove filled with epoxy (**Fig. 3.12b**). Finally, a repairing material overlay was applied above. Details of the different slab specimens are given in **Table 3.3** and **Fig. 3.13** and are described below:

- Slab SF2 (concrete grade of 24 MPa): 6 grooves of 15x15 mm were first cut inside the concrete part. Then, epoxy and CFRP rods were installed into the grooves. The distribution of NSM rods is indicated in **Fig. 3.13**. The distance between the longitudinal steel bar and the NSM rod was 20 mm.

- Slab SF3 (concrete grade of 24 MPa): Similarly to slab SF2, 6 grooves of 15x15 mm were first cut inside the concrete part, which were filled with epoxy and NSM rods, but their distribution was different from slab SF2. The distance between the longitudinal steel reinforcement and the NSM rod was 100 mm, except for the extreme rods in which was 50 mm. In this case, the dimension of groove also was 15x15 mm and CFRP rod in full depth of groove.

- Slab SF4 (concrete grade of 35 MPa): the design, distributions and dimensions were similar to SF3.

- Slab SF5 (concrete grade of 35 MPa): in this case the reinforcement was placed in the repairing material. The 6 CFRP rods were installed onto the surface of the concrete and located at the same position on the horizontal axis as for slabs SF3 and SF4.

- Slab SF6 (concrete grade of 35 MPa): 6 grooves of 15x7.5 mm were first cut into the concrete part and epoxy was used to fill the grooves. Only the half of every CFRP rod was installed inside the groove. The other half was covered by repairing material instead of epoxy (**Fig. 3.13**).

a) Sawing
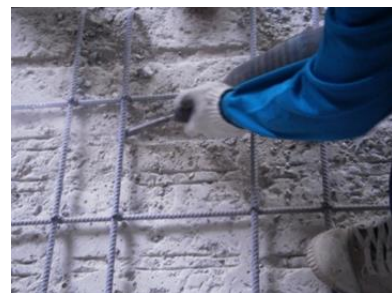
b) Removing concrete from the groove

c) Smoothing the surface

d) Final groove aspect

Figure 3.11 Cutting grooves into concrete.

a) Installing epoxy into the groov

b) Installing CFRP rod into the groove filled with epoxy

Figure 3.12 Installing CFRP rods into concrete.
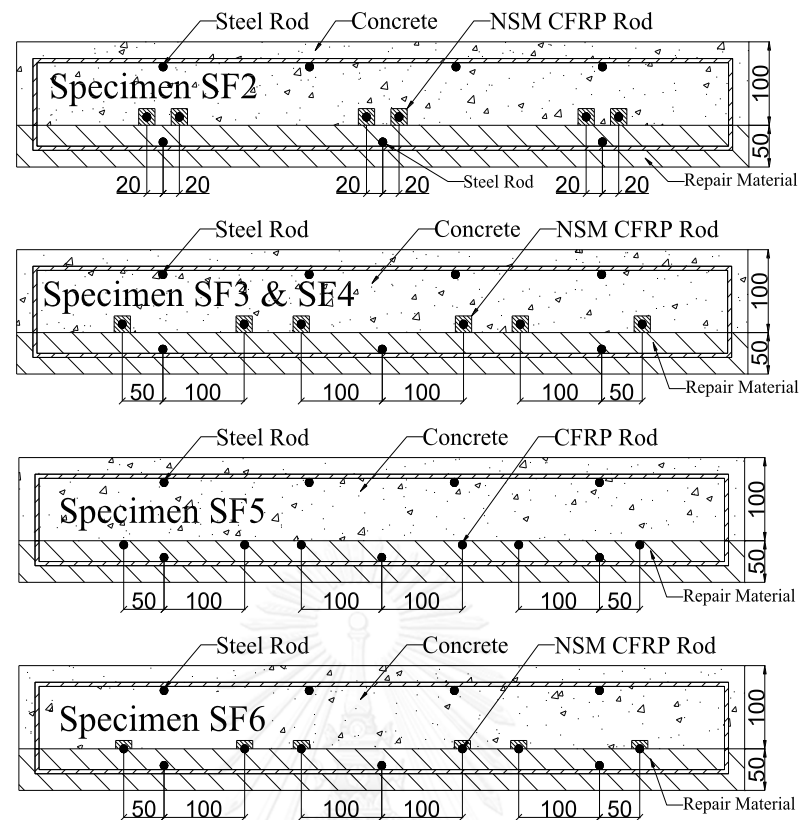
Figure 3.13 The design of fire-damaged reinforced concrete slabs strengthening with NSM CFRP rods.

Table 3.3 Details of slabs.

Slab code	Concrete Strength (MPa)	Dimension of groove (mm)	Note		Depth of repairing material (mm)
SC1	24	-	-	Unfired	-
SC2	35	-	-	Unfired	-
SF1	24	-	-	Fired-Unrepaired	-
SF2	24	15x15	NSM rod in full depth groove	Fired-Repaired	50
SF3	24	15x15	NSM rod in full depth groove	Fired-Repaired	50
SF4	35	15x15	NSM rod in full depth groove	Fired-Repaired	50
SF5	35	-	No groove and filling material.	Fired-Repaired	50
SF6	35	15x7.5	NSM rod in a half depth groove	Fired-Repaired	50

3.2.5 Step 5: installing the repairing material

In the last step of the procedure, repairing material was applied to replace the weakened concrete layer that had been removed in step 3. A steel frame was fixed around the slab as a mold to cast the repairing material layer (**Fig. 3.14**). Before the installation of repairing material, a resin was applied directly to the concrete substrate to improve bond between concrete and repairing material. Finally, the repairing material was poured on to get the thick of 50 mm and subsequently the surface was smoothed (**Fig. 3.15** and **Fig. 3.16**).

Figure 3.14 Installing steel frame around the slab to cast repairing material.

Figure 3.15 Installing the repairing material.

Figure 3.16 The slab after repairing.

3.2.6 Step 6: Flexural test

All the specimens were cured at room temperature for 28 days before the bending test. The simply supported slabs with a clear span of 800 mm were tested under three-point bending test to determine the load-deflection curves. The applied load was controlled by a hand-operated hydraulic jack with full capacity of 500 kN under a loading rate 7 kN/min and was monitored by the load cell. A LVDT was placed at the middle point on the top of the slab and two other LVDTs were placed at 1/4 point of the span to

obtain the deflection profiles. Strain gauges were bonded to the CFRP rods to measure the strain profiles. **Fig. 3.17** shows details of the setup of strain gauges on CFRP rods in strengthened slabs. In every slab, a total of nine strain gauges were bonded on three CFRP rods (three strain gauges on each). They were installed along half of the bond length of the CFRP rods in a half of the slab.
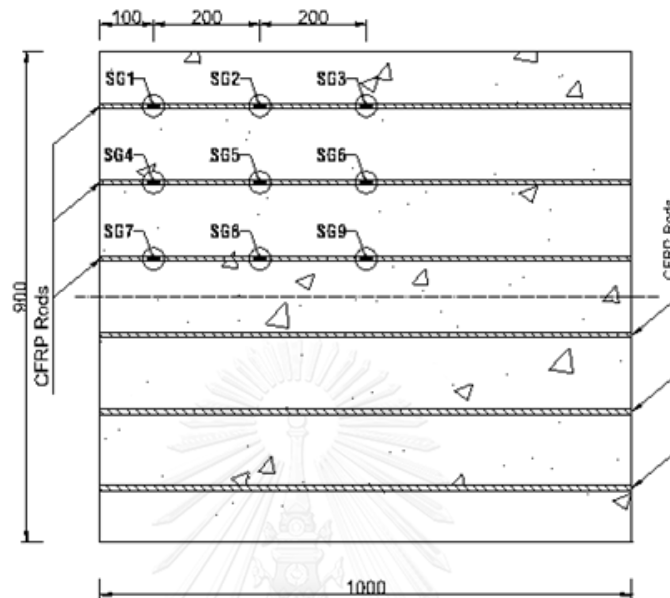
Figure 3.17 Position of strain gauges (SG) on CFRP rods in slab.

3.3 Material properties

The slabs were cast by using ready mixed concrete with two concrete grades of 24 and 35 MPa. The compressive strengths obtained from the tests performed on standard cylinders (150x300mm) were 24.5 and 35.4 MPa. Epoxy paste SIKADUR®-30 was used for the embedment of the NSM CFRP rods, which had a compressive strength and tensile strength of 85 MPa and 26 MPa, respectively, at curing temperature of 35°C after seven days. It had compressive and tensile E-modulus of 9600 and 11200 MPa. SIKADUR®-32TH was used as a resin for bonding of repairing material to concrete substrate. Its compressive and tensile strengths were 60 and 18 MPa, while the bond strength to concrete reached 2.5 MPa. The type of repairing material was SIKA®MONOTOP®-614T, which had a compressive strength of 60 MPa at a curing time of sixty days and a bond strength of 2.0 MPa to concrete. These parameters were provided by the supplier. A spirally-wound CFRP rod was used and its properties were determined on direct pull-out test, including tensile strength of 2220 MPa and E-modulus of 133 GPa. The length of the CFRP rod was 1000 mm, while the diameter was 9 mm.

Chapter 4

TEST RESULTS AND DISCUSSION

4.1 Bond test

4.1.1 Failure pattern

The types of failure are reported in **Table 4.1**. The pull-out failure at the interface between CFRP rod and epoxy or repairing material was the critical mechanism in all cases. A very thin layer of epoxy was observed along the bonded length of the rod. This indicates that the interface failure occurred due to cohesive shear failure in the epoxy. It may be similar to the observations were reported by Sharaky, Torres [50], and Galati and De Lorenzis [51]. As for specimens of groups B and C, a very thin layer of repairing material was also observed on the rod, which could be caused by cohesive shear failure in the repairing material. Since the CFRP rod and groove were covered by repairing material, it was not possible to observe the failure in the substrate adjacent to the groove during the test. No visible cracks were observed on the surface of repairing material and the concrete block. At the loaded end of specimens C3, C4, C5 and C6, a layer of repairing material in the form of cone-shaped crack has been still attached on the surface of the rods (**Fig. 4.1**). This was not observed for specimens C1 and C2.

Table 4.1 The results of bond tests.

Group	Specimen Code	Maximum Load P_{max} (kN)	Average bond stress (MPa)	Average slip at P_{max} (mm)	Failure mode
A	C-1	16.1	2.843	4.31	Pull-out (rod-epoxy)
	C-2	15.2	2.691	4.46	Pull-out (rod-epoxy)
B	C-3	13.4	2.363	4.29	Pull-out (rod-epoxy and repairing material)
	C-4	16.7	2.955	5.78	Pull-out (rod-epoxy and repairing material)
C	C-5	39.1	6.917	4.92	Pull-out (rod-repairing material)
	C-6	43.4	7.669	4.99	Pull-out (rod-repairing material)
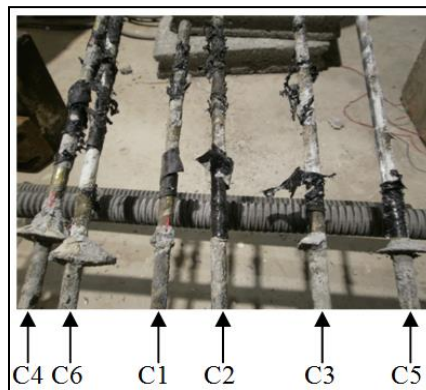
Figure 4.1 CFRP rods after testing.

4.1.2 The maximum load

Fig. 4.2 shows that the ultimate load of specimens having grooves was different negligible (13 – 16 kN). On the contrary, the ultimate load for specimens without grooves (C5, C6) was around three times higher than the others. Based on these results and the observed failure patterns, it seems that the location of CFRP rod significantly affected the load capacity and that the repairing material supplied higher bond strength than the epoxy. This effect is also discussed in the section of bond behavior below.
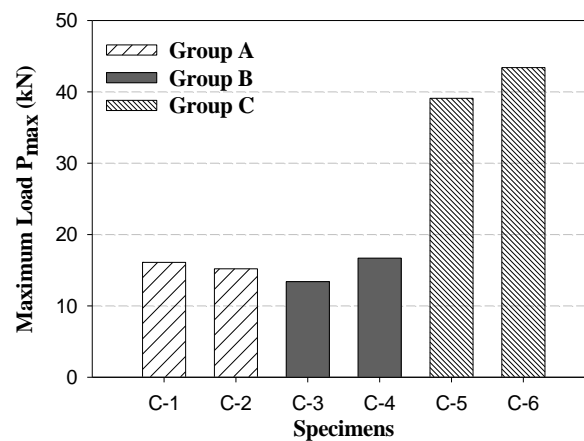
Figure 4.2 Maximum load values of C-shaped specimens.

4.1.3 The tensile strain distribution along CFRP rod

The tensile strain distributions along the CFRP rods are reported in **Fig. 4.3** for all specimens. The values on horizontal axis starts from the free-end to loaded end along the bonded length of the rod and each curve correspond to a specific load level. At the lower load levels, the strains decreased toward the free end with a distribution that, in general, tended to be nonlinear. As the load increased, the strain distribution could be approximated by a linear distribution along the bonded length with the highest value

obtained at the position near load end. This is similar to previously reported on C-shaped pull-out test [27, 52, 53]. This result indicates that the bond stresses between CFRP rod and epoxy redistributed along the bonded length as the load increased. The values of strain from specimens in group C were higher than other groups due to their high load capacity.
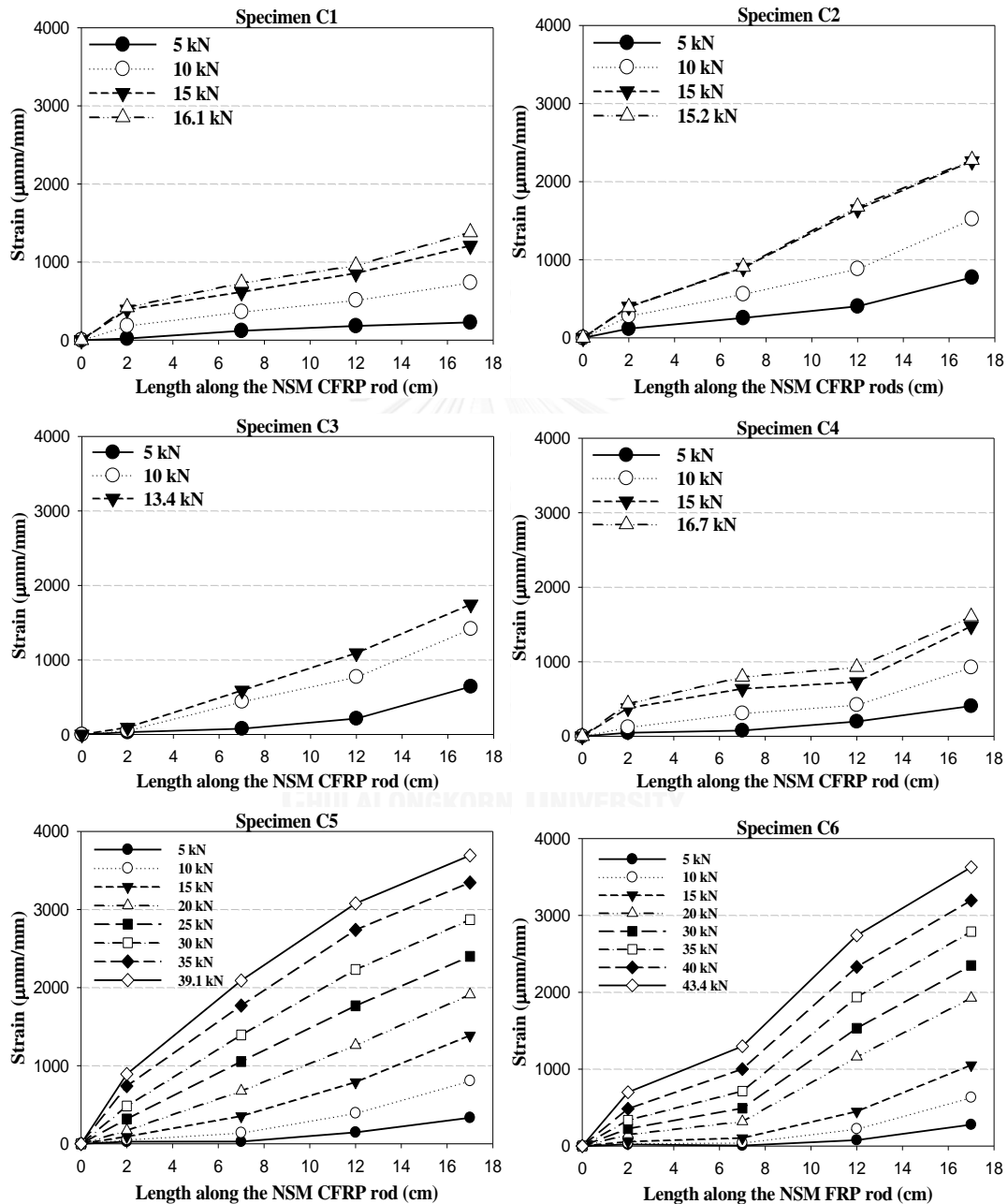
Figure 4.3 Tensile strain distribution along the length of CFRP rods.

4.1.4 Bond stress-slip relationship

Based on the well-known Bertero-Popov-Eligehausen (BPE) relationship (Eligehausen, Popov [54]) for bond of steel reinforcement in concrete, the bond-slip curve for pull-out test of CFRP rod has been adopted from the equations of ascending branch and descending branch [4]:

$$\tau(s) = \tau_m \left(\frac{s}{s_m}\right)^{\alpha}, 0 \leq S \leq S_m \tag{4-1}$$

$$\tau(s) = \tau_m \left(\frac{s}{s_m}\right)^{\alpha'} \tag{4-2}$$

where τ is the local bond stress, s is the local slip, τ_m is maximum bond stress and s_m is correspondingly maximum slip. Parameter α and α' were calibrated by best fitting of the experimental results. The value of α can be obtained by equating the area underneath the ascending branch of the experimental curve to the value [4]:

$$A_\tau(0, S_m) = \int_0^{S_m} \tau_m \left(\frac{s}{s_m}\right)^{\alpha} ds = \frac{\tau_m s_m}{1+\alpha} \tag{4-3}$$

As visible in **Fig. 4.4**, the bond-slip behavior of all specimens has an initial ascending branch until the maximum value, followed by a rather smooth softening branch toward an asymptotic value of bond stress due to the residual friction.
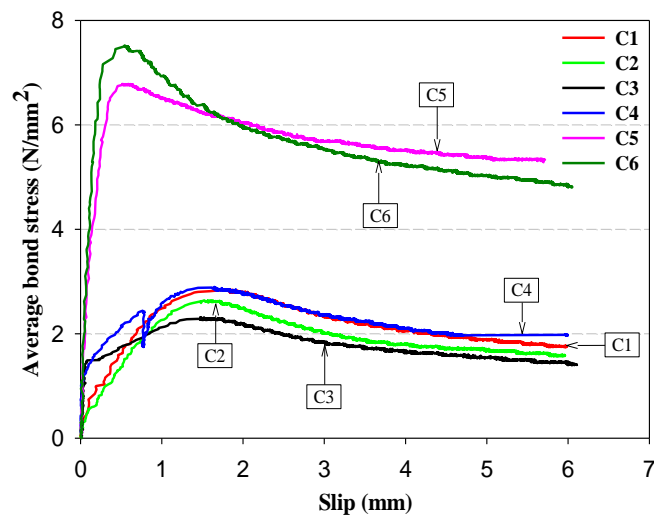
Figure 4.4 Experimental bond-slip curve.

The curves of specimens in groups A (C1, C2 - NSM in full depth groove) and B (C3, C4 - NSM in a half depth groove) are not much different, and their highest bond strengths were below 3 N/mm². However, the ascending branch of specimens C3 and C4 have a higher slope at the initial load levels in comparison with those of specimens C1 and C2. Group C (C5, C6 – CFRP rod in repairing material) reached maximum bond strengths of more than 6 N/mm², about three times higher than the other specimens, with higher slope in the initial branch. Based on the observation of failure patterns and the bond stress – slip curves, it could be concluded that the location of CFRP rod was a main parameter affecting the bond performance of the NSM systems

that were used in this study. Appearance of repairing material in this case affected the bond stress on NSM rod and lead to higher bond performance than the epoxy resin.

In case of group B, with half of rod embedded in repairing material, a higher slope in the bond-slip response could be observed in comparison with group A (the rod in full depth groove with surrounding epoxy). Therefore, at lower slips, the higher bond force could help the rod of specimens in group B to prevent the pull-out load, or delay the slip for similar loads. The initial slope of group B was similar to that of group C, however it showed a change for a value around 1.5 N/mm^2 to follow a trend similar to specimens of group A. As a result, group B could not get a so high bond stress as group C. Based on previous researches. In this study the dimensions of square groove were selected to have a width-to-diameter ratio of approximately 1.7. De Lorenzis and Teng [7] reported a minimum value of 1.5 for lightly sand-blasted bars, which was enough to prevent splitting failure of the epoxy cover [52]. Based on it, the groove dimension were not likely to affect the observed results.

4.1.5 Development length

The fracture energy of the bonded joint can be obtained from the curves in **Fig. 4.4** by equating the area underneath the bond-slip curve. In case of FRP reinforcing rods, this value is usually infinite due to an unlimited post-peak friction branch as can be observed in the figure, hence a development length always exists [7]. Herein, the value of development length will be compared in each case. First, the equilibrium equation of tensile force on rod is used:

$$\pi \frac{d_b^2}{4} d\sigma = \pi d_b \tau dx \tag{4-4}$$

$$\sigma = E \frac{ds}{dx} \tag{4-5}$$

where σ is tensile stress in rod and E is the elastic modulus of the rod. From Eqs. (4-4) and (4-5), the limit tensile stress in the rod σ_1 that can be achieved corresponds to a slip equal to s_m and to an average bond stress τ_m, according to the following equation [55]:

$$\sigma_1 = \sigma(S_m) = \sqrt{\frac{8E\tau_m S_m}{d_b(1+\alpha)}} \tag{4-6}$$

Furthermore, the development length l_m can be calculated from Eqs. (4-4), (4-5) and (4-6):

$$l_m \pi \tau_m d_b = \pi \frac{d_b^2}{4} \sigma(S_m) \Rightarrow l_m = \sqrt{\frac{E d_b S_m}{2\tau_m(1+\alpha)}} \tag{4-7}$$

The values of development length are reported in **Table 5** for each specimen. According to these values, a minimum embedment length needed for NSM CFRP rod to prevent the failure at epoxy-rod interface in case of C5 and C6 (CFRP rod was embedded inside repairing material) was approximately 18.50 mm. Meanwhile, this value with respect to C1, C2 (CFRP rod was embedded inside concrete) and C3, C4 (CFRP rod was embedded between concrete and repairing material) should be at least 3 times higher than the case of C5, C6. Besides, the relationship of the tensile stress in

the rod σ versus the dimensionless development length l/d_b was also predicted as show in **Fig. 4.5** by equation [55]:

$$l = l_m \left(\frac{\sigma}{\sigma_1}\right)^{\frac{1-\alpha}{1+\alpha}}$$

(4-8)

Table 4.2 Calibrated parameters in the bond-slip relationships and values of l_m.

Specimen Code	τ_m (N/mm^2)	s_m (mm)	A_τ (N/mm)	α	α'	l_m (mm)
C-1	2.837	1.763	3.641	0.374	-0.40	52.03
C-2	2.638	1.520	2.637	0.520	-0.38	47.62
C-3	2.317	1.474	2.755	0.240	-0.35	50.82
C-4	2.897	1.648	3.792	0.259	-0.35	45.45
C-5	6.784	0.513	2.526	0.378	-0.10	18.12
C-6	7.521	0.544	3.209	0.275	-0.18	18.43

The curves in **Fig. 4.5** have been derived by equating the development length for each value of the stress. In case of installing CFRP rod inside repairing material without groove and epoxy, the embedment length is always shorter than other cases. For example, if the tensile stress on the rod can reach 2000 N/mm^2 then the embedment length in this case only needs approximately 24 times the diameter of the rod. However, the embedment length ranging from 87 to 101 times the rod diameter with respect to two remaining cases.
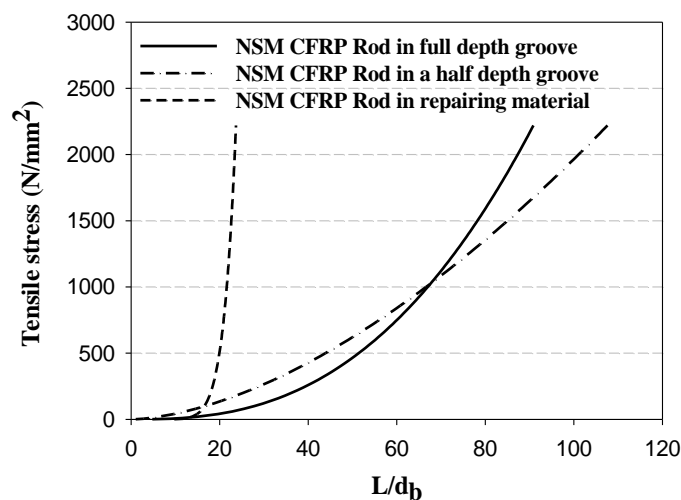
Figure 4.5 Stress σ versus the dimensionless development length l/d_m.

4.2 Flexural test

4.2.1 Failure pattern

The crack patterns of each specimen are depicted in **Fig. 4.6**. For the two control slabs (SC1 and SC2) the failure patterns corresponded to typical bending cracks located in the maximum moment zone. This type of failure can be observed in normal flexural RC members. In case of SF1, slab after fire without strengthening by CFRP rods, the observed bending cracks were also similar to the failure pattern of SC1 and SC2. However, the cracks appeared earlier due to the loss of load capacity of the slab after fire. The initial cracks were observed at the load of 60 kN on slab SF1 while the cracks started at 80 kN on slabs SC1 and SC2.
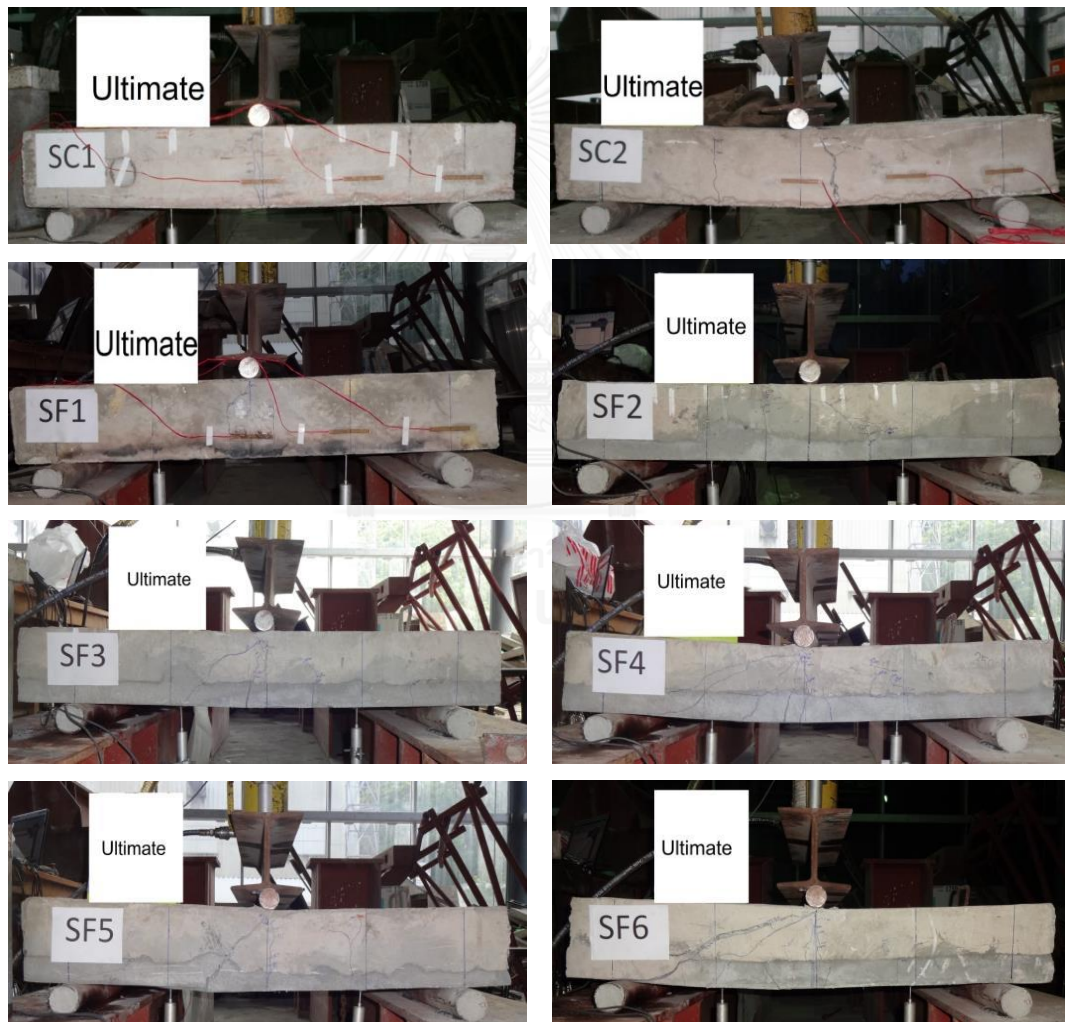
Figure 4.6 Failure modes of slabs after testting.

All slabs repaired with CFRP rods and repairing material cracked at an early stage of 60 kN and initial flexural cracks started on the side of repairing material at the highest moment zone. As the load increased, major bending cracks propagated towards the compression side and the crack width increased until failure occured. At higher load levels, inclined shear cracks appeared towards the load point. The cracks propagated in the slabs without any change in their angle at the intermediate layer. This indicated that a good bond between concrete and repairing material was obtained in all repaired slabs.

4.2.2 Load-defection relationship

Based on the results of monotonic static loading test, it is clear that slabs strengthened with CFRP rods had a significant increase in teh stiffness in comparison with control slabs and, obviously, fired-slab. The ultimate load for the strengthened slabs was two times higher than the control slabs. In general the curves of the strengthened slabs can be approximately divided into three stages: before cracking, steel yielding and post-yeilding stage. This behavior was mentioned in the research of Al-Mahmoud, Castel [6]. The first stage is short and it follows a linear elastic behavior. In the second stage, cracks appear, starting at the maximum moment zone. As load increased and reached the value that led to the yielding of steel bars, this stage will end. The last stage occurred between the steel yielding and the slab failure. At this stage, the steel has yielded, whereas the CFRP rods behaviour is elastic and control the crack widths until failure [32]. Moreover, the increase in deflection has a higher rate than the previous stage. In the comparison between the strengthened slabs, the location of NSM CFRP rods had affected their performance as mentioned below.
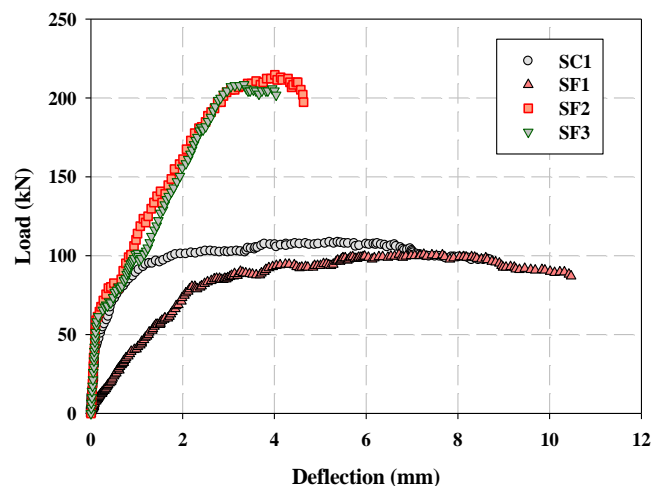
Figure 4.7 Load-deflection relationship of slabs – 24 MPa.

Fig. 4.7 shows the test results of slabs SF2 and SF3 with concrete strength of 24 MPa. It is observed that strengthened slabs got higher ultimate load and stiffness than control specimen SC1 and fire-damaged slab without strengthening SF1. Slab SF1 only reached the ultimate load about 80% over control slab. Meanwhile, slabs SF2 and SF3 reached an ultimate load of higher 200 kN, about more 2 times higher than the control specimen. In the comparison between SF2 and SF3, the curve of slab SF2 shows a higher ultimate load and higher stiffness than the specimen SF3. Both of the slabs were strengthened with NSM CFRP rods inside concrete, but they had the difference in distance from NSM CFRP rod to longitudinal steel reinforcements. These values of the distance were 20 mm for SF2 and 100 mm for SF3. So this difference may have led to the change in redistribution of stress, which as a result of the difference of bending behavior over slabs.
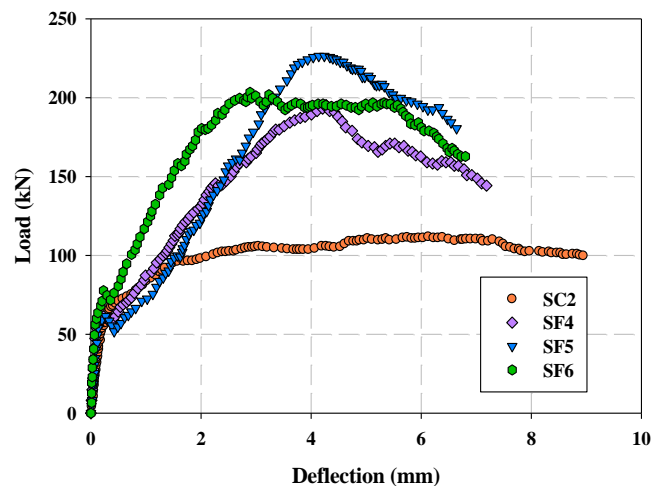
Figure 4.8 Load-deflection relationship of slabs – 35 MPa.

The load-deflection relationship of specimens with concrete strength of 35 MPa are shown in **Fig. 4.8**. The purpose is to evaluate the effect of location of CFRP rods with 3 cases: 1) inside concrete part (SF2); 2) between concrete and repairing material; 3) inside repairing material. The distance from the NSM CFRP rod to longitudinal steel reinforcement was fixed to 100 mm. It is clear to detect the highest value of ultimate load about 220 kN can achieve with respect to slab SF5 which CFRP rods in repairing material. Meanwhile, slabs SF6 and SF4 obtained approximately 200 kN. This indicates that both these strengthening ways did not have any significant difference on the strengthening effectiveness. It may have been due to the bond behaviour between NSM CFRP ros and substrate, which mentioned above in the bonding test of C-shaped specimens. This is in coincidence with the bond test where the highest bond stresses were obtained for CFRP rods embedded in the repairing material while the other two cases showed lower results.
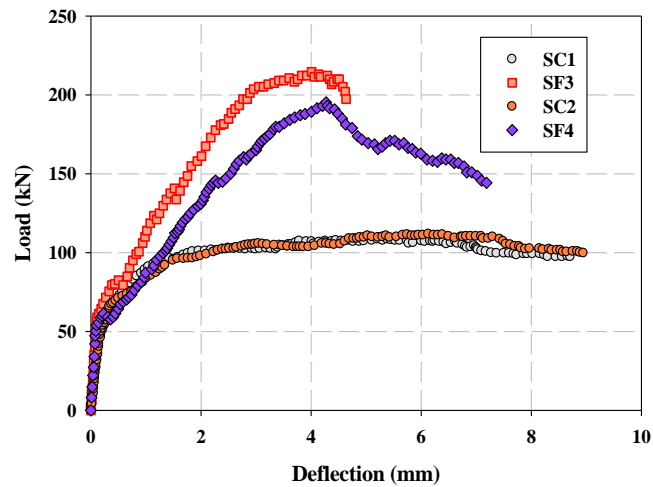
Figure 4.9 Load-deflection relationship of SC1, SC2, SF3 and SF4.

Fig. 4.9 shows the comparison between slabs SF3 and SF4, which have the same strengthening design, but different concrete strength. The deflection of SF3 was smaller than SF4 as the load increased and even the maximum load of SF3 was also higher, although the concrete strength of slab SF3 was lower than SF4. On the other hand the test results of control slabs SC1 and SC2 were quite similar due to steel yielding failure. These results indicate negligible influence of concrete strenght in the case of rods totally embedded in the concrete groove, which showed a relatevely low bond strenght compared to specimens with rods in the repairing material.
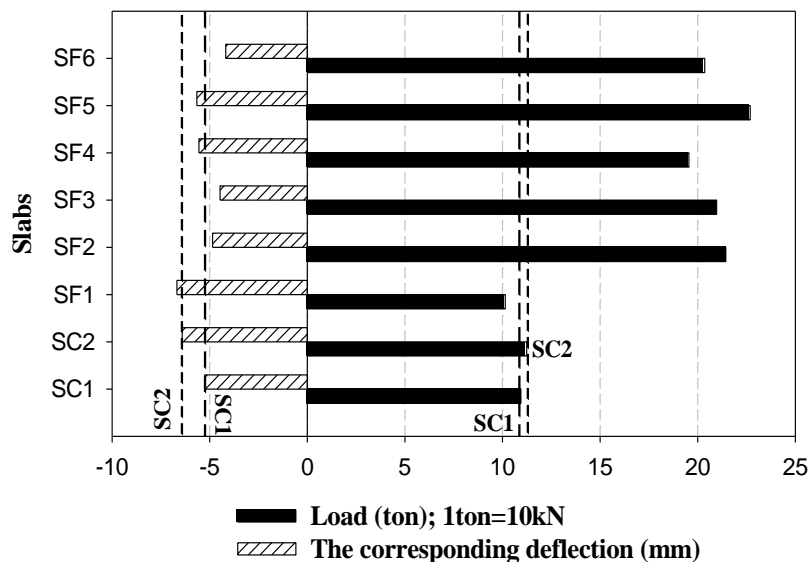
Figure 4.10 Comparison of maximum load and the corresponding deflection.

In order to evaluate the strengthening effectiveness, the results of maximum load capacity and corresponding deflection of strengthened and control slabs are compared in **Fig. 4.10**. All strengthened slabs had higher maximum loads than the control slabs, while their deflections were smaller. On the contrary, the lowest load capacity value was evidently obtained for the case of fired-slab SF1 (101.4 kN) along with the highest deflection value (6.68 mm). As for the results of slabs with concrete grade of 24 MPa, slab SF2 achieved a highest load value of 214.4 kN equal to 2 times the value of control slab SC1. Moreover, slab SF2 also reached a higher maximum load value than SF3, which indicated that the position or distance from the NSM CFRP rod to steel bar was a factor that affected to the strengthening effectiveness.

Among the specimens with concrete strength of 35 MPa, the highest load value was reached for slab SF5 (226.9 kN) equal to 2 times the value of SC2. It may be observed the value of maximum load in descending order over slabs SF5, SF6 and SF4. This means that a higher effectiveness could be obtained by locating CFRP rods into repairing material overlay without grooves and epoxy, which corresponds with the results from bond test of C-shaped specimens that were reported above.

4.2.3 Strain distribution

Fig. 4.11 shows the typical results of strain distributions along half of the bond length of CFRP rods in a half of slab at different loads from 0 to 200 kN, recorded by three strain gauges on every rod. Detail of the setup is shown in **Fig. 3.17** . Some strain gauges (SG8 in slab SF3; SG1, SG2, SG3 in slab SF4; SG4 in slab SF5) failed during the test and their values could not be recorded. In all cases the strain values rose gradually from near end point to mid point of CFRP rod due to the distribution of moment with the highest value at midspan. At the same way all strains increased as the load increased.

A comparison of the strain on the CFRP rod at the point located at 50 cm point among all slabs is showed in **Fig. 4.12**. At the initial load levels the strain values had an inconsiderable increase in every slab. However, the strain show a more evident increase at 80 kN (close to the ultimate load obtained on control slab). This indicated that the CFRP rod carried the additional load as the steel yielding had reached. Therefore, the strain value on CFRP rods had corresponding increased at higher load levels until the failure happened.
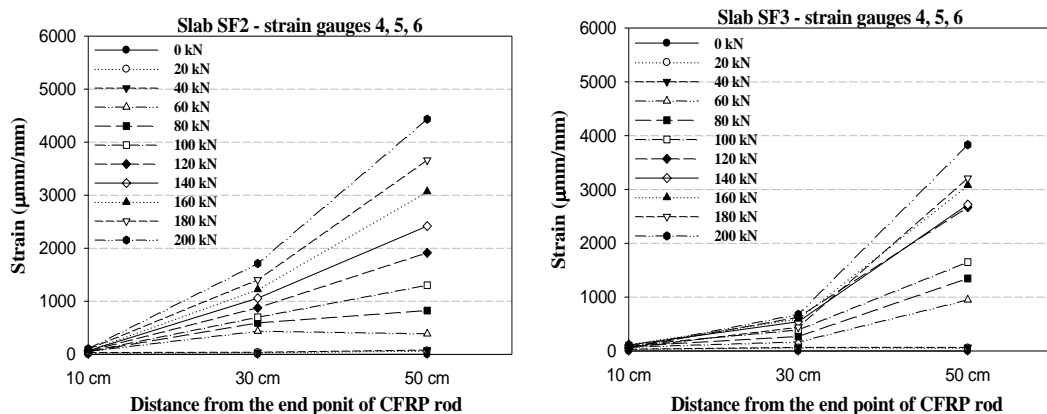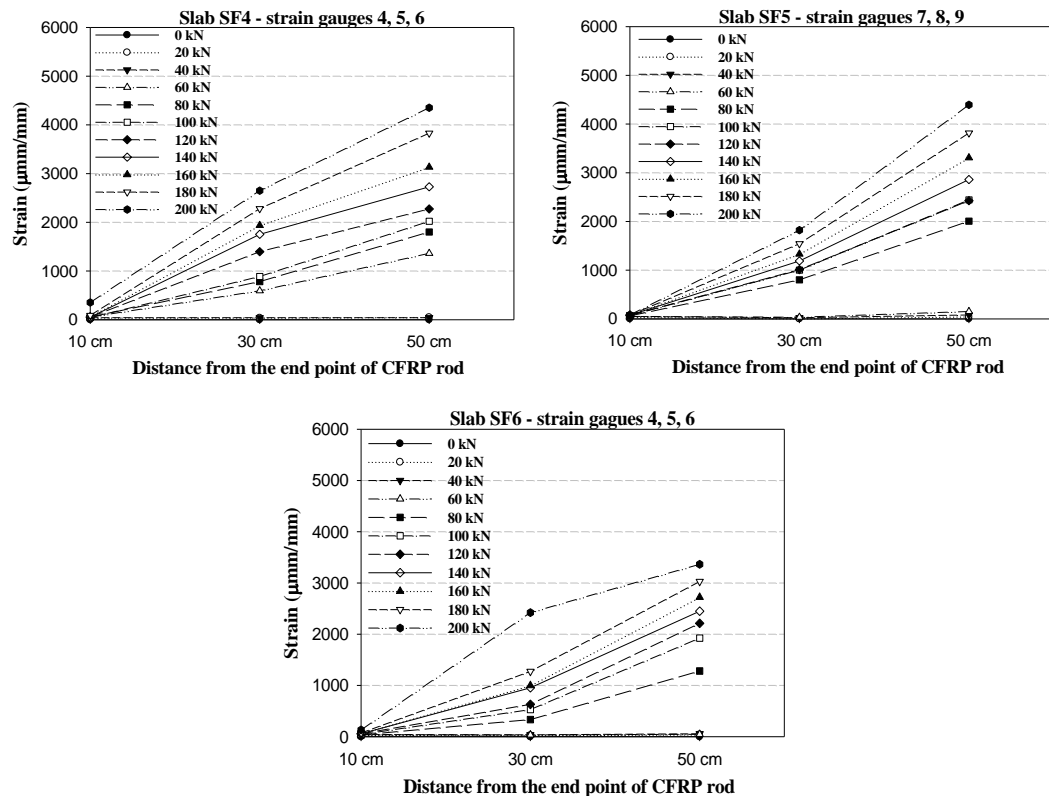
Figure 4.11 Tensile strain distribution along half of the bond length of CFRP rods.
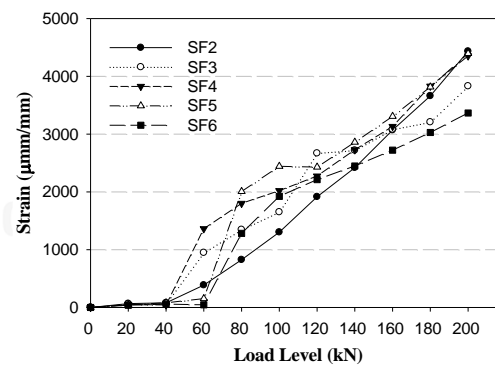
Figure 4.12 Tensile strain on CFRP rods at the position of 50 cm from the end point of CFRP rod.

4.3 Summary

In this chapter, a new method to repair and strengthen fire-damaged flexural RC structures by using the NSM FRP reinforcement method was introduced. An experimental program was carried out to evaluate the effectiveness of this technique on fire-damaged slabs. CFRP rods, epoxy resin and repairing material were used according to three different ways to rehabilitate fire-damaged slabs while a comparison of effectiveness among these three ways was also estimated. In addition, the bond behavior of NSM CFRP rods in case of using with concrete and repairing material were also evaluated through the bond test on C-shaped specimens. Based on the test results the following conclusions can be drawn:

- The results from bond test show that the bond stress – slip law of the NSM FRP system analyzed in this study was similar to the bond law for the typical NSM FRP. The bond stress – slip curves had an initial ascending branch, followed by a rather smooth softening branch after the peak point. However, the location of CFRP rod significantly influenced the bond behavior of the method.

- In both cases NSM FRP rods in full depth groove and in a half depth groove, the bond stresses obtained were not much different and the highest values were below 3 N/mm^2. The latter could delay the slip at the initial low load level. Meanwhile, the bond stress with respect to the case which NSM rod was embedded in repairing material reached 3 times higher than the others.

- The bond failure at the rod-epoxy/repairing material interface with cohesive shear failure in the epoxy/repairing material was observed as the critical failure pattern in all cases.

- Based on the bond test results, the minimum embedded length for NSM rod to prevent pull-out failure in case of CFRP rod in repairing material is approximately 3 times shorter than the other cases.

- In flexural tests, the bending cracks were observed in all slabs, while shear cracks occurred at high load levels in case of the strengthened slabs. The cracks propagated from the repairing material layer toward the concrete layer without any change in their angle, which indicated the good bond between two layers (concrete – repairing material).

- The experimental results show that all strengthened slabs improved their performance when compared to control specimens and fire – damaged slabs. Their maximum loads were 2 times higher than control slabs while the deflections were smaller. The highest load capacity (226.9 kN) was reached for slab SF5 with CFRP rods embedded inside the repairing material. This location of CFRP rods also brought out the highest results in bond tests. Therefore, in comparing the three strengthening methods proposed in this study, the method in which the CFRP rods were installed inside the repairing material could be considered as the most effective. This method also offers advantages such as ease of installation and economy, as epoxy resin was not used and it does have the need to make grooves.

Chapter 5

FINITE ELEMENT MODELLING

5.1 General

The analysis in this chapter is carried out using the finite element package ABAQUS, which is suitable for finite element analysis of structures including linear and nonlinear, dynamic and static, large and small strain analyses [56]. This chapter presents a numerical investigation utilizing non-linear FE analysis to predict the flexural behavior of RC slab before and after exposure to fire as well as the behavior of slabs strengthened with CFRP rods.

5.2 Constitutive models for materials

5.2.1 Concrete

The Concrete Damaged Plasticity (CDP) model was used in FE code ABAQUS to define the concrete behavior [56]. In this model, the elastic stiffness of concrete is assumed to be the same under tension and compression. Two main damage mechanisms of concrete are considered including cracking formation and propagation in tension, elasto-plasticity in compression. The CDP model uses the Drucker-Prager hyperbolic function to assess the flow potential (G) as follows [56]:

$$G = \sqrt{(e\sigma_{t0}\tan\Psi)^2 + \bar{q}^2} - \bar{p}\tan\Psi \qquad (5.1)$$

where σ_{t0} is the uniaxial tensile stress at failure, e is the flow potential eccentricity that adjusts the shape of meridional plane (herein assumed as a hyperbola) at which the function approaches the asymptote. The recommended default value is e = 0.1, which implies that the material has almost the same dilation angle (Ψ) over a wide range of confining pressure stress value [56].

a)   b)
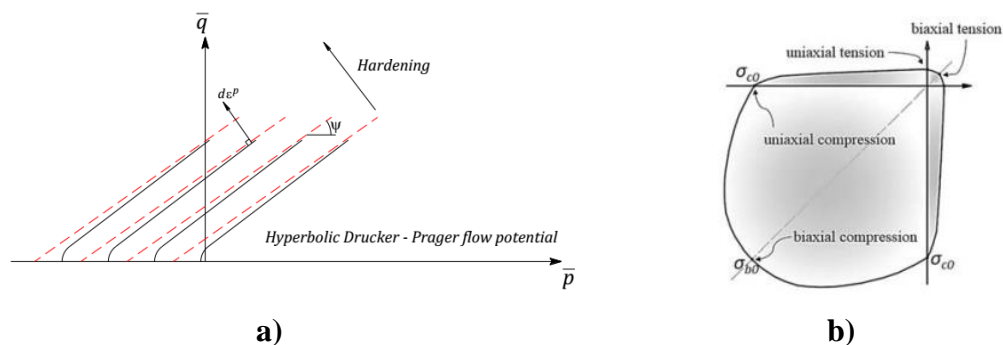
Figure 5.1 a) Hyperbolic flow potentials in the p-q plane, b) yield surface in plane stress [56].

In addition, the dilation angle (Ψ) is the inclination of the failure surface towards the hydrostatic axis at high confining pressure measured in the meridional plane (p-q) (**Fig. 5.1**). The CDP model is non-associated potential plastic flow in the p-q plane (resulting in a non-symmetric stiffness matrix) when the dilation angle and the

material friction angle (β) are different [56]. On the other hand, this hyperbolic model provides associated potential plastic flow in the p-q plane only when Ψ = β. The recommended default value is Ψ: 34 - 43°. For simulation of normal concrete Ψ = 36° is acceptable [57, 58]. In the CDP model, the stress-strain behavior of concrete under uniaxial loading in tension and compression is shown in **Fig. 5.2**.
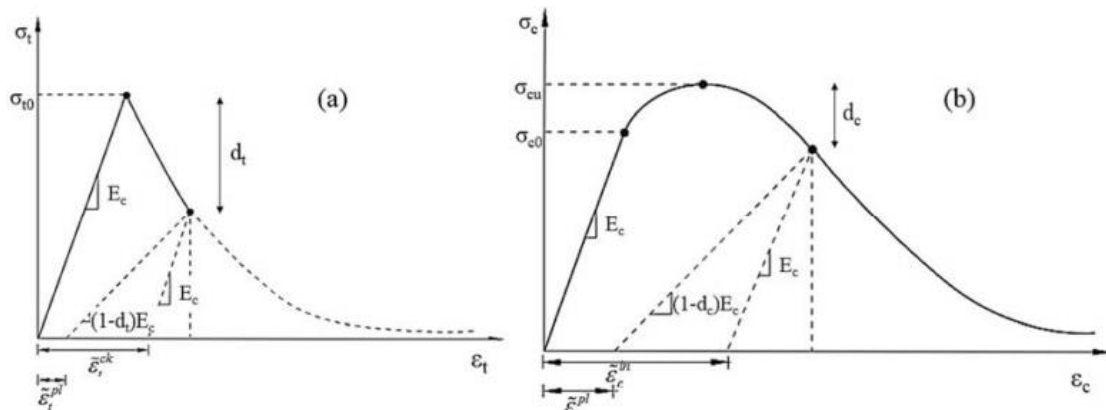
Figure 5.2 Stress-strain behavior of concrete under uniaxial loading in: a) tension, b) compression [56].

where $\tilde{\varepsilon}_c^{in}$ and $\tilde{\varepsilon}_t^{ck}$ are the crushing strain and the cracking strain while $\tilde{\varepsilon}_t^{pl}$ and $\tilde{\varepsilon}_c^{pl}$ are the tensile and compressive equivalent plastic strain. Besides, d_c and d_t are the scalar stiffness degradation variables in a compression and tension zone, respectively.

Furthermore, the ratio of initial biaxial compressive yield stress to initial uniaxial compressive yield stress (f_{b0}/f_{c0}) must be defined in the CDP model, which is taken as 1.16 following the recommend of ABAQUS. In addition, CDP model requires K_c that describes the ratio of the distance between the hydrostatic axis and respectively the compression meridian and the tension meridian in the deviatory cross section [56]. It is recommended to assume $K_c = 2/3$.

For the numerical simulation carried out in this study, the assumed constitutive parameters of the CDP model are indicated in **Table 5.1**.

Table 5.1 Constitutive parameters of CDP model.

CDP parameters	Dilation angle Ψ	Plastic eccentricity e	Stress ratio f_{b0}/f_{c0}	Shape of loading surface K_c	Viscosity parameter V
	36°	0.1	1.16	0.67	0

The uniaxial compressive stress-strain relationship for concrete is modeled following the fib Model Code 2010 [59]. The compressive response of concrete is assumed to be linear elastic up to the uniaxial yield stress, followed by a strain-hardening curve up to the peak compressive stress, after which a descending branch represents the post-peak softening behavior of concrete (**Fig. 5.3a**).

a) uniaxial compression [59]   b) Tensile stress-strain curve [60]
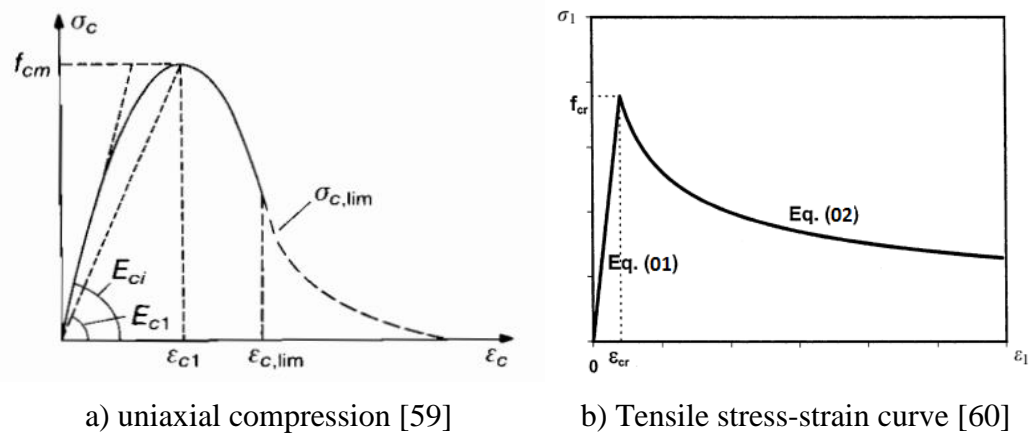
Figure 5.3 Constitutive Models for Concrete.

where σ_c = compression stress; ε_c = compression strain; f_{cm} = maximum compressive stress; E_{c1} = secant modulus from the origin to the peak compressive stress f_{cm}; E_{ci} = tangent modulus; ε_{c1} = 0.0035; $\sigma_{c,lim}$ = 0.5f_{cm}; $\varepsilon_{c,lim}$ = the compression strain at the stress $\sigma_{c,lim}$.

For the tensile behavior of concrete, it is assumed to be linear elastic before cracking, followed thereafter by a descending branch. A tension model proposed by Hsu is used in this study [60] as shown in **Fig. 5.3b** where the ascending and descending branches are given as:

$$\sigma_1 = E_c\varepsilon_1 \qquad \varepsilon_1 \leq \varepsilon_{cr} \tag{5-2}$$

$$\sigma_1 = f_{cr}\left(\frac{\varepsilon_{cr}}{\varepsilon_1}\right)^{0.4} \qquad \varepsilon_1 > \varepsilon_{cr} \tag{5-3}$$

where σ_1 = tension stress; ε_1 = tension strain; E_c = modulus of elasticity of concrete; f_{cr} = cracking stress of concrete; ε_{cr} = cracking strain of concrete.

When concrete is exposed to elevated temperatures, its stress-strain behavior will change due to the decrease of modulus of elasticity, compressive strength and tensile strength. The tensile strength at temperature θ is taken as 0.1 of the compressive strength at temperature θ [61]. A stress-strain diagram of concrete under compression at elevated temperatures can be obtained based on the Eurocode model [62]:

$$\sigma_{c,\theta} = f_{c,\theta}\left[3\left(\frac{\varepsilon_{c,\theta}}{\varepsilon_{cu,\theta}}\right) / \left\{2 + \left(\frac{\varepsilon_{c,\theta}}{\varepsilon_{cu,\theta}}\right)^3\right\}\right] \tag{5-4}$$

$$f_{c,\theta} = k_{c,\theta}f_c \tag{5-5}$$

where $\sigma_{c,\theta}$ = compression stress at temperature θ; $f_{c,\theta}$ = compression strength at temperature θ; $\sum_{\chi,\theta}$ = compression strain at temperature θ; $\sum_{\chi\upsilon,\theta}$ = the strain corresponding to $\phi_{\chi,\theta}$; κ = the reduction factor; f_c = compression strength at ambient temperature.

According to the above models, the stress − strain curves in compression and tension of concrete at different temperatures could be drawn as shown in **Fig. 5.4** and **Fig. 5.5**.
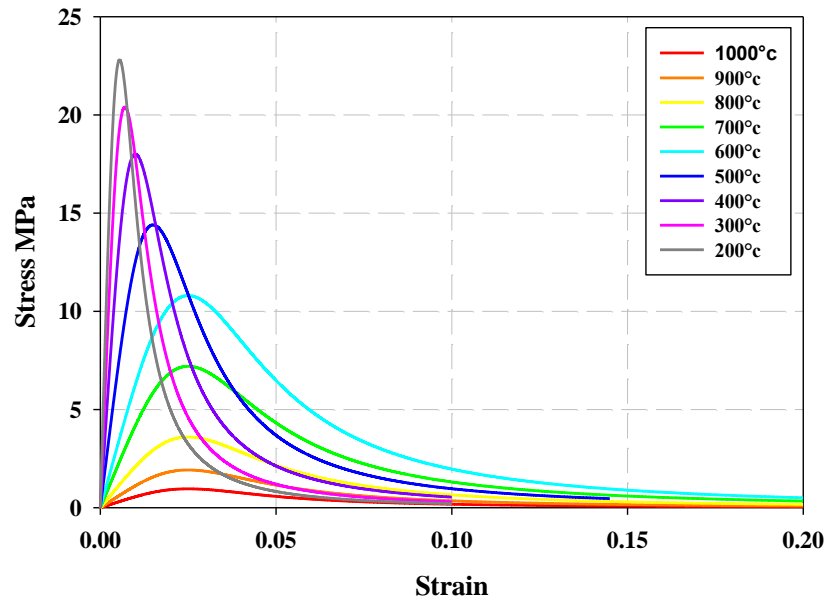
Figure 5.4 Compression stress-strain models of concrete at different temperatures.
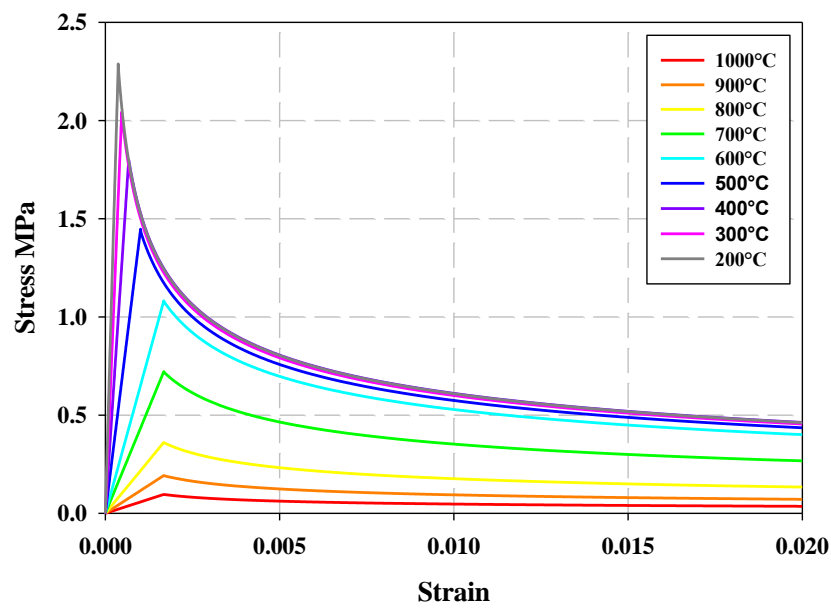
Figure 5.5 Tension stress-strain models of concrete at different temperatures.

5.2.2 Steel and CFRP reinforcement

The typical stress-strain relationship for steel bars is shown in **Fig. 5.6a**. The steel bar has approximately linear elastic behavior at low strain values. At higher strain magnitudes, it begins to have nonlinear, which is referred to as plasticity. The shift from elastic to plastic behavior occurs at the yielding point. Once the stress in the steel exceeds the yield stress, plastic deformation begins to occur. The stiffness of the

steel decreases once the material yields. After heating and cooling to the temperature, it may have a notable decrease in yield strength but the influence on the modulus of elasticity is generally less significant [63]. In general, the shape of the stress-strain curve of steel, heated and cooled to room temperature, is the same as before heating. With respect to simulate the tensile behavior of CFRP bars, a linear elastic stress-strain relation up to tensile strength is adopted (**Fig. 5.6b**).
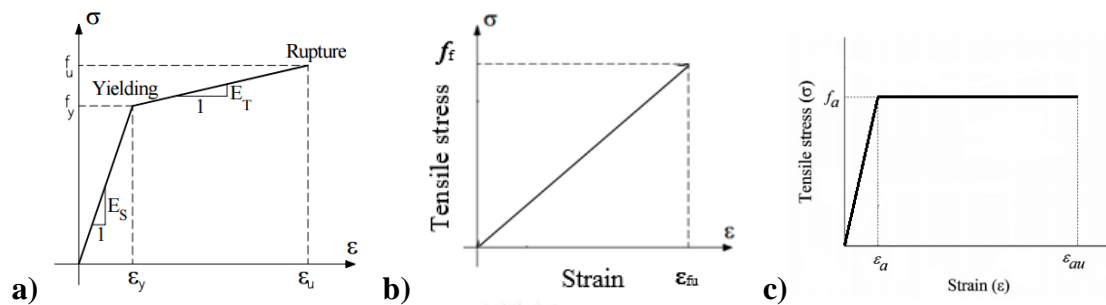
Figure 5.6 Stress-strain curve for: a) Steel reinforcement [64]; b) CFRP reinforcement; c) Adhesive resin.

5.2.3 Epoxy and repairing material

A normal elasto – plastic model is used to simulate the behavior of epoxy adhesive as shown in **Fig. 5.6c**. Besides, due to the lack of studies on proposing the model for repairing material, this research assumes that the behavior of the repairing material can be simulated by using the constitutive model of concrete. The properties of epoxy and repairing material were mentioned in the chapter of experimental program.

5.3 FEM modelling

5.3.1 General

The developed three-dimensional (3D) FE models were created using the finite element code ABAQUS/Explicit [56]. In this numerical simulation, the explicit solver was chosen in order to eliminate the convergence problem. It has been used to perform a quasi-static analysis and in this case, the load should be applied as slow velocity to make the dynamic effects negligible and get more accurate results [58]. For this modelling, the time step is set to be 0.3 for all models. Regarding the element type, concrete, repairing material and epoxy were simulated by using 3D 8-Node solid elements, defined by eight nodes, each node having three translational degrees of freedom in x, y and z directions. In addition, the 3D 2-Node truss element was utilized to model the steel reinforcement bars and CFRP rods. An assumption of perfect bond between the reinforcement bars and concrete was utilized in this analysis for all of modelling situations. Therefore rebars were fully embedded in the concrete using a type of "embedded region" when modelling the interaction between steel rods and concrete. The 3D 8-Node elements were used to simulate the steel rods working as supports and loading pin in bending test.

5.3.2 Numerical simulation of RC slabs – control specimen

3D Finite Element Method (FEM) model of control slab was simulated as shown in **Fig. 5.7**. The element size used in the analysis of RC slab was 10x10x10mm. The loading and boundary conditions of the model were applied according to the particularities of the test setup.
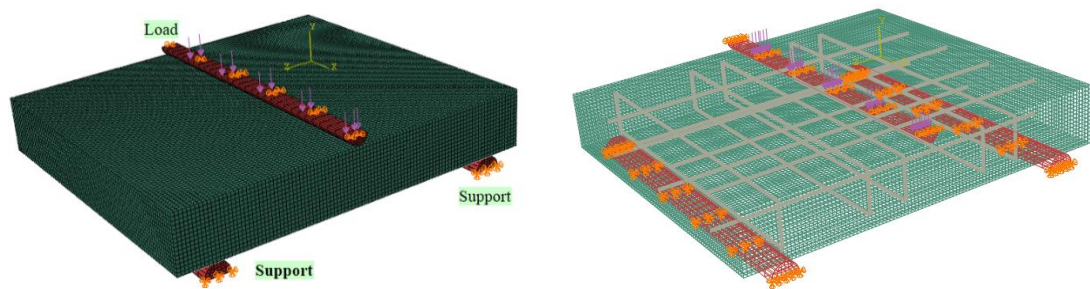
Figure 5.7 FEM model for RC slab.

In order to assess the predictive performance of the described numerical model, the load versus mid-span deflection response is compared in **Fig. 5.8** with experimental data. It can be observed that the numerical model showed similar stiffness before concrete cracking compared with experimental diagram. It reached a cracking load around 40 kN, thence a decrease in stiffness occurred similarly as in the behaviour obtained in the test sample. Moreover, the model also captured the post yielding stage observed in testing. In general, it can be concluded that the numerical simulation showed a good agreement in comparison with the load-deflection behaviour from tests, with little difference in stiffness and load carrying capacity compared with test data.
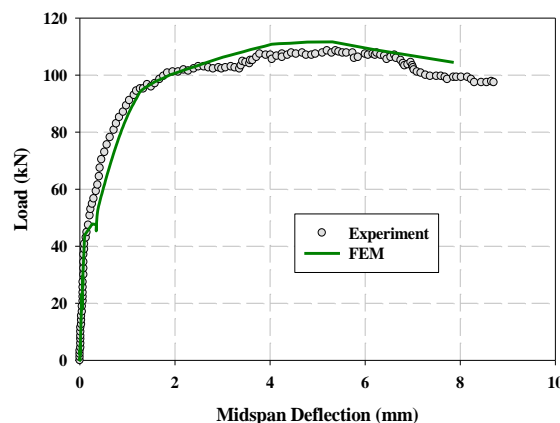
Figure 5.8 FEM results of control specimen.

For the failure pattern, a typical flexural failure with small cracks at the mid-span of slab were observed in the experimental test. Though the FEM model could not capture exactly every crack line, it indicated the flexural failure pattern or the cracking area similar to the observation in bending test. Herein, the failure pattern or the cracking area in concrete was estimated through the distribution of concrete tensile strains in the Z direction of the model. **Fig. 5.9** shows the failure pattern of the control slab in

bending test and the concrete tensile strain field based on the PE33 output (plastic strain in Z direction).
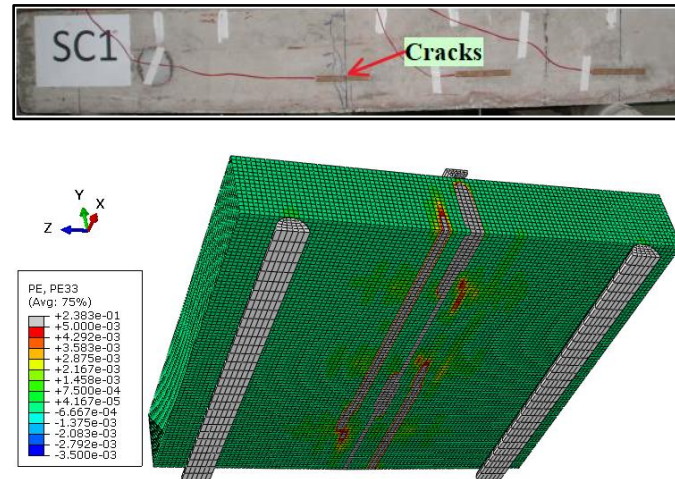
Figure 5.9 Experimental and FEM pattern of concrete failure for control specimen.

5.3.3 Numerical simulation of fire-damaged RC slabs

To simulate the fire-damaged slabs, the temperature distribution from the exposure surface was considered. This research aimed to propose a simple method to predict the flexural behavior of RC slabs after exposure to fire by dividing the fire-damaged part into several layers. At each layer, the mechanical properties, or the stress-strain relationship of concrete, will change correspondingly to the temperature distribution versus the depth of slab. Because the mechanical characteristics of concrete cannot recover from damage due to temperature increase, it could be assumed that the stress-strain relation of concrete after cooling down is similar to that of the heated concrete [11]. Therefore, it was required to know the highest temperature attained at different depths inside the concrete, thence the relative stress-strain relation would be assigned in modelling.

In the fire tests of this study, some thermocouples were installed to record the temperature distribution in the slabs during the heating time. The maximum temperatures registered from thermocouples are shown in **Table 5.2**.

Table 5.2 The maximum temperature recorded in the slab.

Distance from exposure surface (mm)	Max. temperature (°C)
125	130.7
75	131.0
25	358.4
0	949.0

Regarding to the fire-damaged part in the slab, a layer with a thickness of 50mm was removed for repairing. In order to simulate this layer in the model, the temperature distribution in this part was required. However, due to the lack of data from the test, only two positions at the exposure surface and the depth of 25 mm were recorded (**Table 5.2.**). These values were not enough for modelling the fire-damaged slab based on the method mentioned above.

Therefore, an assumption of temperature distribution in this layer was carried out relying on the data obtained from the test and the other references, which determined the temperatures measured versus the cross section concrete depth [9]. With respect to steel bars, its material properties are significantly affected by the temperature increase. However, after heating and cooling to the room temperature, it may have a notable decrease in yield strength but the influence on the modulus of elasticity is generally less significant [63]. Moreover, the previous studies reported that the strength reduction was more than 10% for structural steel. In general, the shape of stress-strain curve of steel reinforcement after heating and cooling to room temperature is the same as before heating. These assumptions for modelling steel bars were applied in this numerical simulation.

To apply the proposed method in this numerical simulation, the bottom of the slab model was divided into 5 small layers of 10 mm thickness. The details are shown in **Figure 5.10**. The stress-strain relationship of concrete was different for each layer (layer 01 – 05) according to the maximum temperature that was assumed in them.
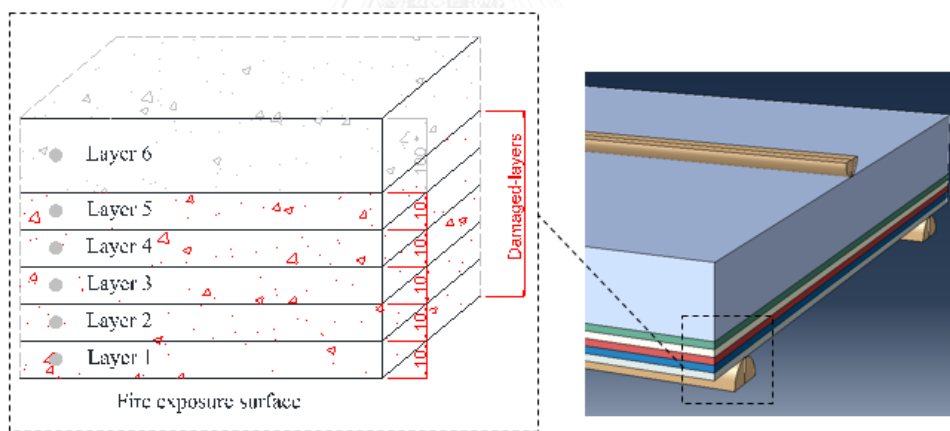
Figure 5.10 Modelling the fire-damaged RC slab.

Table 5.3 shows the values of temperature assumed for each layer with three different situations of temperature distribution (Case A, B and C). The remaining part of the slab from layer 06 up to the top, is considered to be undamaged concrete, so the stress-strain relation of concrete at normal temperature could be assumed. The results are shown in **Fig. 5.11**, which includes a comparison on load-deflection behavior between FE models for heated slab and control specimen.

Table 5.3 Temperature distribution in the fire-damaged zone.

Layer	Case A	Case B	Case C
Layer 05	200°C	200°C	200°C
Layer 04	200°C	200°C	200°C
Layer 03	400°C	400°C	400°C
Layer 02	600°C	600°C	800°C
Layer 01	900°C	800°C	800°C
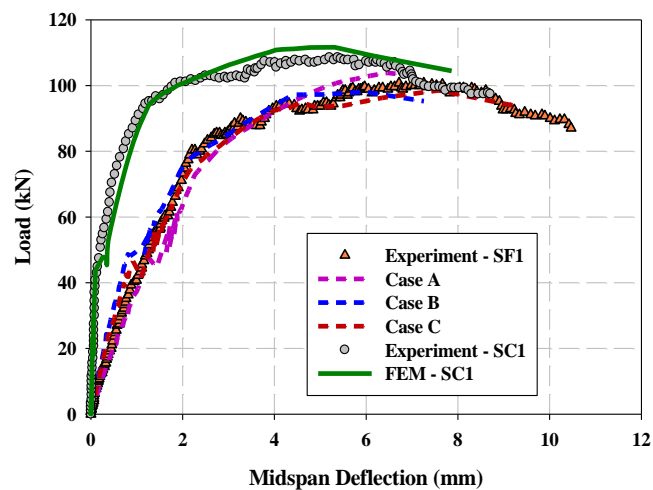
Figure 5.11 FEM results for the simulation of fire-damaged slab.

Due to the influence of fire attack, the stiffness of concrete decreased, which caused a reduction in the slab stiffness as shown in **Fig. 5.11** for experimental curves. Regarding to the curves from simulation, it could be said that the numerical model is capable to predict the flexural behavior of the fire-damaged slab. All of three situations A, B and C showed the stiffness reduction with slight differences in comparison with the experimental curve. Although there was a small disparity between the load carrying capacity from FEM and experimental curves, the post yielding stage of the load-deflection diagram from the model indicated an acceptable agreement with the actual test. This loading capacity was lower than that of the model for control specimen. Besides, the numerical simulation also showed a failure pattern, based on the PE33 output, which was quite similar with the observation in experimental test (**Fig. 5.12**). Based on the evaluation of obtained FEM results, it is possible to apply this numerical simulation for predicting the load-deflection relation of fire-deteriorated slab. In this simulation technique, an accurate result could be attained if temperature distribution profile was supplied adequately.
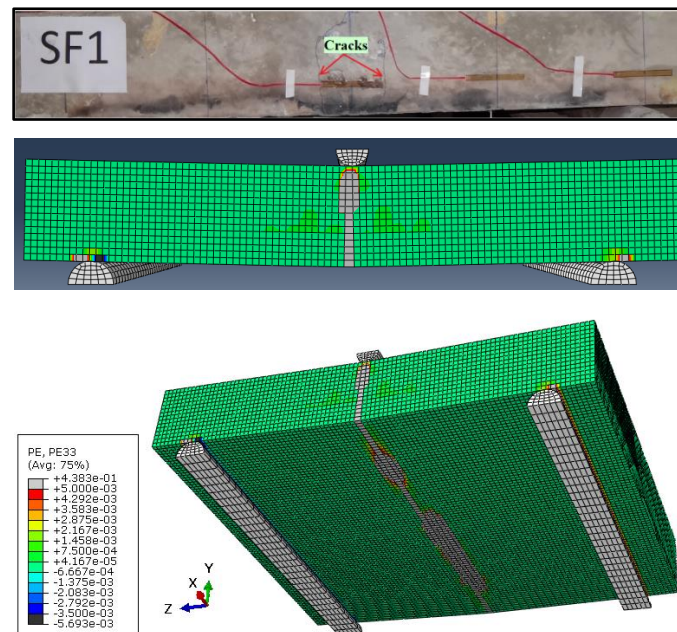
Figure 5.12 Experimental and FEM pattern of concrete failure for fire-damaged slab.

5.3.4 Numerical simulation of repaired RC slabs

5.3.4.1 Assessment of the numerical model

With respect to the repaired slabs, the fire-damaged concrete layers were replaced by repairing material. This research assumed that the behavior of repairing material in simulation could be assigned by using the constitutive model for concrete (CDP model). Among the repaired slabs, slabs SF2 and SF3 were chosen to simulate. The bottom parts in these models with the thickness of 50mm were assigned by the property of repairing material. In order to save the computational time, a half of slab was simulated due to the symmetric in z direction. The details are shown in **Fig 5.13**.
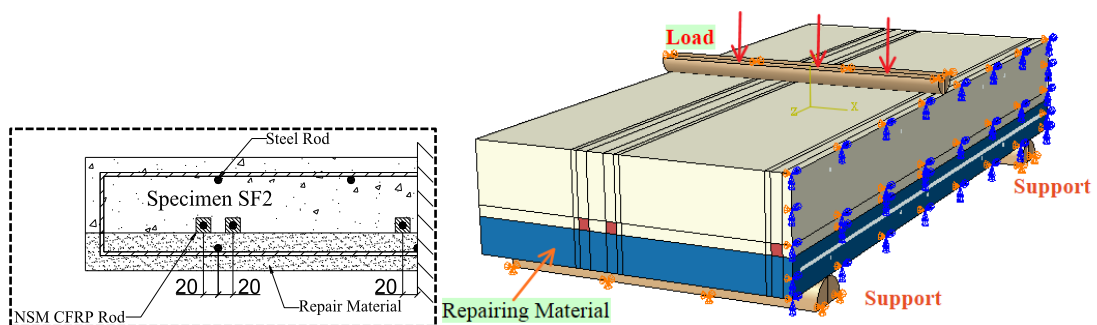
Figure 5.13 The model of ½ slab in ABAQUS.

A fine mesh with the element size of 5x5x5 mm was applied for both of two models SF2 and SF3, this small size element was expected to yield accurate results. In additions, the NSM CFRP bars were assumed to be fully embedded in concrete, hence "embedded region" was applied in order to simulate the bonding behavior between NSM system and concrete. In the next part, another method is conducted for

modelling this contact and the results from both of simulation ways are compared. The details of slabs SF2 and SF3 are shown in **Fig. 5.14**.
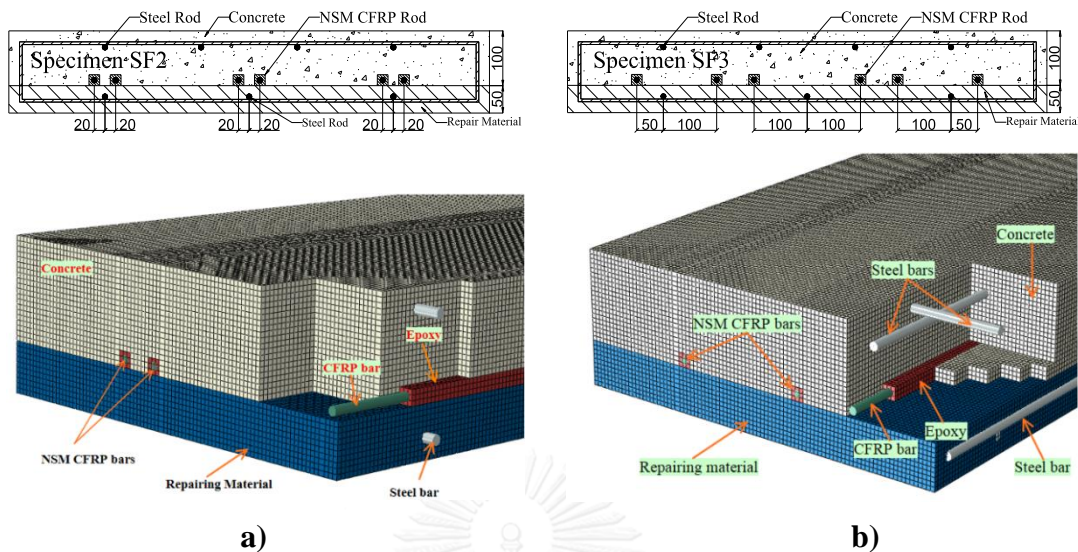
Figure 5.14 The model of slab SF2 (a) and SF3 (b) in small element size.

The relation between force and mid-span deflection of repaired slab SF2 from numerical simulation is reported in **Fig. 5.15** in a comparison with the result from control slab SC1.
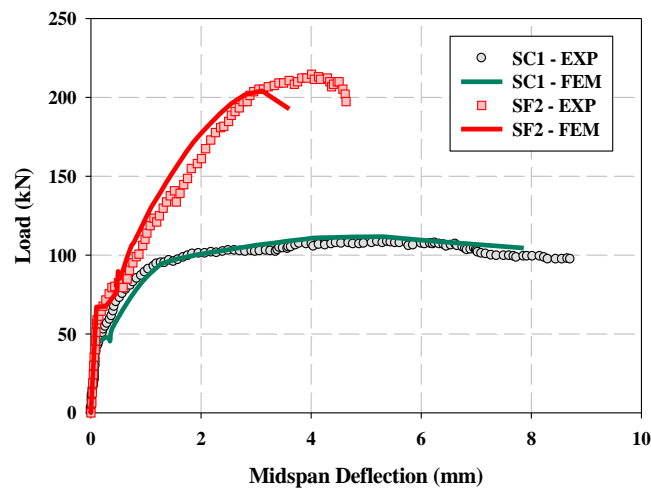
Figure 5.15 FEM results of model SF2 compared with experimental result.

In general, the load-deflection curve obtained from the simulation of slab SF2 showed out a similar shape with the experimental diagram. It can be observed that a good agreement attained in the elastic stage. In the post yielding stage, the stiffness of slab reduced and this change was also captured in the simulation. However, in this stage, the stiffness of FEM curve is higher than experimental curve. The bonding model for CFRP bars and concrete might affect to this point. Regarding to the maximum load carrying capacity, the value obtained from FEM model equals 95% of the experiment. Nevertheless, the deflection corresponding with the maximum load of FEM model

(3.1 mm) was lower than the experimental value (4.5 mm). The slab in simulation achieved the failure point earlier than the observation in the test.
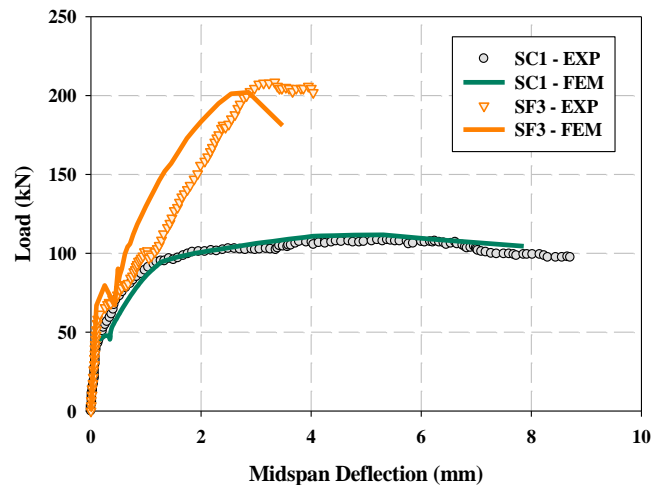
Figure 5.16 FEM results of model SF3 compared with experimental result.

The results from the numerical simulation for slab SF3 is described through of the load-deflection relation in **Fig. 5.16**. The model of repaired slab SF3 showed higher load carrying capacity compared with the simulation results of control specimen SC1 as expected. In the assessment with its corresponding experimental data (SF3-EXP), the load-deflection diagram from the model showed a good agreement with experimental curve in the elastic stage. Although an analogous shape of the diagram observed in post yielding stage, but the slab stiffness attained from the model was evident higher than that of experimental slab. As well as the prior model (SF2-FEM), model SF3-FEM also reached an approximate value of maximum load carrying capacity but the corresponding deflection was lower in comparison with the experimental value.
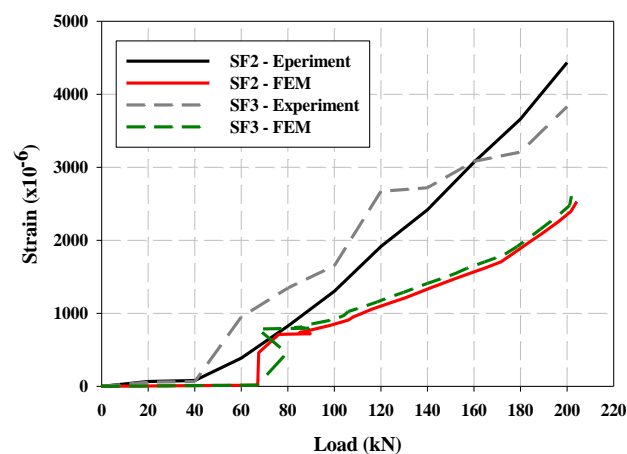
Figure 5.17 The comparison of FRP strain.

Fig. 5.17 showed out a comparison about the CFRP strain profile at the middle of bar between the results from FEM and experiment. At the initial load levels (0-40 kN),

the CFRP strain in both of experiment and simulation had an inconsiderable increase. After that the strain increased with additional load, which means it started to carry the load and help to enhance the load carrying capacity of the slab. As the load raised, the FRP strain from FEM model increased but the obtained values were lower than that of experiment. So the stress that FRP sustained in modelling was lower than that in the real test.

5.3.4.2 Influence of meshing size

Although the fine mesh may provide accurate result but it takes longer computing time. Obviously, smaller element size or coarse mesh lead to less accurate result but smaller accurate result. In this part, a coarse mesh with the element size of 15x15x15mm was applied in order to check ability if the model can provide a quick and rough estimation of design. Thence both of models SF2 and SF3 were modified with the coarse mesh as shown in **Fig. 5.18**.
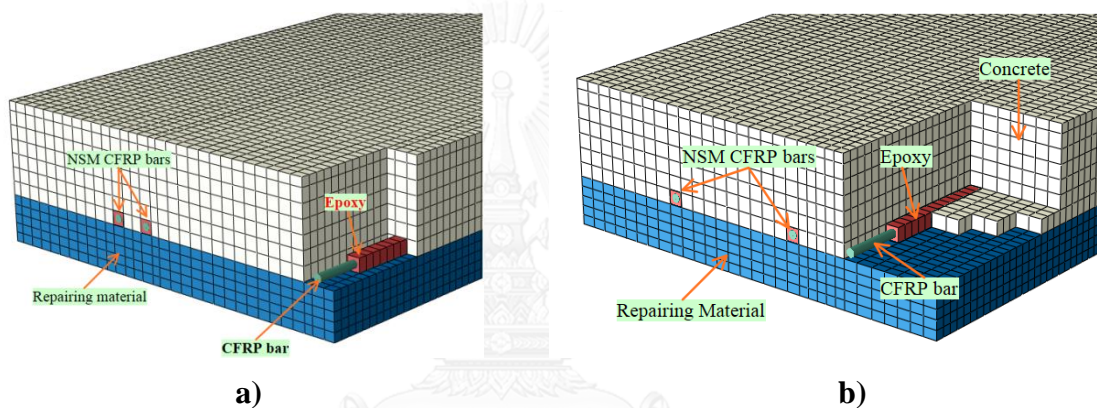
Figure 5.18 The model of slab SF2 (a) and SF3 (b) in coarse mesh.
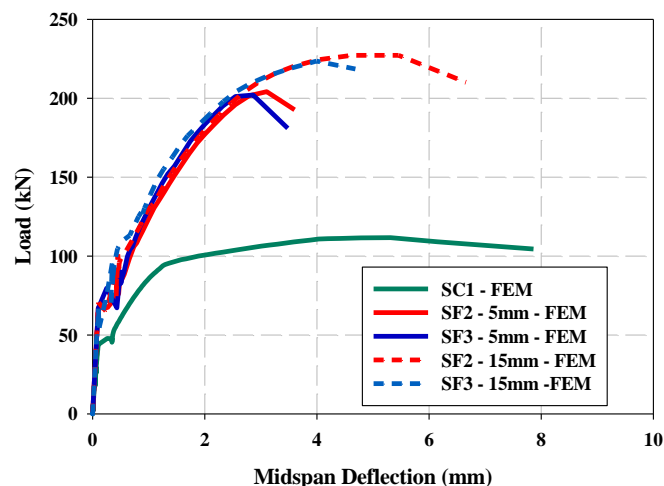
Figure 5.19 FEM results of models fine and coarse mesh.

The influence of different element sizes in meshing was evaluated based on the load-deflection diagrams in **Fig. 5.19**. There are not much different in the elastic stage and post yielding stage in comparison between two situations of 5mm and 15mm element size for both of two models SF2 and SF3. But models FEM-15mm showed higher

load carrying capacity and corresponding deflection compared with models FEM-5mm. Therefore, it could be concluded that in regards to save computational time, a coarse mesh model is also possible to predict the general behavior of repaired slab except the degree of accuracy for load carrying capacity.
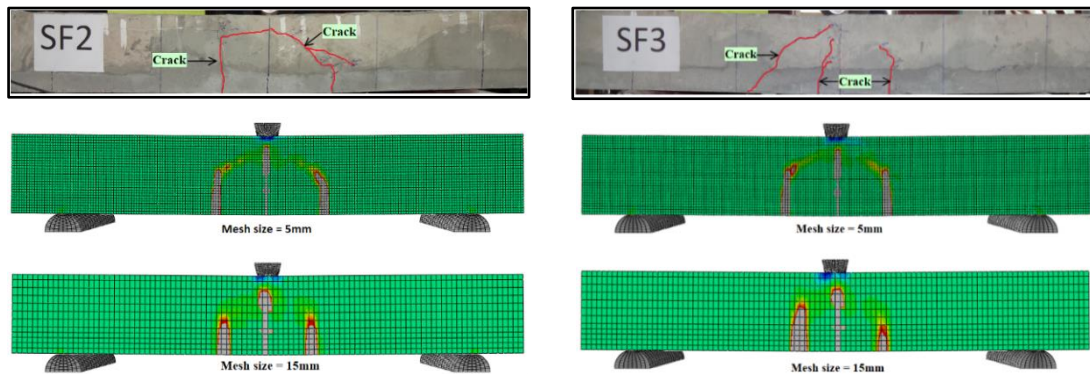
Figure 5.20 Distribution of concrete tensile strain based on the PE33 output.

The change of element size also affected to the failure pattern or the distribution of concrete tensile strain in the model. **Fig. 5.20** shows the distribution of concrete tensile strain in z direction for two models in cases of small and large element size. It can be observed from the figure that the cracking area detected in model FEM-15mm looks larger compared with model FEM-5mm. Model FEM-5mm carried out the cracking pattern that is quite close with the cracking lines observed in the test. Therefore, the cracking pattern could be predicted well if a small meshing size was applied.

5.3.4.3 Influence of interfacial bond model

In this part, the bond behavior between NSM FRP system and concrete are considered and a method using connector element was applied in order to simulate this contact. The interfacial bond model was assigned between epoxy and concrete while a full bond was assumed for CFRP bar and epoxy. This is done since the observed failure mode of the pull-out test specimens was a separation at the interface between concrete and epoxy.

Connector elements with connection type AXIAL were employed to connect pairs of nodes between epoxy and concrete. This element type provides a connection between two nodes where the relative displacement is along the line separating the two nodes (**Fig. 5.21**). It models discrete physical connections such as axial springs, axial dashpots, or node-to-node (gap-like) contact [56]. In this numerical simulation the type axial spring element was chosen to simulate the contact.
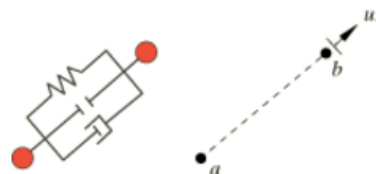
Figure 5.21 Connection element type AXIAL [56].

Due to the limitation of memory of computer and the computational time, only model with coarse mesh size was used to apply this interfacial bond model. The details of connector elements in this numerical simulation are shown in **Fig. 5.22**.
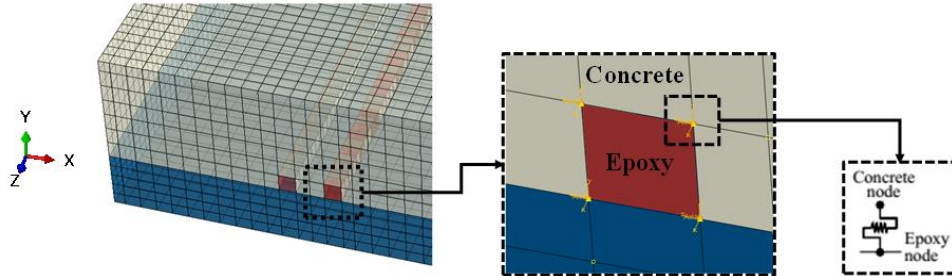
Figure 5.22 The contact between concrete and epoxy nodes in model of slab.

The governed law of connector behavior was based on a bilinear force-motion diagram as shown in **Fig 5.23**. It assumes that the connector response is linear elastic and after damage initiation a linear damage evolution is desired. The ascending branch depicts a linear elastic behavior based on equation:

$$F_i = E_{ii} \times u_i \tag{5-1}$$

where F_i is the force in the ith component of relative motion, u^i is connector displacement in the ith direction and E_{ii} is the elastic stiffness.

If damage were not specified, the response would be linear elastic (a straight line passing through the origin). Conversely, damage has initiated, assume at point I, the corresponding constitutive motion at this point is u_o. If the load increases further such that the constitutive motion increases to u_c, the connector force response at point C becomes F_c. The response is diminished by $d \times F_{eff}$ (d is damage variable) when compared to the effective response F_{eff} (the elastic response with no damage). Thus, $F_c = (1 - d)F_{eff}$. If unloading occurs at point C, the unloading curve of slope $(1 - d)E$ is followed.
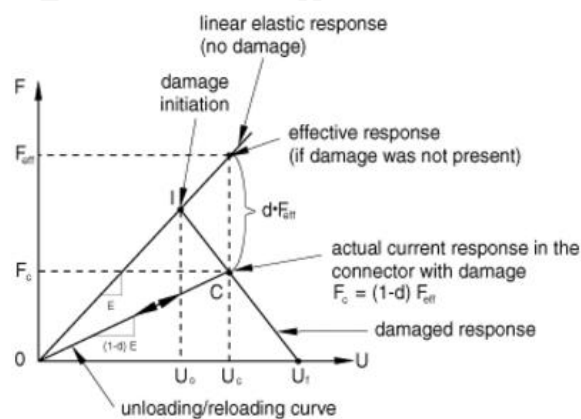
Figure 5.23 Bilinear force-motion law [56].

In order to get the required parameters for the simulation, the data from pull-out test was used. Herein, the maximum force from pull-out test was 16.1 kN and the corresponding slip of FRP bar was 1.7 mm. Before applying this bond model into the simulation of slabs, a model of pull-out test on C-shaped concrete block was run

based on mentioned parameters to assess the result. Detail of C-shaped concrete block model is shown in **Fig. 5.24**. The epoxy part in this model was meshed with the same element size and the contact pairs of connector elements were created similar as it would be simulated in the models of slabs. The connector elements were located in Y direction that also is the direction of slip.
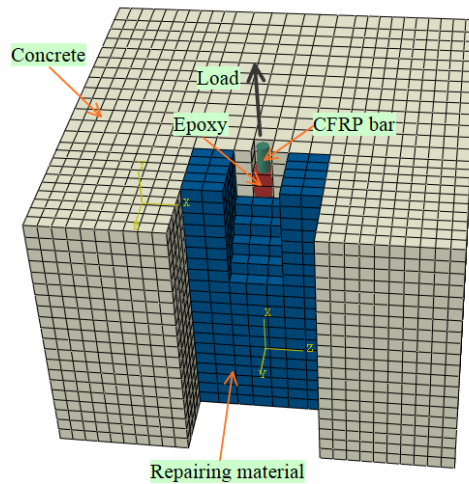
Figure 5.24 The model of C-shaped concrete block in pull-out test.
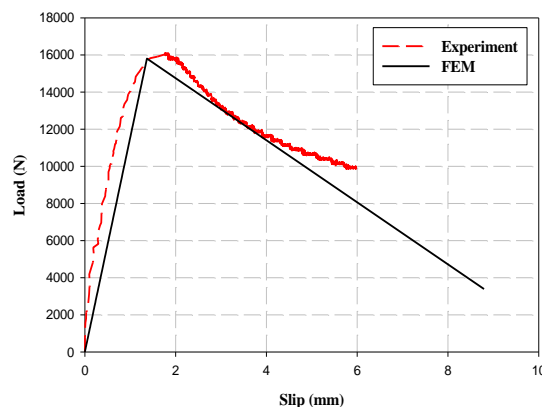
Figure 5.25 The result from numerical simulation of pull-out test.

The result obtained from the model of pull-out test are shown in **Fig. 5.25**. Although the results were in linear for both of ascending and descending branch but it showed the values of maximum force and corresponding slip that are close to the real test. It could be capable to apply this type of interface bond model for the numerical simulation of slab. However, in direct pull-out test, the data is presented in one direction but in the flexural member a three directions behavior would occur for the bond between NSM system and concrete. In the models of slabs, the connector elements were oriented in Z direction while a hard contact property provided by ABAQUS [56] was applied for the simulation of the normal direction (Y and X direction). It aimed to prevent the penetration between concrete and FRP material but transmitting the pressure force.
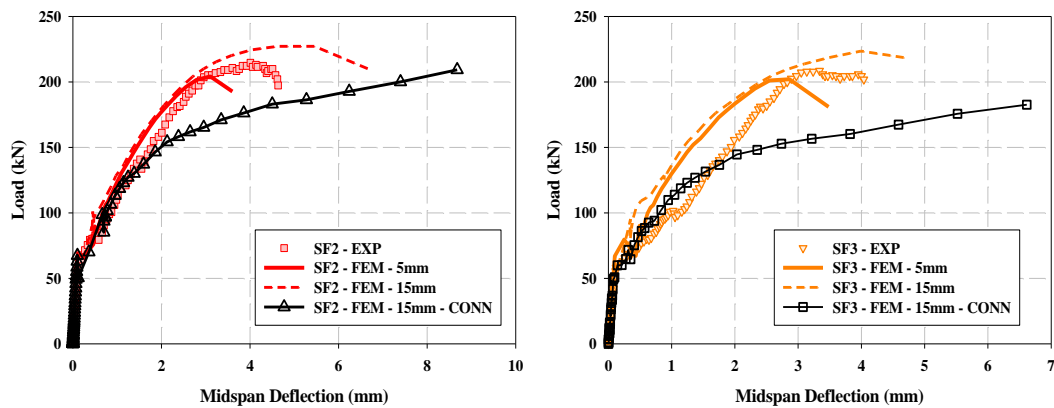
Figure 5.26 The load-deflection curves when the interface bond mode was applied.

After applying the bond model as mentioned above into the model of slab, the load-deflection relations of slabs SF2 and SF3 were attained as shown in **Fig. 5.26**. It is clear to observe the decrease in stiffness of slab, the diagrams become closer with the experimental curve in comparison with the prior models using the contact type "embedded". This means the contact model has a potential to simulate the real bond behavior for NSM FRP-concrete system. However, when the load reached ¾ of the maximum value, the slope of curve decreased and the value of deflection becomes higher than that of experiment at the same load level.

5.3.5 Parametric study

In the parametric study, the influence of CFRP length and a potential of using partially-bonded system are evaluated. Because the bond model has been developing so a fully bonded or contact type "embedded" was applied for the numerical simulation in this parametric study.

5.3.5.1 Influence of CFRP length

In this study, CFRP bars were applied for full span of the structure as presented in the experiment. However, there is not necessary to apply CFRP reinforcement for full span of the flexural member in all cases. Longer length of FRP leads to take high cost for repairing process. Therefore a shorter length can be employed for saving cost but it still must ensure the working capacity as expected. Nevertheless, this length should be extended up to a certain distance from the loading section in shear span to avoid the premature failure modes (such as concrete cover delamination and debonding of the CFRP laminate from the concrete substrate) before the CFRP rupture [65]. Standard ACI-440-2R-08 [66] required the CFRP bonded length should be extended at its both extremities of the maximum bending moment region as a required development length (l_{db}). Because the NSM system in this strengthening is different with the normal NSM system mentioned in the standard (without a cover by repairing material at the bottom part), so the value for development length l_{db} in this study was calculated based on the experimental data (see chapter 4). Thence, a numerical simulation was performed in order to predict the flexural behavior of slab SF2 and SF3 in case of reducing the CFRP bonded length.

Based on the data of development length versus diameter of CFRP bar in **Fig. 4.5** the value of development length is obtained: $l_{db} \geq 20 \times D = 20 \times 9 = 180$ mm. In this numerical simulation, two values of development length l_{db} of 300 mm and 200 mm were applied in models (**Fig. 5.27**). The notations of models are: FB = full bonded length of CFRP bar; C600 = the length of CFRP bar is 600 mm (l_{db} = 300mm); C400 = the length of CFRP bar is 400mm (l_{db} = 200mm).
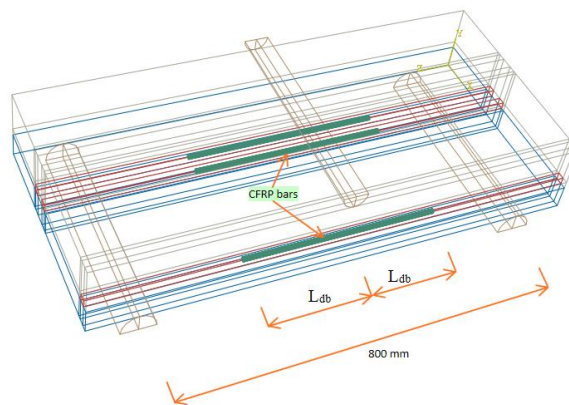
Figure 5.27 Change the length of CFRP bar in model of strengthened slab.

The effect of changing CFRP reinforcement length to load-deflection relation in model SF2 is shown in **Fig. 5.28**. Among the curves for three situations obtained from the numerical simulation, it can be observed that the load-deflection diagrams of slab strengthened by CFRP bars with 600mm length is similar with the case of full-bonded length. Meanwhile, the model of slab strengthened by 400mm length CFRP bars showed an obvious decrease in load carrying capacity compared with the others. A decrease in stiffness also was observed as the load increased over 150 kN. The load-deflection curves of models with fine and coarse mesh showed the same stiffness and the difference is about the value of maximum loading capacity as well as the corresponding deflection, which also was observed for the prior models reported above.
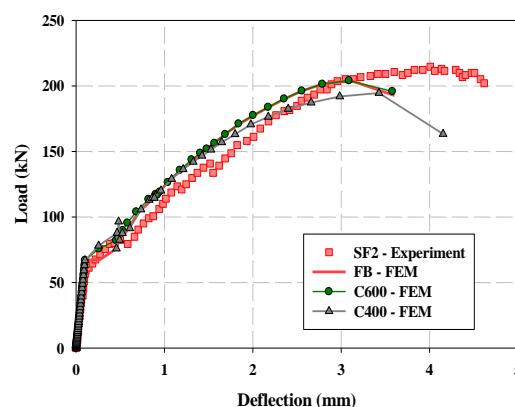
Figure 5.28 FEM results for the changes of CFRP length – SF2.
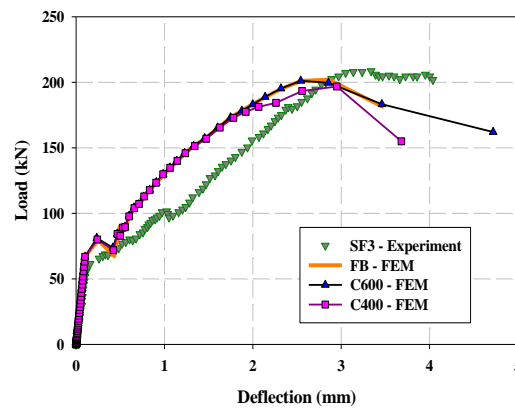
Figure 5.29 FEM results for the changes of CFRP bar length – SF3.

The above figure brings out the results of load-deflection diagrams when changing the length of CFRP bars for model SF3. As CFRP bars with the length of 600 mm were applied, there were no change in the load-deflection relation compared with the situation of 1000 mm. This is similar with the results indicated regarding to model SF2. Furthermore, using 400mm CFRP bars could make a decrease in stiffness as the load reached higher than 170 kN and a lower maximum load carrying capacity. Based on the results obtained from numerical simulation, in order to save material as well as save the repairing cost in the real application, a shorter length of CFRP bars are still possible to enhance the load carrying capacity. Obviously, it is required to satisfy the requirement of development length.

5.3.5.2 Influence of partially-bonded system

Another part of this parametric study, the influence on the flexural behavior of strengthened slabs as partially-bonded (PB) system was applied instead of using fully bonded system. In this numerical simulation, the partially-bonded system was simulated by changing the un-bonded length (L_{ub}) of 600 mm and 400 mm in both of models SF2 and SF3. The details are shown in **Fig. 5.30**. The notations of models are: FB = full bonded length; PB300 = partially bonded length of 300 mm or L_{ub} = 400 mm; PB200 = partially bonded length of 400 mm or L_{ub} = 600 mm.
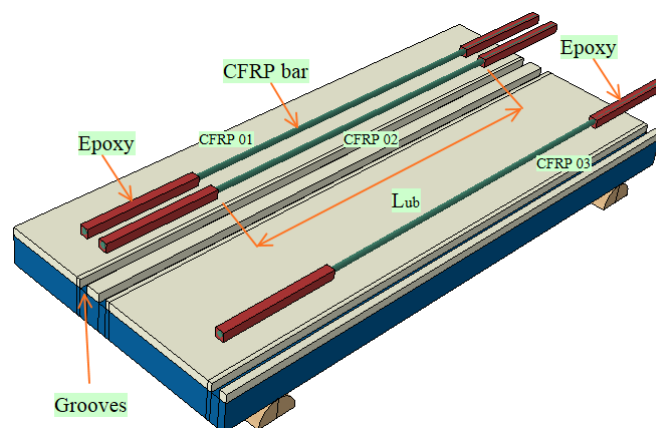
Figure 5.30 The partially-bonded system applied in the numerical simulation.
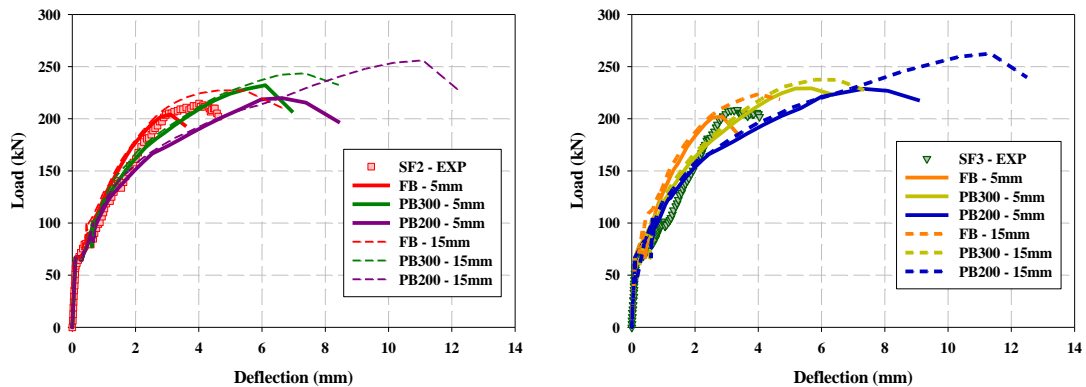
Figure 5.31 FEM results for different cases of partially-bonded system.

The results of numerical simulation for models SF2 and SF3 with the application of partially-bonded system are shown in **Fig. 5.31** based on the load-deflection curves. For both models of SF2 and SF3, the stiffness of the slabs was decreased with increasing the un-bonded length at the post-yield stage. This effect is similar with the results reported by the prior studies that applied partially-bonded system on the beams [38, 41, 67]. As a result, the deformability of the partially-bonded slabs was increased at the same applied load compared to the fully bonded one. In order to compare the deformability of each models, the deflections at ultimate and yielding load were recorded from the simulation as reported in **Table 5.4.** Thence the deformability μ was calculated $\mu = \Delta_u/\Delta_y$ [38] and the results are shown in **Fig. 5.32**. The charts in figure shows that a clear increase of deformability for partially-bonded slabs compared with fully bonded slabs but only a slight enhance when increasing the un-bonded length. It might be due to the small size of the specimen. If the larger specimen is applied, the change could be clearer.

Table 5.4 Deflections at ultimate and service load obtained from numerical simulations.

Slab name	SF2			SF3		
Model group	Δy (mm)	Δu (mm)	μ	Δy (mm)	Δu (mm)	μ
FB	2.005	3.105	1.5	1.151	2.863	2.5
PB300	2.683	6.105	2.3	1.358	5.687	4.2
PB200	2.534	6.630	2.6	1.531	7.326	4.8

The strain profiles of CFRP prior to steel yielding and post yielding stage with respect to models of partially-bonded and fully-bonded systems are shown in **Fig. 5.33**. Unlike the fully-bonded system, the strain was constant throughout the un-bonded region in case of partially-bonded slabs, which indicated that the FRP stress was uniform within the un-bonded length. Prior to steel yielding, the strain in CFRP bars with regard to partially-bonded systems was lower than that of fully-bonded slabs. So the FRP stress in partially-bonded slabs was lower in comparison with fully-bonded systems. This means that the stresses in steel reinforcement and concrete were higher than that of fully-bonded slabs.

In post yielding stage, the stress in steel reinforcement could not increase, so it lead to the rise of stress in FRP as additional applied. As a result, the stress in FRP in partially-bonded system enhanced to almost equal to that of fully-bonded slab. This can be observed based on the strain profiles of FRP reinforcement in post yielding stage.
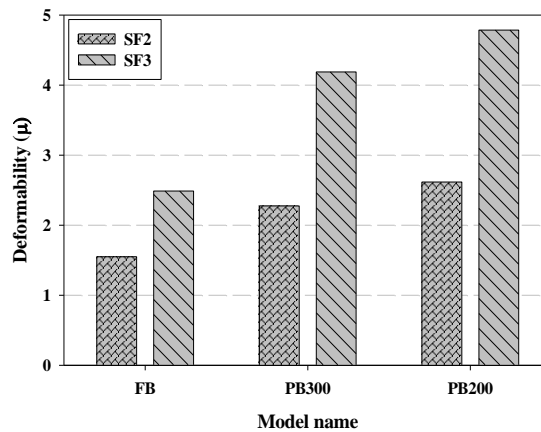
Figure 5.32 The comparison of deformability of models.
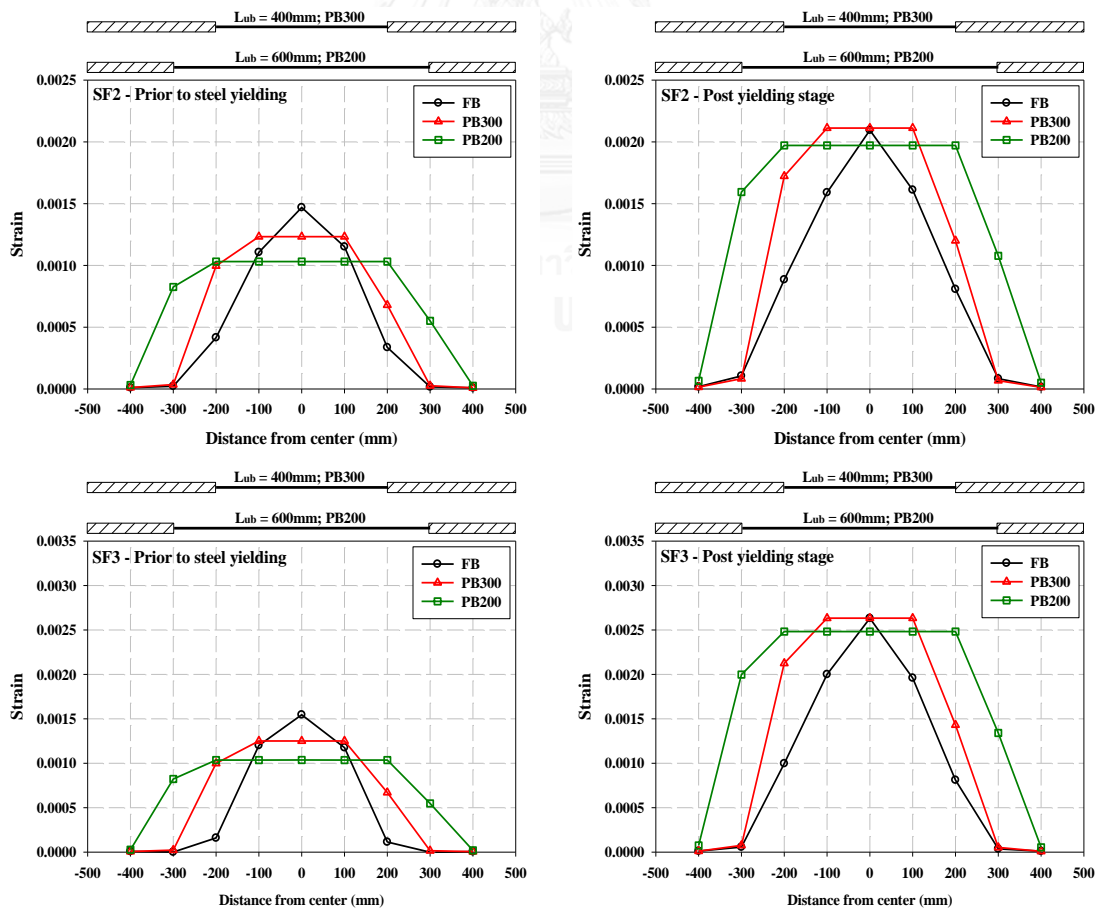
Figure 5.33 Comparison of FRP strains prior to steel yielding and post yielding stage in models of SF2 and SF3.

5.4 Analytical work

In this part, an analytical work is carried out to predict the values of load capacity for slabs repaired by NSM FRP system that proposed in this study. The calculation was based on standard fib Bulletin 14 [18].
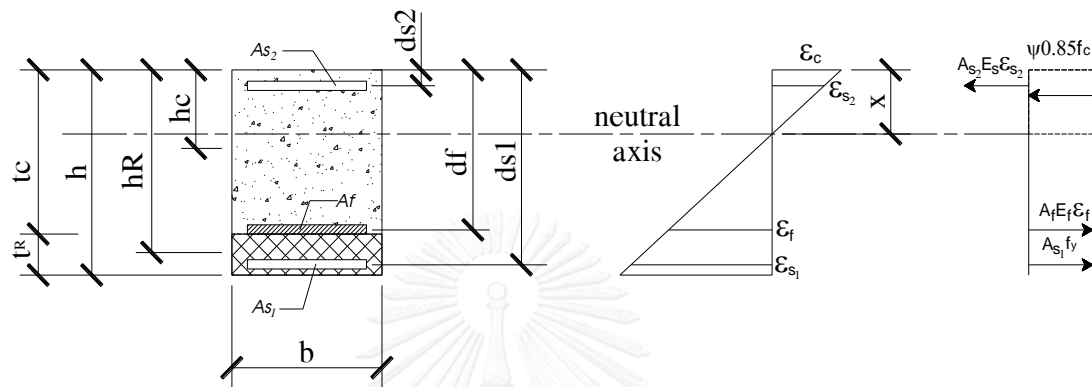
Figure 5.34 Analysis of cross section.

where b = 900 mm; h =150 mm; t_c = 100 mm; t_R = 50 mm; d_f = 92.5 mm; d_{S1} = 120 mm; d_{S2} = 30mm; h_R = h-t_R/2 = 125 mm; A_f = 381.51 mm^2; A_{s1} = 235.5 mm^2; A_{s2} = 314 mm^2; n_R = E_R/E_c = 1.58; n_f = E_f/E_c = 5.78; n_S = E_S/E_c = 8.70.

❖ Cracking load

Calculation of neutral axis depth:

$$x = \frac{bt_ch_c+n_Rbt_Rh_R+n_fA_fd_f+n_SA_{S1}d_{S1}+n_SA_{S2}d_{S2}}{bt_c+n_Rbt_R+n_fA_f+n_SA_{S1}+n_SA_{S2}} = 82.8 \text{ mm}$$

Moment of inertia:

$$I_0 = \frac{bx^3}{3} + \frac{b\times[(h-x)-t_R]^3}{3} + n_R\left[\frac{b\times t_R^3}{12} + b \times t_R \times \left((h-x) - \frac{t_R}{2}\right)^2\right] + n_S\left[A_{S_2} \times (x - d_{S_2})^2\right] +$$
$$n_S\left[A_{S_1} \times (d_{S_1} - x)^2\right] + n_f\left[A_f \times (d_f - x)^2\right] = 324\,142\,515 \text{ mm}^4$$

Cracking moment:

$$M_c = \frac{f_t \times I_0}{h - y_{0na}} = 9\,652\,893.458 \text{ N.mm}$$

Cracking load:

$$P_C = \frac{M_C \times 4}{L} = 48\,264.47 \text{ N}$$

where L = 800 mm.

❖ Failure load

Calculation of neutral axis depth:

$$0.85\Psi f_c bx + A_{S_2} E_S \varepsilon_{S_2} = A_{S_1} f_y + A_f E_f \varepsilon_f$$

where $\Psi = 0.8$ and

$$\varepsilon_{S_2} = \varepsilon_{cu} \left(1 - \frac{d_{S_2}}{x}\right)$$

$$\varepsilon_f = \varepsilon_{cu} \left(\frac{d_f}{x} - 1\right)$$

→ The depth of neutral axis: x = 30.4 mm

Failure moment:

$$M = A_{S_1} f_y \left(d_{S_1} - \delta_G x\right) + A_f E_f \varepsilon_f (h - \delta_G x) + A_{S_2} E_s \varepsilon_{S_2} \left(\delta_G x - d_{S_2}\right) = 45839980.57 \text{ N.mm}$$

Failure load:

$$P = \frac{M \times 4}{L} = 229\ 199.9 \text{ N}$$

5.5 Conclusions

- In this chapter, a numerical simulation was developed based on 3D nonlinear FE approach in order to predict the flexural behavior of RC slabs before and after fire damage. This simulation also aimed to evaluate the performance of fire-damaged RC slabs after repairing by NSM CFRP bars.

- Based on a comparison with the results from real test, it is possible to use this numerical simulation in order to predict the behavior of fire-damaged slab as well as the normal structure.

- Besides, the proposed model is also capable for predicting a general behavior of fire-damaged slabs repaired by NSM CFRP bars. However, in order to improve the simulation for a better result compared with the experimental, an interfacial bond model using connector element was conducted. Although the result in model of pull-out test was acceptable but it is required to have more evaluation about the necessary parameters for connector elements as applying to the model of slab.

- Furthermore, a parametric study based on the developed model evidenced that if the FRP length satisfied the required development length as calculated based on the pull-out test, the slab still can have ability to enhance the load carrying capacity compared with the control specimen. In addition, an application of partially-bonded system in case of this repairing method is possible to increase the deformability of strengthened slab and still ensure its bearing capacity.

Chapter 6

CONCLUSIONS AND RECOMMENDATIONS

6.1 Conclusion

The current research mainly aimed to propose a method for repairing and strengthening fire-damaged reinforced concrete slabs based on NSM CFRP technique in combination with repairing material. This method was expected to enhance the load carrying capacity of fire-damaged slabs without changing original size after repairing process. Moreover, the influence of location of CFRP bars was the main parameter for evaluating. To attain comprehensive and complementary achievements, experimental and numerical works were carried out. In this chapter, the main conclusions of this work and the recommendations for future research are presented.

6.1.1 Experimental results

The experimental work in this study was carried out to evaluate the performance of a new method for repairing fire-damaged RC slab based on NSM CFRP system combined with using repairing material. The location of CFRP bars was the main parameter affected to the result of this technique.

Based on the results from direct pull-out test, the bond stress in the situation which NSM rod was embedded in repairing material layer attained 3 times higher than the other situations: 1) inside concrete; 2) between concrete and repairing material.

All strengthened slabs showed an increase in load carrying capacity over control specimens and fire – damaged slab. The highest load capacity (226.9 kN) was reached in regards to slab SF5 with CFRP rods embedded inside the repairing material part.

Among three strengthening designs proposed in this study, the situation which CFRP rods were installed inside the repairing material cover could be considered as the most effective method. It also offers advantages such as ease of installation, saving cost because making groove and epoxy resin were not required.

Finally, it could be concluded that the proposed method is totally possible to repair fire-deteriorated flexural structure without changing its initial size. Moreover, in the design, CFRP bars could be protected from the external agents during service process after the rehabilitation.

6.1.2 FEM results

A numerical simulation was developed based on 3D nonlinear FE approach in order to predict the flexural behavior of RC slabs in the experiment.

The simulation showed a good agreement with the test results in modelling the RC slab before and after exposure to fire.

A simple method as mentioned in this study is suitable to simulate the behavior of slab after exposure to fire. The result from this numerical simulation could be more

accurate if the data of temperature distribution inside the specimen is supplied adequately.

With respect to the simulation of repaired slabs, an assumption for the fully bond between FRP system and concrete and also the assumption for the model of repairing material similar with the constitutive model of concrete were applied. In this case, the model was able to predict the flexural behavior of repaired slabs.

In additions, in order to save computational time, a coarse mesh model was carried out. It also predicted similar load-deflection relation for model of repaired slab except a different of maximum load capacity. Therefore, the simulation with coarse mesh as proposed in this study would be used if the assessment is only on general behavior.

The parametric study based on the developed model evidenced that if the FRP length satisfied the required development length as calculated based on the pull-out test, the slab still can have ability to enhance the load carrying capacity compared with the control specimen. In addition, an application of partially-bonded system in case of this repairing method is possible to increase the deformability of strengthened slab and still ensure its bearing capacity.

6.2 Recommendations for future work

In order to apply the proposed method to real structures, further researches and investigations are considered.

- The influence of the shape and the type of FRP should be evaluated in the experiment for a larger application of FRP material.

- Because this method is expected to protect the FRP system from the external agents after the rehabilitation during service process. Therefore, it is necessary to have experimental studies to evaluate the ability of repaired structure using this technique as it is exposed to fire attack.

- Based on the results from parametric study, it is possible to apply the partially-bonded system for this method if a requirement of deformability is considered but it should be experimentally evaluated.

- In order to improve the proposed numerical simulation, it is required to have a deeper investigation on the bond model between CFRP system and concrete or repairing material.

- In addition, the behavior of repairing material in this research was assumed as same as the behavior of concrete for modelling. It makes the results from numerical simulation would not reflect exactly the real behavior of structure. So it is required to have an experiment for evaluating the mechanical property of repairing material as well as its constitutive model for simulation. Besides, further researches can study the performance if the other kind of repairing material is applied.

REFERENCES

[1] Sangluaia H, Natarajan and Rajaraman. Behaviour of Reinforced Concrete Slab Subjected To Fire. International Journal Of Computational Engineering Research. 2013;3:195-206.

[2] Haddad RH, Al-Mekhlafy N, Ashteyat AM. Repair of heat-damaged reinforced concrete slabs using fibrous composite materials. Construction and Building Materials. 2011;25:1213-21.

[3] Kai X, Guohui W, Jiangtao Y, Zhoudao L. Flexural strengthening of fire-damaged reinforced concrete continuous T-beams with CFRP sheets. Electric Technology and Civil Engineering (ICETCE), 2011 International Conference: IEEE; 2011. p. 372-9.

[4] De Lorenzis L, Rizzo A, La Tegola A. A modified pull-out test for bond of near-surface mounted FRP rods in concrete. Composites Part B: Engineering. 2002;33:589-603.

[5] Sharaky IA, Torres L, Baena M, Miàs C. An experimental study of different factors affecting the bond of NSM FRP bars in concrete. Composite Structures. 2013;99:350-65.

[6] Al-Mahmoud F, Castel A, François R, Tourneur C. RC beams strengthened with NSM CFRP rods and modeling of peeling-off failure. Composite Structures. 2010;92:1920-30.

[7] De Lorenzis L, Teng JG. Near-surface mounted FRP reinforcement: An emerging technique for strengthening structures. Composites Part B: Engineering. 2007;38:119-43.

[8] fib. Fire design of concrete structures - materials, structures and modelling2007.

[9] fib. Fire design of concrete structures - structural behaviour and assessment. Switzerland: the International Federation for Structural Concrete (fib); 2008.

[10] Arioz O. Effects of elevated temperatures on properties of concrete. Fire Safety Journal. 2007;42:516-22.

[11] Chung C-H, Im CR, Park J. Structural Test and Analysis of RC Slab After Fire Loading. Nuclear Engineering and Technology. 2013;45:223-36.

[12] Erlin B, Hime WG, Kuenning WH. Evaluating fire damage to concrete structures. Concrete Construction. 1972;17:154-9.

[13] GangaRao HV, Taly N, Vijay P. Reinforced concrete design with FRP composites: CRC press; 2006.

[14] Quayyum S. Bond behaviour of fibre reinforced polymer (FRP) rebars in concrete. 2010.

[15] Bisby L. ISIS Educational Module 2: An Introduction to FRP Composites for Construction. ISIS Canada, Intelligent Sensing for Innovative Structures, A Canadian Network of Centres of Excellence, University of Manitoba, Winnipeg. 2003;100.

[16] Balaguru P, Nanni A, Giancaspro J. FRP composites for reinforced and prestressed concrete structures: a guide to fundamentals and design for repair and retrofit: Taylor & Francis US; 2008.

[17] MATTHYS S. FRP Material Characteristic. University of Ghent2015.

[18] Du Béton FI. Externally bonded FRP reinforcement for RC structures. Bulletin. 2001;14:138.

[19] El-Hacha R, Rizkalla SH. Near-surface-mounted fiber-reinforced polymer reinforcements for flexural strengthening of concrete structures. ACI Structural Journal. 2004;101.

[20] Asplund S. Strengthening bridge slabs with grouted reinforcement. ACI Journal Proceedings: ACI; 1949.

[21] Lee D, Cheng L, Yan-Gee Hui J. Bond Characteristics of Various NSM FRP Reinforcements in Concrete. Journal of Composites for Construction. 2012;17:117-29.

[22] HPU. http://www.hpu.edu.vn/. 2012.

[23] De Lorenzis L, Nanni A, La Tegola A. Strengthening of reinforced concrete structures with near surface mounted FRP rods. International Meeting on Composite Materials, PLAST 2000, Proceedings, Advancing with Composites2000. p. 9-11.

[24] Parretti R, Nanni A. Strengthening of RC members using near-surface mounted FRP composites: Design overview. Advances in Structural Engineering. 2004;7:469-83.

[25] Blaschko M, Zilch K. Rehabilitation of concrete structures with CFRP strips glued into slits. Proceedings of the twelfth international conference of composite materials, ICCM1999.

[26] Teng J, De Lorenzis L, Wang B, Li R, Wong T, Lam L. Debonding failures of RC beams strengthened with near surface mounted CFRP strips. Journal of composites for construction. 2006;10:92-105.

[27] Hassan T, Rizkalla S. Bond mechanism of NSM FRP bars for flexural strengthening of concrete structures. ACI Struct J. 2004;101:830-9.

[28] Alkhrdaji T, Nanni A, Chen G, Barker M. Upgrading the transportation infrastructure: solid RC decks strengthened with FRP. Concrete International. 1999;21:37-41.

[29] Ceroni F. Experimental performances of RC beams strengthened with FRP materials. Construction and Building Materials. 2010;24:1547-59.

[30] Al-Mahmoud F, Castel A, François R, Tourneur C. Strengthening of RC members with near-surface mounted CFRP rods. Composite Structures. 2009;91:138-47.

[31] Soliman SM, El-Salakawy E, Benmokrane B. Flexural behaviour of concrete beams strengthened with near surface mounted fibre reinforced polymer bars. Canadian Journal of Civil Engineering. 2010;37:1371-82.

[32] Sharaky IA, Torres L, Comas J, Barris C. Flexural response of reinforced concrete (RC) beams strengthened with near surface mounted (NSM) fibre reinforced polymer (FRP) bars. Composite Structures. 2014;109:8-22.

[33] Foret G, Limam O. Experimental and numerical analysis of RC two-way slabs strengthened with NSM CFRP rods. Construction and Building Materials. 2008;22:2025-30.

[34] Kreit A, Al-Mahmoud F, Castel A, François R. Repairing corroded RC beam with near-surface mounted CFRP rods. Materials and structures. 2011;44:1205-17.

[35] Moon D-Y, Sim J, Oh H. Detailing considerations on RC beams strengthened with CFRP bars embedded in mortar overlay. Construction and Building Materials. 2007;21:1636-46.

[36] Palmieri A, Matthys S, Taerwe L. Fire tests on NSM FRP strengthened and insulated beams. 6th International Conference on FRP Composites in Civil Engineering (CICE-2012)2012. p. 1-8.

[37] Choi HT, West JS, Soudki KA. Analysis of the flexural behavior of partially bonded FRP strengthened concrete beams. Journal of Composites for Construction. 2008;12:375-86.

[38] Choi HT. Flexural behaviour of partially bonded CFRP strengthened concrete T-beams. 2008.

[39] Lees JM, Burgoyne CJ. Analysis of concrete beams with partially bonded composite reinforcement. American Concrete Institute; 2000.

[40] Choi HT, West JS, Soudki KA. Partially bonded near-surface-mounted CFRP bars for strengthened concrete T-beams. Construction and Building Materials. 2011;25:2441-9.

[41] Sharaky I, Torres L, Sallam H. Experimental and analytical investigation into the flexural performance of RC beams with partially and fully bonded NSM FRP bars/strips. Composite Structures. 2015;122:113-26.

[42] Mufti AA, Newhook JP, Tadros G. Deformability versus ductility in concrete beams with FRP reinforcement. PROCEEDINGS OF THE 2ND INTERNATIONAL CONFERENCE ON ADVANCED COMPOSITE MATERIALS IN BRIDGES AND STRUCTURES, ACMBS-II, MONTREAL 19961996.

[43] Tann D, Delpak R, Andreou E. 2.7 Ductility and deformability of fibre composites strengthened reinforced concrete beams. Advanced Polymer Composites for Structural Applications in Construction: Proceedings of the First International Conference, Held at Southampton University, UK, on 15-17 April 2002: Thomas Telford Services Limited; 2002. p. 117.

[44] Chahrour A, Soudki K. Flexural response of reinforced concrete beams strengthened with end-anchored partially bonded carbon fiber-reinforced polymer strips. Journal of Composites for Construction. 2005;9:170-7.

[45] Novidis D, Pantazopoulou SJ, Tentolouris E. Experimental study of bond of NSM-FRP reinforcement. Construction and Building Materials. 2007;21:1760-70.

[46] ACI. ACI 318-08: Building Code Requirements for Structural Concrete and Commentary. America: American Concrete Institute; 2008. p. 345.

[47] ASTM. ASTM E119: Standard Test Methods for Fire Tests of Building Construction and Materials. West Conshohocken, America: American Society for Testing and Materials; 2000.

[48] Daungwilailuk T. Assessment of Fire-Damaged Concrete. Chulalongkorn University: Chulalongkorn University; 2012.

[49] ASTM. ASTM C 1583-04: Standard Test Method for Tensile Strength of Concrete Surfaces and the Bond Strength or Tensile Strength of Concrete Repair and Overlay Materials by Direct Tension (Pull-off Method). West Conshohocken, America: American Society for Testing and Materials; 2005.

[50] Sharaky IA, Torres L, Baena M, Vilanova I. Effect of different material and construction details on the bond behaviour of NSM FRP bars in concrete. Construction and Building Materials. 2013;38:890-902.

[51] Galati D, De Lorenzis L. Effect of construction details on the bond performance of NSM FRP bars in concrete. Advances in Structural Engineering. 2009;12:683-700.

[52] De Lorenzis L, Nanni A. Bond between near-surface mounted FRP rods and concrete in structural strengthening. ACI structural Journal. 2002;99:123-32.

[53] Soliman SM, El-Salakawy E, Benmokrane B. Bond performance of near-surface-mounted FRP bars. Journal of Composites for Construction. 2010;15:103-11.

[54] Eligehausen R, Popov EP, Bertero VV. Local bond stress-slip relationships of deformed bars under generalized excitations. Proceedings of the 7th European Conference on Earthquake Engineering Vol 4. Athens: Techn. Chamber of Greece1982.

[55] Cosenza E, Manfredi G, Realfonzo R. Development length of FRP straight rebars. Composites Part B: Engineering. 2002;33:493-504.

[56] Simulia. ABAQUS Version 6.13-4 and ABAQUS user's manual. Hibbitt Karlsson & Sorensen Inc2014.

[57] Kmiecik P, Kamiński M. Modelling of reinforced concrete structures and composite structures with concrete strength degradation taken into consideration. Archives of Civil and Mechanical Engineering. 2011;11:623-36.

[58] Shahrokh Esfahani M, Nilforoush Hamedani R. Numerical Evaluation of Structural Behavior of the Simply Supported FRP-RC Beams. 2012.

[59] fib. Model Code 2010. Fédération Internationale du Béton fib/International Federation for Structural Concrete; 2010.

[60] Wang T, Hsu TT. Nonlinear finite element analysis of concrete structures using new constitutive models. Computers & structures. 2001;79:2781-91.

[61] Dai J-G, Gao W-Y, Teng J. Finite Element Modeling of Insulated FRP-Strengthened RC Beams Exposed to Fire. Journal of Composites for Construction. 2014.

[62] EN1994-1-2. Eurocode 4: Design of composite steel and concrete structures - Part 1-2: General Rules - Structural Fire Design. London, UK: British Standards Institution; 2005.

[63] Tao Z, Wang X-Q, Uy B. Stress-strain curves of structural and reinforcing steels after exposure to elevated temperatures. Journal of Materials in Civil Engineering. 2012;25:1306-16.

[64] Neale K, Ebead U, Abdel Baky H, Elsayed W, Godat A. Modelling of debonding phenomena in FRP-strengthened concrete beams and slabs. International Institute for FRP in Construction. 2005.

[65] Rezazadeh M. Innovative methodologies for the enhancement of the flexural strengthening performance of NSM CFRP technique for RC beams. 2015.

[66] Institute AC. ACI 440.2R-08. Guide for the design and construction of externally bonded FRP systems for strengthening of concrete structures. Michigan2002.

[67] Seo S-y, Choi K-b, Kwon Y-s, Lee K-s. Flexural Strength of RC Beam Strengthened by Partially De-bonded Near Surface-Mounted FRP Strip. International Journal of Concrete Structures and Materials. 2016:1-13.

APPENDIX

VITA

Name: Cao Nguyen Thi

Date of Birth: 30 September, 1988

Education:

2006 - 2011, Bachelor's degree in Civil Engineering, Department of Construction Materials, Faculty of Civil Engineering, Hochiminh City University of Technology, Hochiminh City, Vietnam.

2011 - 2013, Master's degree in Construction Materials Technology, Department of Construction Materials, Faculty of Civil Engineering, Hochiminh City University of Technology, Hochiminh City, Vietnam.

2013 - 2016, Doctoral degree in Structural Degree, Department of Civil Engineering, Faculty of Engineering, Chulalongkorn University.

Job:

2011 - present, Lecturer at Tien Giang University, Tien Giang province, Vietnam.